Ore Geology Reviews 111 (2019) 103001

Contents lists available at ScienceDirect

Ore Geology Reviews

journal homepage: www.elsevier.com/locate/oregeorev

Petrogenesis and metallogenic implications of volcanic rocks from the Lawu basin, eastern Tibet: Insights into the intracontinental Eocene-Oligocene porphyry copper systems

Yue Xu[a,b,c], Leiluo Xu[c,*], Xianwu Bi[c], Ruizhong Hu[c,e], Xilian Chen[d], Rui Ma[c], Jingjing Zhu[c], Hongjun Yu[a], Baohua Liu[a], Juan Li[c]

[a] *National Deep Sea Center, State Ocean Administration, Qingdao 266237, China*
[b] *Ocean University of China, Qingdao 266100, China*
[c] *State Key Laboratory of Ore Deposit Geochemistry, Institute of Geochemistry, Chinese Academy of Sciences, Guiyang 550081, China*
[d] *Key Laboratory of Mineralogy and Metallogeny, Guangzhou Institute of Geochemistry, Chinese Academy of Sciences, Guangzhou 510640, China*
[e] *School of Earth and Planetary Sciences, University of Chinese Academy of Sciences, Beijing 100049, China*

A R T I C L E I N F O

Keywords:
Potassic volcanic rocks
Sr-Nd-Hf-O isotope
Yulong Porphyry Copper belt
Intracontinental mineral systems
The Lawu basin

A B S T R A C T

Generally, porphyry Cu deposits are associated with the comagmatic porphyry (or subvolcanic)-volcanic systems of high magmatic H_2O-fO_2 conditions. The volcanic rocks, as the counterpart of the porphyries, thus can provide some significant insights into the fertility of the porphyries to some extent. For this reason, we have used the Lawu volcanic rocks and spatial-temporal closely-related porphyries in the newly discovered porphyry Cu prospects (e.g., Seli, Zongguo, Mamupu) in the southern segment of the Yulong intracontinental porphyry Cu belt to illustrate the relationship between the porphyries and volcanic rocks, petrogenesis of the volcanic rocks, and then to evaluate the ore potential of the porphyries based on the magmatic H_2O-fO_2 conditions.

Both the Lawu volcanic rocks and Seli-Zonguo-Mamupu porphyries are shoshonitic and metaluminous, and have similar REE patterns, and Sr-Nd-Hf isotopic compositions, which suggest a comagmatic relation between the volcanic rocks and porphyries. An episodic magmatism model is proposed to explain the slightly younger age (~36–35 Ma) and less evolved nature of volcanic rocks than the porphyries. The Lawu volcanic rocks of mainly intermediate composition (SiO_2 = 54.25–64.68 wt%) have high K_2O (4.75–5.94 wt%) and high K_2O/Na_2O ratios (1.69–2.00), broadly similar to the coeval Yulong fertile granitic porphyries and the Nangqian mafic lavas. The $(^{87}Sr/^{86}Sr)_i$ and $\varepsilon_{Nd}(t)$ values, uniform zircon $\varepsilon_{Hf}(t)$ and $\delta^{18}O$ values, and lack of inherited zircons of the Lawu volcanic rocks don't support their formation by mixing between the mantle-derived Nangqian mafic lavas and crust-derived Yulong felsic porphyries or assimilation and fractional crystallization (AFC) of mafic magmas. They are characterized by high Ba/Th, Ba/La and listric-shaped normalized rare earth element profile with significantly negative Nb-Ta-Ti anomalies, and have high initial $^{87}Sr/^{86}Sr$ ratios (0.7071–0.7079) and low $\varepsilon_{Nd}(t)$ values (−5.71 to −3.05), and low zircon ε_{Hf} (t) (−1.53 to 4.09) and clearly high $\delta^{18}O$ values (6.67–8.42‰), suggesting that, they were probably formed by fractional crystallization (FC) of mantle-derived mafic magmas and originated from mantle domains modified by significant amount of H_2O-rich marine sediments of the Paleo-Tethyan oceanic slab.

Magmatic H_2O contents calculated from deepest-crystallized amphiboles indicate that, the Lawu volcanic rocks and Zongguo porphyries have initial magmatic H_2O contents as high as the Yulong fertile porphyries and typical porphyry Cu systems worldwide (commonly > 4 wt% H_2O). Magmatic fO_2 (ΔFMQ) of the Lawu volcanic rocks (0.6–1.3, ave. 0.9 ± 0.1) and the Zongguo porphyries (0.9–1.7, ave. 1.4 ± 0.2) are clearly lower than the fertile porphyries in the giant Yulong deposit (ΔFMQ = 1.6–3.3, ave. 2.3 ± 0.5) and typical porphyry Cu deposits in the world (commonly ΔFMQ > 2). The slightly lower magmatic H_2O contents and slightly higher magmatic fO_2 of the Zongguo porphyries than the Lawu volcanic rocks were ascribed to variable degassing during magmatic evolution. These suggest that, in spite of the high magmatic H_2O contents, the comagmatic porphyries (at least the Zongguo porphyries) of the Lawu volcanic rocks in the southern segment of the Yulong porphyry Cu belt are unlikely to produce large-scale porphyry Cu mineralization like the giant Yulong deposit, due to the low magmatic fO_2 conditions.

* Corresponding author.
E-mail address: xuleiluo@vip.gyig.ac.cn (L. Xu).

https://doi.org/10.1016/j.oregeorev.2019.103001
Received 23 February 2019; Received in revised form 1 June 2019; Accepted 3 July 2019
Available online 05 July 2019
0169-1368/

1. Introduction

Formation of porphyry copper deposits is commonly connected with the comagmatic porphyry (or subvolcanic)-volcanic systems, typically of intermediate to felsic composition (Richards, 2003; Sillitoe, 2010). In this comagmatic system, due to rapid volcanic eruption, the volcanic rocks in composition are commonly less evolved and more close to the original magmas than the porphyries formed by the more evolved magmas in the deep chambers, and thus can provide significant information on the origin and some physical-chemical conditions (e.g., oxidation states, water contents, sulfur fugacity, etc.,) of the magmas (Carmichael, 1991; de Hoog et al., 2004; Richards, 2003; Sillitoe, 2010). High magmatic oxygen fugacity (fO_2) and water (H_2O) contents are crucial for the fertility of the porphyry Cu systems, largely because high magmatic fO_2 can suppress the formation of significant amounts of magmatic sulfide phases which would strip the magmas of the metal Cu at early stage of the magma evolution, and facilitate transportation of Cu into upper crustal levels in the fractionating magmas, and furthermore, hydrous magma can provide enough exsolving magmatic H_2O for formation of the hydrothermal ore-forming fluids (Ballard et al., 2002; Mungall, 2002; Richards, 2009; Richards and Celâl Şengör, 2017). Therefore, magmatic fO_2-H_2O conditions are widely examined and used as important signatures to evaluate the ore potential of the porphyries in many porphyry Cu ore districts or prospects (Ballard et al., 2002; Liang et al., 2006; Shen et al., 2015; Wang et al., 2014a,b, 2018; Xu et al., 2016a, 2019a; Zhu et al., 2018).

In the Eastern Qiangtang terrane of Tibet, the intermediate to felsic volcanic rocks in the Lawu basin are spatially-temporally closely associated with the newly discovered Seli-Zongguo-Mamupu porphyry Cu prospects, which are situated in the southern segment of the giant Yulong porphyry Cu belt (YPCB), and were formed in post-collisional intracontinental setting during the Eocene to Oligocene (Chen et al., 2016; Hou et al., 2003; Lin et al., 2018; Pan et al., 2010).

In this study, in combination with published data, zircon U-Pb ages and Hf-O isotopes, and whole-rock geochemistry and Sr-Nd isotopes were determined to illuminate the association of the Lawu volcanic rocks with the porphyries in the Seli-Zongguo-Mamupu porphyry Cu prospects and the petrogenesis of the Lawu volcanic rocks, and then, the magmatic fO_2 and H_2O conditions estimated from amphibole compositions of the Lawu volcanic rocks and Zongguo porphyries are used to evaluate ore potential of the porphyries in the Seli-Zongguo-Mamupu porphyry Cu prospects.

2. Geological background and sampling

2.1. The Eastern Qiangtang terrane

The eastern Tibetan Plateau is composed of (from north to south) the Songpan-Ganze complex, Eastern Qiangtang terrane, Western Qiangtang terrane and Lhasa terrane from north to south, separated from each other by the Jinsha River (or Jinshajiang in Chinese), Longmu Tso-Shuanghu and Bangong-Nujiang sutures, respectively (Fig. 1a; e.g., Deng et al., 2014a,b; Yin and Harrison, 2000; Zhu et al., 2013). The Eastern Qiangtang terrane was derived from the Indian Gondwana (He et al., 2011; Pullen et al., 2008; Tao et al., 2014; Usuki et al., 2013; Wang et al., 2013; Zhu et al., 2013). The Jinshajiang suture represents the late Triassic collision of the Eastern Qiangtang terrane with Triassic flysch of the Songpan-Ganze terrane (Wang et al., 2017). From Devonian to Triassic, the Jinshajiang Paleo-Tethyan ocean was subducted westwards beneath the Eastern Qiangtang terrane, recorded by the Jiangda-Weixi arc belt in the eastern margin of the Eastern Qiangtang terrane (Fig. 1b; Deng et al., 2014b; Mo et al., 1993; Metcalfe, 2013; Wang et al., 2017). Paleo-Tethyan subduction-related igneous rocks of Jiangda-Weixi arc belt include Jiyidu tonalite, Tongpu quartz diorite, Cuiyibi volcanic formation and Jijiading basalts of Jiangda-Weixi arc belt (Wang et al., 2014a,b; Wu et al., 2013a,b; Zi et al., 2012a,b). Jiyidu and Tongpu intrusions (283–263 Ma) have a slab-melt origin (Wu et al., 2013a,b; Zi et al., 2012b), whereas Cuiyibi and Jijiading volcanic rocks (247–237 Ma) originated from an enriched lithospheric mantle source that had been metasomatized by fluids derived from subducted sediments (Wang et al., 2014a,b; Zi et al., 2012a). During the Cenozoic, the closure of the Neo-Tethyan ocean led to the

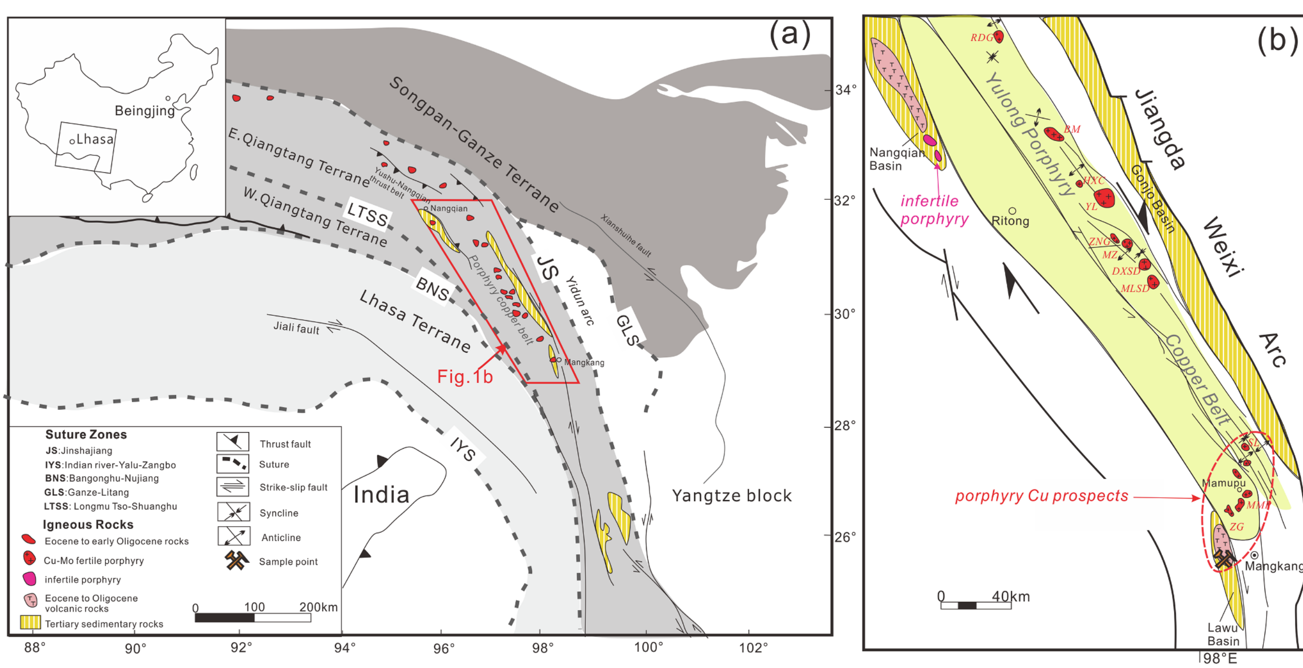

Fig. 1. (a) Simplified tectonic framework of the Himalayan-Tibetan orogen (modified after Hou et al., 2003; Yin and Harrison, 2000); (b) distribution of the volcanic rocks in the Lawu and Nangqian basins and Cu deposits in the YPCB (modified after Hou et al., 2003; Lin et al., 2018). The fertile porphyries are defined as the causative magmatic rocks leading to ore formation, whereas infertile porphyries refer to intrusions absent of mineralization (Lu et al., 2016). Deposits in the YPCB: RDG-Ridanguo; BM-Baomai; HXC-Hengxingcuo; YL: Yulong; ZNG-Zhanaga; MZ-Mangzong; DXSD-Duoxiasongduo; MLSD-Malasongduo; SL-Seli; MMP-Mamupu; ZG-Zongguo.

India-Asian collision initiated at ~65–60 Ma (Ding et al., 2016, 2017; Hu et al., 2017; Wu et al., 2014; Zhu et al., 2017; Zheng and Wu, 2018). The convergence rate of the India-Asian continents suddenly dropped at ~45 Ma, indicating the transition from "soft collision" to "hard collision" (e.g., DeCelles et al., 2002; Kohn and Parkinson, 2002). Owing to such hard collision, the Songpan-Ganze terrane was subducted southwards beneath the Eastern Qiangtang terrane along the Jinshajiang suture, and a series of strike-slip faults and contraction deformation were developed, including the Jinshajiang strike-slip fault system and the Yushu-Nangqian thrust belt (Horton et al., 2002; Hou et al., 2003; Roger et al., 2000; Spurlin et al., 2005; Tapponnier et al., 2001; Xu et al., 2016a,b; Yin and Harrison, 2000). These constructions and structures had controlled the development of the Nangqian basin, the Lawu basin, and the Yulong porphyry copper belt (Fig. 1; Horton et al., 2002; Hou et al., 2003; Spurlin et al., 2005).

2.2. The Yulong porphyry copper belt and the porphyry Cu prospects in the south

The Yulong porphyry copper belt (YPCB), over 300 km long and 15–30 km wide, contains a number of porphyry plutons associated with Cu-(Mo) mineralization (Hou et al., 2003; Xu et al., 2012). One giant (e.g., Yulong), two large (e.g., Malasongduo and Duoxiasongduo), and four medium-sized (e.g., Narigongma, Baomai, Zhanaga and Mangzong) deposits have been identified in the central segment of the YPCB (Appendix Table A2), with zircon U-Pb ages of the fertile porphyry plutons ranging from ~43 to 37 Ma (Appendix Fig. A1 and Appendix Table A3; Chang et al., 2017; Hou et al., 2003; Jiang et al., 2006; Liang et al., 2006, 2007; Lin et al., 2018; Li et al., 2012; Pan et al., 2010; Xu et al., 2012; Yang et al., 2014; Zhang and Xie, 1997). Recently, Cu-(Mo-Au-Ag)-mineralized porphyries have been discovered in the Seli-Zongguo-Mamupu prospects, southern segment of the YPCB (Appendix Table A2; Chen et al., 2016; Zhang et al., 1998, 2012).

Seli porphyry pluton is composed of the monzogranite porphyries, and occurs as a small stock with an outcrop area of 0.009 km^2 (Fig. 2a). This pluton was intruded into the upper Triassic sandstone and shale. Phenocrysts (30–40 vol%) of the monzogranite porphyry mainly consists of K-feldspar, plagioclase, and minor quartz, biotite and amphibole (Table 1; Chen et al., 2016). Amphibole in our samples experienced strong potassic alteration and became secondary biotite (Fig. 3f). Propylitic and potassic alteration and disseminated chalcopyrite, pyrite and pyrrhotite can be found in the pluton (Fig. 3i; Appendix Table A2; Chen et al., 2016; Zhang et al., 1998). Zongguo porphyry pluton occurs as a small stock with an outcrop area of 0.008 km^2 (Fig. 2b). This pluton is composed of quartz monzonite porphyries, and was emplaced into the upper Triassic purplish red sandy conglomerate with tuff and limestone interlayers (Fig. 2b; Chen et al., 2016). Phenocrysts of the quartz monzonite porphyry consist of K-feldspar, plagioclase, amphibole, biotite and quartz (Fig. 3g; Table 1; Chen et al., 2016). Disseminated chalcopyrite mineralization can be found in the porphyries (Fig. 3j; Appendix Table A2). Mamupu porphyry pluton, composed of syenite porphyries, occurs as two dykes with a total outcrop area of 4.1 km^2 (Fig. 2c; Chen et al., 2016). The pluton was intruded into the upper Triassic sandy mudstone, and the Permian-Cretaceous sandy conglomerate, and the wall-rocks experienced hornfelsized and propylitic alteration (Chen et al., 2016). K-feldspar and minor plagioclase,

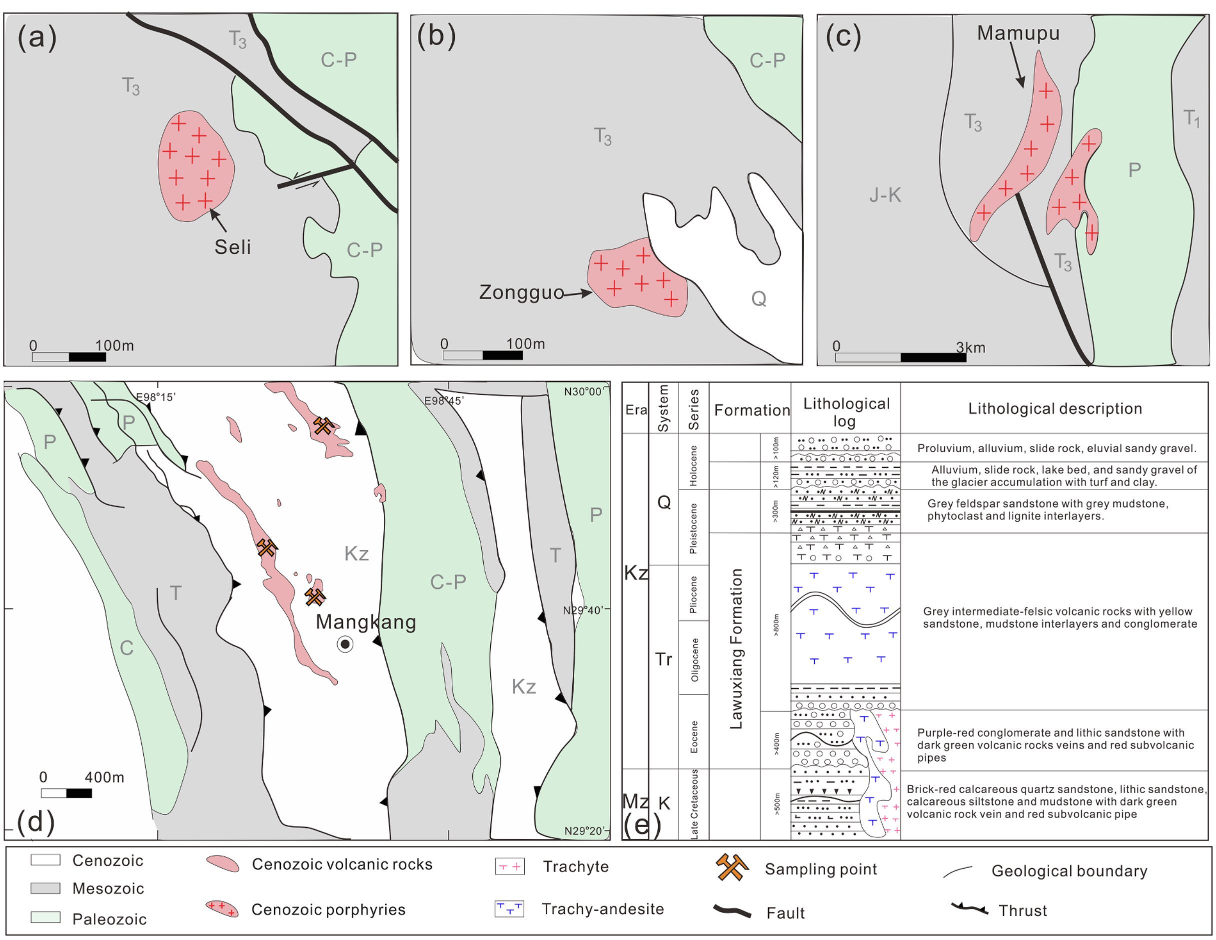

Fig. 2. Simplified geological maps for porphyry plutons from the Seli (a), Zongguo (b), and Mamupu (c) prospects (modified from Chen et al. (2016)); (d) simplified geological map showing distribution of the volcanic rocks in the Lawu basin (modified from Zhang et al. (2005)); (e) Geologic column of the volcanic rocks in the Lawuxiang formation of the Lawu basin (modified from Zhang et al. (2005)).

Table 1
Phenocryst and groundmass mineralogy of the volcanic rocks from the Lawu basin and porphyries from Seli-Zongguo-Mamupu Cu prospects.

Sample no.	Lithology	Texture	Phenocrysts	Groundmass	Reference
the Lawu basin					
LW01-1	trachy-andesite	porphyritic	Cpx(6), Bt(5), Pl(4), Kfs(5)	Zrn, Ap	This study
LW01-3	trachy-andesite	porphyritic	Cpx(5), Bt(4), Pl(3), Kfs(6)	Zrn	This study
LW01-4	trachy-andesite	porphyritic	Cpx(3), Bt(6), Pl(4), Kfs(7)	Pl, Kfs, Zrn, Ap, Mag	This study
LW01-9	trachy-andesite	porphyritic	Cpx(4), Bt(5), Pl(4), Kfs(6)	Pl, Kfs, Zrn	This study
LW04-3	trachy-andesite	porphyritic	Cpx(3), Bt(4), Pl(4), Kfs(4)	Pl	This study
LW04-1	trachy-andesite	porphyritic	Cpx(2), Bt(5), Pl(4), Kfs(3)	Zrn, Ap, Mag	This study
LW04-2	trachy-andesite	porphyritic	Cpx(3), Bt(6), Pl(4), Kfs(5)	Pl, Kfs, Zrn	This study
LW04-10	trachy-andesite	porphyritic	Cpx(3), Bt(5), Pl(4), Kfs(5)	Pl, Kfs, Zrn, Mag	This study
LW05-1	trachyte	porphyritic	Amp(6), Bt(3), Kfs (2), Pl(1), Cpx(1)	Pl, Zrn, Mag	This study
LW05-8	trachyte	porphyritic	Amp(5), Bt(4), Kfs (3), Pl(1), Qz (1)	Pl, Kfs, Zrn, Mag	This study
Seli-Zongguo-Mamupu					
83–90 (Seli)	monzogranite porphyry	porphyritic	Kfs (15), Pl(15), Amp(5), Bt(4), Qz (1)	Pl, Kfs, Zrn, Ap	This study; Chen et al. (2016)
83–86 (Zongguo)	quartz monzonite porphyry	porphyritic	Kfs (15), Pl(15), Amp(5), Bt(3), Qz (3)	Pl, Kfs, Qz, Zrn, Ap	This study; Chen et al. (2016)
83–115 (Mamupu)	syenite porphyry	porphyritic	Kfs (15), Pl(5), Amp(5), Bt(3), Qz (2), Cpx(1)	Pl, Kfs, Zrn, Ap	This study; Chen et al. (2016)

Abbreviations: Amp = amphibole; Ap = apatite; Bt = biotite; Cpx = clinopyroxene; Kfs = K-feldspar; Mag = magnetite; Pl = plagioclase; Qz = quartz; Zrn, zircon. Proportions in percent of phenocrysts shown in parentheses (vol. %).

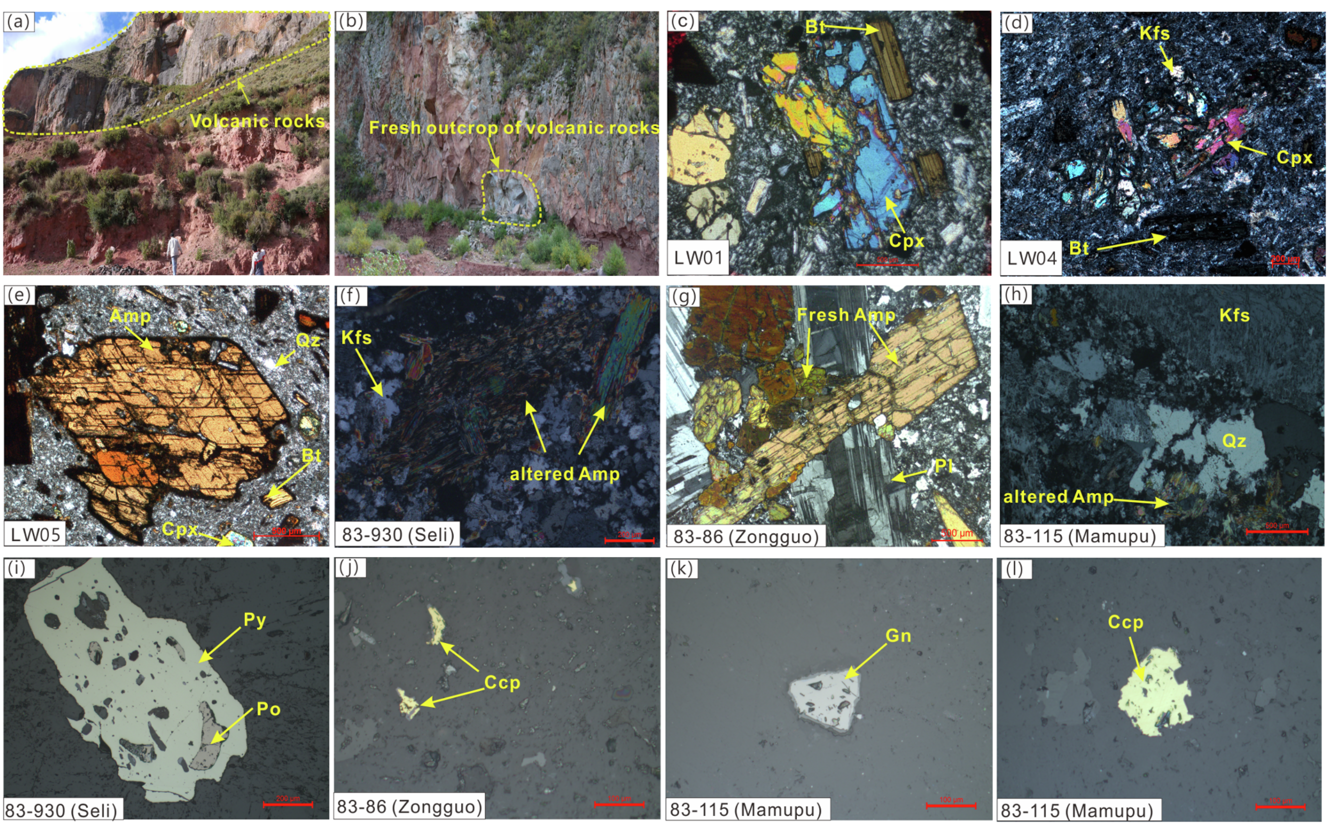

Fig. 3. Field photos (a, b), and photomicrographs of the volcanic rocks from the Lawu basin (c–e) and porphyries from Seli-Zongguo-Mamupu prospects (f–l). Abbreviations: Amp = amphibole; Bt = biotite; Ccp = chalcopyrite; Cpx = clinopyroxene; Gn = galena; Kfs = K-feldspar; Pl = plagioclase; Po = pyrrhotite; Py = pyrite; Qz = quartz.

amphibole, biotite, quartz and clinopyroxene constitute phenocrysts of the syenite porphyries (Fig. 3h; Table 1; Chen et al., 2016). Disseminated chalcopyrite, pyrite and galena mineralization can be found in the porphyries (Fig. 3k, l; Appendix Table A2; Zhang et al., 2012).

Mineralized porphyries in the Seli-Zongguo-Mamupu prospects have biotite/feldspar K-Ar ages of 39.5–34.2 Ma and zircon U-Pb ages of 39.4–38.5 Ma (Appendix Fig. A1 and Table A3), and were suggested to be derived from a source with crust-mantle mixing characteristics (Chen et al., 2016; Zhang and Xie, 1997). Spatially, these porphyries are close to the volcanic suites in the Lawu basin (Fig. 1b).

2.3. The Lawu basin and sampling

The Lawu pull-apart basin is located in the southern segment of the YPCB, and its formation was controlled by NNW-directed fold-thrust structures and strike-slip faults (Fig. 1b). The Lawuxiang formation, a major Eocene-early Pleistocene strata in the Lawu basin, primarily consists of ~400 m thick underlying clastic rocks and ~800 m thick overlying volcanic rocks (Fig. 2e; Pan et al., 2010). The underlying clastic rocks are composed of purple-red conglomerate and lithic sandstone with dark green volcanic rock veins and red subvolcanic pipe, and the overlying volcanic rocks are composed of grey intermediate-felsic volcanic rocks with yellow sandstone, mudstone interlayers and conglomerate (Fig. 2e). The volcanic rocks of the Lawuxiang formation in the Lawu basin (Lawu volcanic rocks) have ages of 34.8–33.5 Ma, with a proposed derivation from enriched mantle (EMII) (Zhang et al., 2005). Spatially and temporally, the Lawu volcanic suites are associated with the Seli-Zongguo-Mamupu porphyry Cu-(Mo-Au-Ag) prospects (Fig. 1b).

Ten grey to dark green volcanic rocks were collected from the Lawuxiang formation in the Lawu basin (Fig. 2d and e). The samples are typical trachy-andesitic to trachytic in composition and have porphyritic texture, set in a glassy to partially devitrified matrix. Mg-rich clinopyroxene (2–6 vol%), Mg- and K-rich biotite (4–6 vol%), and K-rich K-feldspar (3–7 vol%) are found in the trachy-andesitic end-members of this suite (samples Lawu 01 and Lawu 04; Fig. 3c, d). In contrast, the trachytic end-members have less clinopyroxene (1 vol%), biotite (3–4 vol%) and K-feldspar (2–3 vol%), but more amphibole (5–6 vol%) and quartz (1 vol%) phenocrysts (LW05; Fig. 3e). Details of rock types and mineral assemblages for phenocryst and groundmass are summarized in Table 1.

3. Analytical methods

3.1. SIMS zircon U-Pb dating

Three samples from the Lawu basin were collected for zircon separation. The zircon grains for U-Pb dating were roughly separated through standard density and magnetic separation techniques, and then handpicked and mounted in an epoxy resin disk and then polished before being imaged by cathodoluminescence (CL). Zircon *in-situ* U-Pb isotope analyses were performed using a Cameca 1280 secondary ion mass spectrometry (SIMS) at the Institute of Geology and Geophysics, Chinese Academy of Sciences (IGG-CAS), using standard operating conditions (20 × 30 μm, analytical spot size, 8 nA primary O_2^- beam, 7-scan duty cycle and mass resolution ~5400). The standard zircon Plešovice ($^{206}Pb/^{238}U$ = 0.05369, corresponding to 337.1 Ma; Sláma et al., 2008) was used to normalize U-Pb ratios of the unknown samples during analyses, and the standard zircon M257 (U = 840 ppm, Th/U = 0.27; Nasdala et al., 2008) were performed for calculating U, Th and Pb concentrations of the unknowns. The detailed operating and data processing procedures follow those described by Li et al. (2009). The measured $^{206}Pb/^{238}U$ uncertainty during the course of this study is ca. 1% (1 RSD), although the long-term uncertainty of the standard zircons propagated to the unknowns was 1.5% (1 RSD) (Li et al., 2010a). ^{204}Pb-method was used to correct the measured Pb isotopic composition for common Pb. An average present-day crustal Pb composition is used to correct the common Pb due to the extremely small corrections (Stacey and Kramers, 1975). Concordia diagrams and weighted mean age calculations were carried out using the Isoplot/Ex of Ludwig (2012).

3.2. Whole-rock major- and trace-element analyses

Rock samples were cut into thin slabs and the freshest portions were used for bulk-rock analyses. Major element analyses were determined by an X-ray fluorescence spectrometer (PANalytical Axios-advance) at the ALS Laboratory Group, Guangzhou. 1 g powder was heated up to 1100 °C for 1 h to calculate Loss on ignition (LOI). Analytical precision was generally better than 5%, as determined based on the Chinese National standard GSR-3.

Trace elements were measured using a PE DRC-e ICPMS at the state Key Laboratory of Ore Deposit Geochemistry (SKLODG), Institute of Geochemistry, Chinese Academy of Sciences. Rock powder (50 mg) was dissolved in PTFElined stainless steel bombs using a mixture of HF and HNO_3 for 48 h at ~190 °C. As an internal standard, Rh was used to monitor signal drift during counting. The international standards JG-2, SG-3, GSR-1, G-2, NIM-G, and SG-1a were used for monitoring analytical quality. The analytical uncertainty is lower than 5%. The detailed analytical methods were described by Qi et al. (2000).

3.3. Whole-rock Sr-Nd isotope analyses

The Sr-Nd isotopic compositions were analyzed using TRITON Thermal Ionization Mass Spectrometer (TIMS) at the SKLODG. Whole-rock powders were dissolved in Teflon bombs using HF + HNO_3. Sr and Nd were separated in solution using cationic ion-exchange procedures (Fan et al., 2003; Richard et al., 1976; Zhang et al., 2002). Sr and Nd isotopic ratios were normalized based on a $^{86}Sr/^{88}Sr$ of 0.1194 and a $^{146}Nd/^{144}Nd$ of 0.72419. Reference standards NBS987 for Sr yielded average $^{87}Sr/^{86}Sr$ = 0.710260 ± 0.000007 (2σ, n = 100) and La Jolla for Nd yielded $^{143}Nd/^{144}Nd$ = 0.512010 ± 0.000006 (2σ, n = 100).

3.4. Zircon O and Hf isotope analyses

In-situ zircon oxygen isotope analyses were conducted using the Cameca 1280 SIMS at IGG-CAS. The Cs^+ ion beam was accelerated at 10 kV, with an intensity of ~2 nA. The analysis spot that was the same site previously for U-Pb dating was about 20 μm in diameter (Fig. 5). The normal-incidence electron flood gun was used to compensate for sample charging and the NMR (nuclear magnetic resonance) was used to stabilize magnetic field. Oxygen isotopes measurement were conducted using multicollector mode on two off-axis Faraday cups. Details of analytical procedures are same to those described by Tang et al. (2015). The internal precision on individual analysis was generally less than 0.20‰ (1 standard error). The standards of zircon Penglai and Qinghu with a $\delta^{18}O$ value of 5.31‰ ± 0.10‰ (2 SD) and 5.4‰ ± 0.2‰ (2SD), respectively, were used to correct the instrumental mass fractionation factor (IMF) (Li et al., 2010b, 2013). Zircon O-isotope data are listed in Table 5.

Zircon *in-situ* Hf isotopic compositions were conducted using a Neptune MC-ICPMS equipped with a 193 nm FX laser-ablation system at the Laboratory of Geoanalyses and Geochronology, Tianjin Institute of Geology and Mineral Resources. The Hf analyses were conducted on the same spots as the previous oxygen isotope analyses (Fig. 5). The analyses were conducted with spot size of ~55 μm and an 8 Hz repetition rate. During laser ablation analyses, the interference of $^{176}Yb/^{176}Hf$ was corrected using the independent mass bias factors for Yb and Hf. The detailed isobaric interference corrections and instrumental conditions were summarized by Wu et al. (2006). Zircon standards, Mud Tank, GJ-1, 91500 and Temora, were analyzed as quality control standards. During the whole session, average $^{176}Hf/^{177}Hf$ ratios for the Mud Tank and 91,500 were 0.282513 ± 20 (2σ, n = 48) and 0.282309 ± 18 (2σ, n = 20); average $^{176}Hf/^{177}Hf$ ratios for Temora was 0.282684 ± 18 (2σ, n = 20) (Wu et al., 2006) and for GJ-1 was 0.282006 ± 24 (2σ, n = 20), respectively, which agree well with the recommended values (Griffin et al., 2006; Wu et al., 2006; Gerdes and Zeh, 2006). Zircon Hf-isotope data are listed in Table 5.

3.5. Electron microprobe analyses of amphibole

Amphiboles from the Seli and Mamupu porphyry samples are seriously altered, and cannot be used for electron microprobe analyses (Fig. 3f and h). However, amphiboles from the Lawu volcanic rocks and Zongguo porphyries are relatively fresh and selected for electron microprobe analyses. The elemental analyses of amphibole phenocrysts from the Lawu volcanic rocks were acquired from polished thin sections using a JEOL JXA-8230 electron microprobe at Testing Center of Shandong Bureau of China Metallurgy and Geology, China. Element determinations (Si, Ti, Al, Cr, Fe-Total, Mn, Mg, Ca, Na, K, F, Cl) of amphibole were carried out using a beam size of 5 μm, an accelerating potential voltage of 15 kV, and a probe current of 15 nA. Silicate minerals were used as the standards for element calibrating, such as kaersutite for Fe, Ti, Ca, Na, Mg, Si, Al, K, pyrope for Cr, Mn, apatite for F and tugtupite for Cl. Matrix effects were corrected using the ZAF software provided by JEOL. The accuracy of the reported values for the analyses is 1–5% depending on the abundance of the element.

Major element compositions of amphibole from the Zongguo porphyries were determined using a JXA8530F-plus Field Emission electron microscope using wavelength-dispersive spectroscopy at the SKLODG. The operating conditions are accelerating voltage of 25 kV, beam current of 10 nA, and beam diameter of 1–3 μm. All data were corrected based on the ZAF procedure. The following standards were used for element calibrating: kaersutite (for Fe, Ti, Ca, Na, Mg, Si, Al, K), pyrope (for Cr, Mn), apatite (for F) and tugtupite (for Cl).

4. Results

4.1. Zircon U-Pb age data

Zircons from trachy-andesite and trachyte (samples LW01-1, LW04-2 and LW05-1) are euhedral to subhedral and exhibit ellipsoidal or stubby prismatic morphology, with crystal length of 50–150 μm and length-to-width ratio of 3:1–4:1 (Fig. 5). CL images show that they have typical magmatic zoning, with few overgrowth rims or core-mantle structures. Zircon grains have variable concentrations of Th and U (110–1387 and 204–1770 ppm, respectively), with Th/U varying from 0.40 to 1.18 (Table 2). The data are plotted on a Tera–Wasserburg

Table 2
Zircon U-Pb isotopic data obtained by SIMS for the volcanic rocks from the Lawu basin.

Spot	Th(ppm)	U(ppm)	Th/U	$^{238}U/^{206}Pb$	1σ (%)	$^{207}Pb/^{206}Pb$	1σ (%)	$^{206}Pb/^{238}U$(Ma)	1σ(abs.)
LW01-1									
1	506	968	0.52	183.613	1.57	0.04660	3.27	35.0	0.5
2	597	548	1.09	182.898	1.53	0.04802	4.30	35.1	0.5
3	732	1114	0.66	182.525	1.55	0.04637	3.06	35.2	0.5
4	369	507	0.73	181.997	1.50	0.04667	2.65	35.3	0.5
5	278	436	0.64	181.976	1.86	0.04739	4.98	35.3	0.7
6	460	443	1.04	181.810	1.57	0.05026	6.05	35.4	0.6
7	562	875	0.64	180.745	1.74	0.05028	3.50	35.6	0.6
8	384	803	0.48	180.463	1.58	0.04814	4.26	35.6	0.6
9	367	734	0.50	179.760	1.59	0.04912	3.96	35.8	0.6
10	279	427	0.65	179.039	2.00	0.04809	6.07	35.9	0.7
11	110	274	0.40	185.198	1.67	0.04795	2.46	34.7	0.6
12	229	305	0.75	184.350	1.62	0.04546	5.29	34.9	0.6
13	186	234	0.79	178.150	1.63	0.04745	2.85	36.1	0.6
14	166	204	0.81	178.007	1.66	0.04593	2.95	36.1	0.6
15	213	478	0.45	176.980	1.72	0.04784	1.90	36.3	0.6
16	279	642	0.43	175.708	1.56	0.04745	1.98	36.6	0.6
LW04-2									
1	265	396	0.67	180.024	1.66	0.04678	2.35	35.7	0.6
2	676	881	0.77	181.066	1.58	0.04691	2.10	35.5	0.6
3	558	1027	0.54	180.322	1.50	0.04622	1.26	35.7	0.5
4	204	323	0.63	182.591	1.55	0.04576	2.30	35.2	0.5
5	331	564	0.59	182.577	1.57	0.04611	2.77	35.2	0.5
6	464	992	0.47	183.900	1.51	0.04634	2.15	35.0	0.5
7	277	291	0.95	182.818	1.50	0.04761	2.63	35.2	0.5
8	636	946	0.67	181.859	1.51	0.04636	1.80	35.4	0.5
9	283	362	0.78	183.305	1.76	0.04668	2.17	35.1	0.6
10	595	636	0.94	186.839	1.52	0.04822	2.48	34.4	0.5
11	215	348	0.62	181.190	1.53	0.04818	2.08	35.5	0.5
12	703	1069	0.66	179.117	1.52	0.04619	2.04	35.9	0.5
13	126	214	0.59	182.709	1.58	0.04691	2.73	35.2	0.6
14	311	343	0.91	178.945	1.67	0.04840	2.42	35.9	0.6
15	868	734	1.18	176.879	1.50	0.04637	2.06	36.3	0.5
16	179	357	0.50	182.200	1.57	0.04773	2.89	35.3	0.6
17	517	639	0.81	182.209	1.50	0.04784	2.95	35.3	0.5
18	555	827	0.67	182.858	1.51	0.04638	1.92	35.2	0.5
19	316	349	0.90	181.673	1.56	0.04634	3.09	35.4	0.6
LW05-1									
1	541	793	0.68	176.275	1.50	0.04741	1.61	36.5	0.5
2	944	1490	0.63	178.771	1.50	0.04773	1.35	36.0	0.5
3	527	856	0.62	173.707	1.53	0.04623	1.98	37.0	0.6
4	422	880	0.48	176.851	1.53	0.04763	1.56	36.3	0.6
5	1387	1770	0.78	178.287	1.52	0.04699	1.17	36.1	0.5
6	742	1325	0.56	175.764	1.72	0.04619	1.32	36.6	0.6
7	506	916	0.55	178.122	1.50	0.04740	1.73	36.1	0.5
8	590	1183	0.50	180.284	1.50	0.04589	1.46	35.7	0.5
9	538	1103	0.49	181.504	1.51	0.04737	1.98	35.4	0.5
10	412	695	0.59	177.115	1.51	0.04800	1.80	36.3	0.5
11	762	1353	0.56	178.368	1.50	0.04680	1.26	36.0	0.5
12	781	1373	0.57	178.797	1.53	0.04594	2.86	36.0	0.5
13	419	939	0.45	176.886	1.50	0.04591	1.51	36.3	0.5
14	526	1030	0.51	178.522	1.52	0.04718	1.51	36.0	0.5
15	927	1724	0.54	180.513	1.50	0.04771	1.41	35.6	0.5

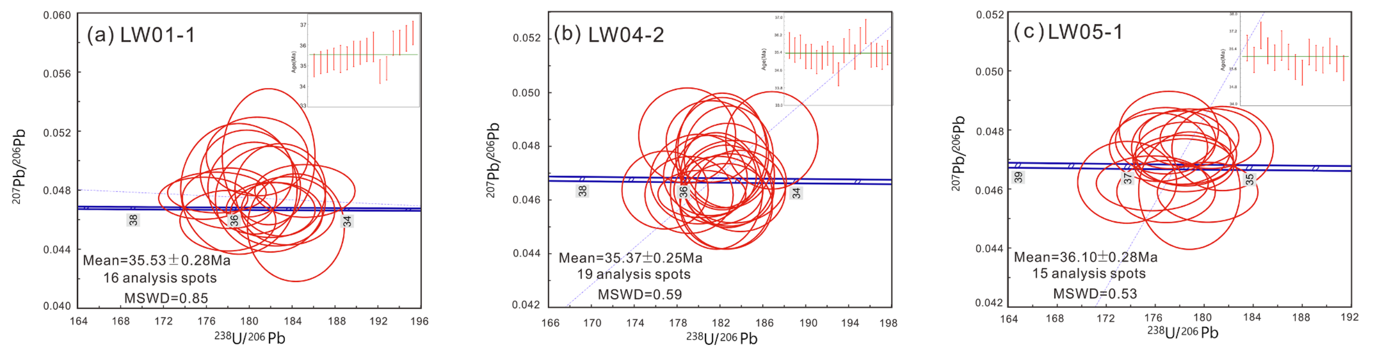

Fig. 4. Zircon U-Pb concordia diagrams for the volcanic rocks of the Lawu basin. Illustrations show weighted mean model ages.

diagram (Tera and Wasserburg, 1972), and Concordia intercept ages were calculated using Isoplot/Ex (Ludwig, 2012), with an anchoring point of $^{207}Pb/^{206}Pb = 0.83 \pm 0.6$ (ratio of average crust composition; Anderson, 2002). Analyzed zircon grains from samples LW01-1, LW04-2 and LW05-1 yielded weighted mean $^{206}Pb/^{238}U$ ages of 35.53 ± 0.28 Ma (2σ, MSWD = 0.85, n = 16), 35.37 ± 0.25 Ma (2σ, MSWD = 0.59, n = 19) and 36.10 ± 0.28 Ma (2σ, MSWD = 0.53, n = 15), respectively (Fig. 4).

4.2. Whole-rock major and trace element data

Major- and trace-elemental data are summarized in Table 3. As illustrated in a total alkali-silica diagram (Fig. 6a), samples from Lawu basin are trachy-andesites and trachytes. They have 54.25–64.68 wt% SiO_2, 2.44–3.35 wt% MgO, 4.75–5.94 wt% K_2O values, varying from alkaline to subalkaline series. The Lawu samples have high K_2O/Na_2O raitos (1.59–2.00) with A/CNK [molar ratio $Al_2O_3/(CaO + Na_2O + K_2O)$] ratios of 0.60–0.80 and A/NK [molar ratio $Al_2O_3/(Na_2O + K_2O)$] ratios of 1.19–1.45, showing shoshonitic and metaluminous characteristics (Fig. 6).

On the primitive mantle-normalized trace element diagram (Fig. 7a and c), the Lawu samples are enriched in light rare earth elements (LREE) and large ion lithophile element (LILE, e.g. Rb, Th, and U) with negative anomalies of Nb, Ta and Ti. Chondrite-normalized REE patterns show that, they are moderately enriched in LREE relative to MREE and HREE ($[La/Yb]_N$ = 11.98–17.04), with slightly negative Eu anomalies (Eu/Eu* = 0.77–0.85), and flat HREE patterns ($[Er/Yb]_N \sim 1$) (Fig. 7b and d).

4.3. Whole-rock Sr-Nd isotope data

Whole-rock Sr-Nd isotopic data for the studied volcanic rocks are listed in Table 4 and plotted in Fig. 8. The Lawu volcanic rocks have $^{87}Sr/^{86}Sr$ ratios of 0.707401–0.708123 and $^{143}Nd/^{144}Nd$ ratios of 0.512329–0.512467, with calculated $(^{87}Sr/^{86}Sr)_i$ ratios of 0.7071–0.7079 and $\varepsilon_{Nd}(t)$ values of −5.71 to −3.05. The two-stage depleted Mantle Nd model ages (T_{DM2}) of the volcanic rocks range from 0.97 to 1.30 Ga.

4.4. In-situ zircon Hf-O isotope data

In-situ zircon Hf-O isotope data are listed in Table 5. Hf isotope compositions are relatively homogeneous with calculated $\varepsilon_{Hf}(t)$ values for samples LW01-1, LW04-2 and LW05-1 ranging from 0.58 to 4.09, −0.92 to 3.09 and −1.53 to 2.77, respectively, and the corresponding T_{DM2} ages are 0.85–1.08 Ga, 0.92–1.17 Ga and 0.94–1.21 Ga, respectively. These zircons have a relatively narrow oxygen isotope composition, with $\delta^{18}O$ values of 6.67–8.42‰.

4.5. Amphibole composition data

Amphibole grains occur as euhedral phenocrysts in the Lawu volcanic rocks and Zongguo porphyries (Fig. 3e and g). Amphibole compositions and calculated parameters, such as magmatic H_2O contents and fO_2 conditions, and crystallization pressure-temperature conditions of amphibole, are presented in Appendix Table A1 and illustrated in Fig. 11.

The crystallization temperatures for amphibole are calculated with the equation of Ridolfi and Renzulli (2012), the crystallization pressures for amphibole are calculated using the spreadsheet presented by Mutch et al. (2016), and the magmatic H_2O contents and fO_2 conditions are calculated based on the spreadsheet of Ridolfi et al. (2010). The estimated crystallization temperatures and pressures for amphibole of the Lawu volcanic rocks range from 718 to 868 °C (ave. 763° ± 31 °C, n = 39) and from 3.6 to 5.5 kbar (ave. 4.5 ± 0.4 kbar, n = 39), respectively. Crystallization depths of amphibole grains, assuming conditions of lithostatic pressure ($\rho crust = 2.7 \times 10^3 kg/m^3$), are 13.8–20.9 km (ave. 17.1 ± 1.5 km, n = 39). Estimated magmatic H_2O contents and fO_2 conditions (ΔFMQ) range from 4.2 to 5.2 wt% (ave. 4.6 ± 0.2 wt%, n = 39), and from 0.6 to 1.3 (ave. 0.9 ± 0.1, n = 39) (where FMQ is the fayalite-magnetite-quartz buffer; O'Neill, 1987), respectively.

For the Zongguo porphyries, the estimated crystallization temperatures and pressures of amphibole range from 668° to 776 °C (ave. 716° ± 21 °C, n = 35) and from 2.7 to 4.0 kbar (ave. 3.2 ± 0.3 kbar, n = 35), respectively. Crystallization depths of amphibole grains are 10.4–15.4 km (ave. 12.2 ± 1.0 km, n = 35). Estimated magmatic H_2O contents and fO_2 conditions (ΔFMQ) range from 3.0 to 3.9 wt% (ave. 3.5 ± 0.2 wt%, n = 35), and from 0.9 to 1.7 (ave.1.4 ± 0.2, n = 35), respectively.

5. Discussion

5.1. Relationship between volcanism and porphyry magmatism in the southern segment of the Yulong porphyry Cu belt

The Eocene-Oligoene magmatism and associated porphyry Cu mineralization in the southern segment of the Yulong porphyry Cu belt mainly occurred in the Lawu basin and adjacent Seli-Zongguo-Mamupu porphyry Cu prospects (Fig. 1). Understanding the relationship of volcanism in the Lawu basin and porphyry magmatism in the adjacent Seli-Zongguo-Mamupu porphyry Cu prospects is critical for revealing the petrogenesis and porphyry Cu mineralization in the Yulong intracontinental porphyry Cu belt. Zircon U-Pb ages show that the Lawu volcanism occurred at ~36–35 Ma, contemporary with the porphyry magmatism in the Seli-Zongguo-Mamupu porphyry Cu prospect (Appendix Fig. A1 and Table A3). Both the volcanic rocks and porphyries are shoshonitic and metaluminous (Fig. 6a–c), exhibit linear trends in the Harker diagrams (Fig. 6d–f), and have similar REE patterns and Sr-Nd-Hf isotopic compositions (Figs. 7, 8 and 12b), which

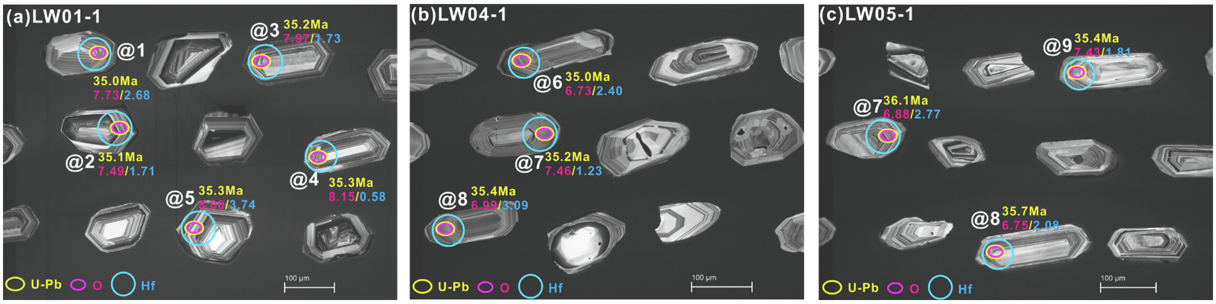

Fig. 5. Cathodoluminescence images of representative zircon grains for the volcanic rocks of the Lawu basin. The yellow, red and blue circles indicate the analytical areas for SIMS U–Pb dating, O-isotopes and LA-MC-ICPMS Lu–Hf isotopes. Numerals in yellow, red and blue color indicate U–Pb age (Ma), $\delta^{18}O$ (‰) and $\varepsilon_{Hf}(t)$ values, respectively. The white scale bars represent 100 μm. (For interpretation of the references to color in this figure legend, the reader is referred to the web version of this article.)

Table 3
Major (wt%) and trace element (ppm) concentrations for the volcanic rocks from the Lawu basin.

Locality	the Lawu basin									
Sample no.	LWL01-1	LW01-3	LW01-4	LW01-9	LW04-3	LW04-1	LW04-2	LW04-10	LW05-1	LW05-8
Rock type	TA	TA	TA	TA	TA	TA	TA	TA	T	T
SiO_2	60.48	58.62	59.88	61.72	56.78	56.85	54.25	55.87	64.21	64.68
TiO_2	0.69	0.71	0.69	0.70	0.63	0.63	0.66	0.63	0.56	0.57
Al_2O_3	14.15	14.12	14.10	14.34	13.66	13.62	13.24	13.39	13.63	13.48
TFe_2O_3	4.20	4.26	4.15	4.27	5.09	5.12	5.54	5.12	4.28	4.46
MnO	0.06	0.07	0.06	0.06	0.09	0.09	0.11	0.10	0.07	0.08
MgO	2.88	2.94	2.78	2.91	2.91	2.96	3.35	3.06	2.44	2.48
CaO	4.26	4.32	4.16	4.37	5.22	5.07	6.09	5.17	4.05	4.12
Na_2O	2.87	2.81	2.89	2.96	3.05	3.04	2.93	2.94	3.28	3.23
K_2O	4.96	4.75	4.88	5.04	5.85	5.94	5.55	5.88	5.36	5.13
P_2O_5	0.365	0.373	0.367	0.373	0.537	0.520	0.590	0.524	0.398	0.412
LOI	4.18	6.73	5.48	2.51	5.62	5.33	6.83	6.12	0.76	0.85
Total	99.40	100.00	99.73	99.55	99.71	99.45	99.43	99.07	99.29	99.73
A/CNK	0.79	0.80	0.80	0.78	0.66	0.66	0.60	0.65	0.73	0.73
A/NK	1.40	1.45	1.40	1.39	1.20	1.19	1.22	1.20	1.22	1.24
K_2O/Na_2O	1.73	1.69	1.69	1.70	1.92	1.95	1.89	2.00	1.63	1.59
Cr	59.4	60.6	55.8	61.3	66.3	66.2	81.9	65.3	63.4	63.5
Co	42.2	40.9	47.9	48.3	31.6	33.9	31.4	33.7	46	46.9
Ni	25.9	25.8	24.2	26.5	24.4	23.7	27.7	24.3	18.4	22.8
Cu	23.8	32.2	25.8	27.1	28.1	30.0	32.6	30.7	17.0	17.8
Rb	208	186	197	202	238	232	217	228	210	212
Sr	1150	1120	1120	1140	1140	1140	1190	1080	1030	998
Y	28.0	28.8	27.8	27.9	28.6	28.0	29.5	27.5	26.7	27.7
Zr	266	266	264	263	236	246	239	239	163	175
Nb	20.4	19.7	19.4	19.5	18.7	18.6	18.6	18.3	17.2	17.9
Ba	1510	1510	1490	1480	1190	1230	1300	1150	1100	1030
Ta	1.25	1.21	1.20	1.20	1.10	1.06	1.10	1.06	1.03	1.16
Pb	49.5	48.6	48.9	49.1	52.7	49.7	53.6	55.5	35.2	35.1
Th	20.7	20.3	20.0	19.9	19.5	18.5	18.0	19.1	19.4	20.3
U	6.20	5.95	6.06	6.20	5.12	5.48	5.62	5.43	5.51	5.37
Hf	6.55	6.67	6.23	6.52	6.24	6.46	6.23	6.35	4.64	4.64
La	57.0	56.1	55.6	55.6	48.8	47.4	50.4	46.9	42.6	44.4
Ce	107	105	104	104	95.5	92.2	99.8	92.0	81.5	85.1
Pr	11.9	12.2	11.7	11.8	10.7	10.3	11.1	10.5	9.1	9.6
Nd	45.1	44.9	44.1	44.2	40.6	39.3	43.1	39.4	35.4	37.6
Sm	8.51	8.42	8.13	8.09	7.36	7.42	7.83	7.36	6.82	7.21
Eu	2.03	2.11	2.05	1.96	1.91	1.77	1.89	1.88	1.79	1.83
Gd	7.20	7.23	6.87	6.75	6.14	6.14	6.56	6.05	6.51	6.83
Tb	1.10	1.12	1.05	1.05	1.01	0.997	1.05	0.990	0.934	1.00
Dy	4.92	5.16	4.93	4.93	5.11	4.95	5.22	4.83	4.64	4.95
Ho	0.967	0.959	0.894	0.908	0.99	0.953	1.01	0.981	0.901	0.961
Er	2.93	2.92	2.73	2.66	2.98	2.91	3.06	2.85	2.76	2.95
Tm	0.375	0.37	0.374	0.388	0.435	0.398	0.426	0.393	0.396	0.408
Yb	2.44	2.48	2.34	2.5	2.69	2.69	2.85	2.73	2.55	2.56
Lu	0.347	0.368	0.354	0.352	0.446	0.407	0.400	0.392	0.385	0.386
$(La/Yb)_N$	16.76	16.23	17.04	15.95	13.01	12.64	12.68	12.32	11.98	12.44
Eu/Eu*	0.77	0.80	0.82	0.79	0.85	0.78	0.79	0.84	0.81	0.79
$(Er/Yb)_N$	1.23	1.21	1.20	1.09	1.14	1.11	1.10	1.07	1.11	1.18

T, trachyte; TA, trachy-andesite. *Total Fe is given as Fe_2O_3. $Eu/Eu^* = Eu_n/(Sm_n \times Gd_n)^{1/2}$.

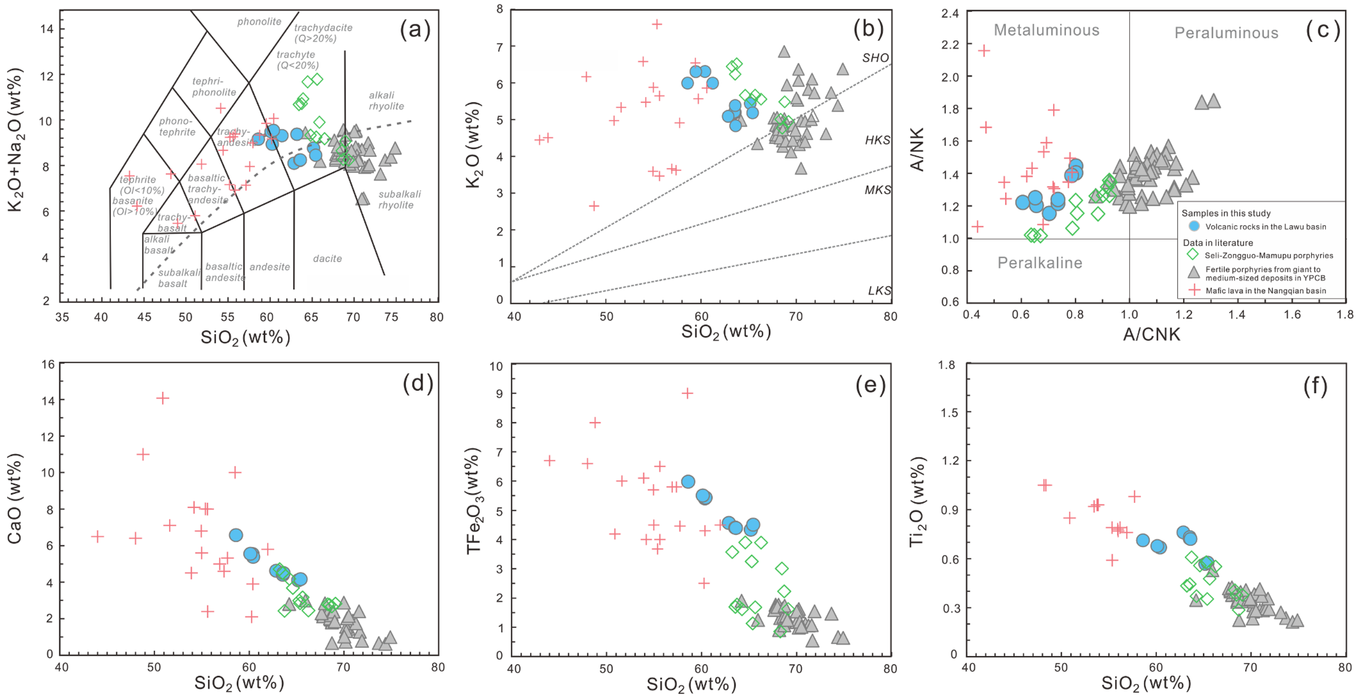

Fig. 6. Geochemical classification of the volcanic rocks in the Lawu basin. (a) TAS diagram (Le Maitre et al., 1989); the dashed line separating alkaline series from subalkaline series is from Irvine and Baragar (1971). (b) K_2O vs SiO_2 diagram, modified from Peccerillo and Taylor (1976) and Gill (2012). SHO, HKS, MKS and LKS are shoshonitic series, high-K calc-alkaline series, medium-K calc-alkaline and low-K tholeiite series, respectively. (c) A/CNK [molar ratio Al_2O_3/($CaO + Na_2O + K_2O$)] vs A/NK [molar ratio Al_2O_3/($Na_2O + K_2O$)] diagram (Kemp and Hawkesworth, 2003). (d–f) CaO, TFe_2O_3, TiO_2 vs SiO_2. All the major element values are normalized to 100% on a volatile-free basis. Literature data for the fertile porphyries from the YPCB and mafic lava from the Nangqian basin are shown for comparison. Data source: fertile porphyries from the giant to medium-sized deposits: (Hou et al., 2003; Jiang et al., 2006; Lin et al., 2018); porphyries from Seli-Zongguo-Mamupu deposit prospect: (Chen et al., 2016); mafic lavas from the Nangqian basin: (Deng et al., 2001; Spurlin et al., 2005; Xu et al., 2019b).

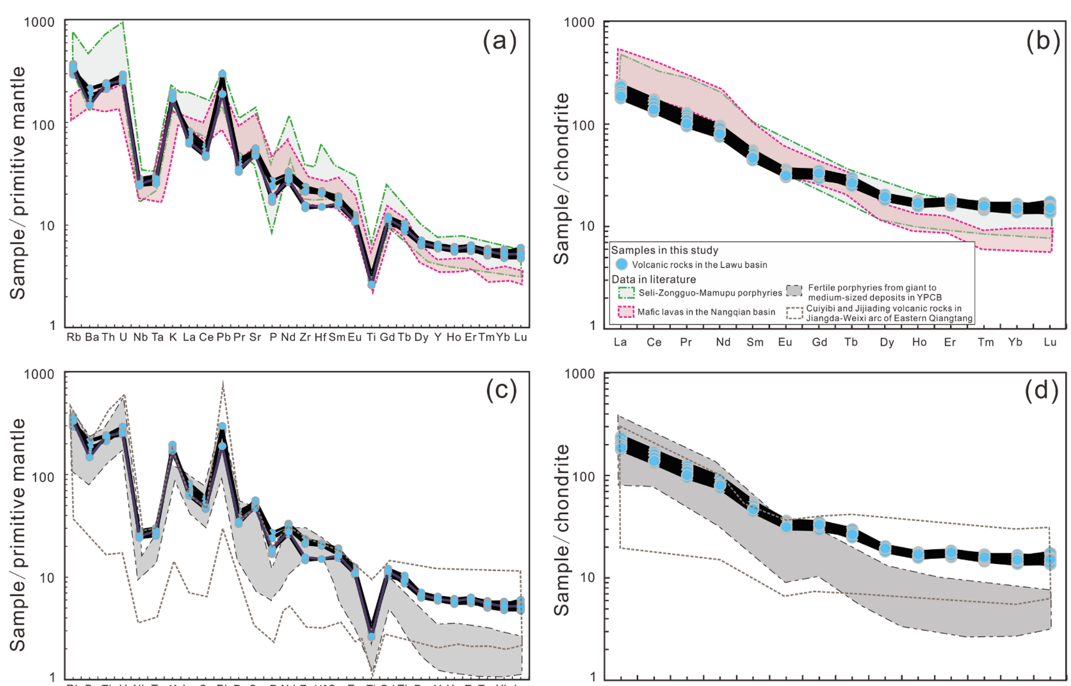

Fig. 7. (a, c) Primitive mantle normalized multi-element and (b, d) chondrite-normalized rare earth element (REE) patterns diagrams for the volcanic rocks in the Lawu basin. Chondrite and primitive mantle normalizing values are from Sun and McDonough (1989). Literature data for the giant to medium-sized deposits fertile porphyries are from (Hou et al., 2003; Jiang et al., 2006; Lin et al., 2018); Data for the Seli-Zongguo-Mamupu deposit prospects porphyries are from (Chen et al., 2016); Data for the Nangqian mafic lavas are from (Deng et al., 2001; Spurlin et al., 2005; Xu et al., 2019b); Data for Paleo-Tethyan subduction-related Cuiyibi and Jijiading volcanic rocks in the Jiangda-Weixi arc belt from (Wang et al., 2014a,b; Zi et al., 2012a).

Table 4
Sr-Nd isotopic data for the volcanic rocks from the Lawu basin.

Sample no.	Rock type	age(Ma)	$^{87}Rb/^{86}Sr$	$^{87}Sr/^{86}Sr$	± 2σ	$(^{87}Sr/^{86}Sr)_i$	$^{147}Sm/^{144}Nd$	$^{143}Nd/^{144}Nd$	± 2σ	$(^{143}Nd/^{144}Nd)_i$	ε_{Nd} (t)	T_{DM2} (Ga)
LW01-1	TA	37.0	0.5234	0.708090	12	0.707815	0.1141	0.512332	8	0.512304	−5.67	1.30
LW01-3	TA	37.0	0.4972	0.708123	14	0.707862	0.1127	0.512329	6	0.512302	−5.71	1.30
LW01-4	TA	37.0	0.4806	0.708098	16	0.707846	0.1134	0.512334	6	0.512307	−5.61	1.30
LW04-3	TA	35.0	0.6042	0.707421	10	0.707121	0.1096	0.512434	4	0.512409	−3.59	1.14
LW04-1	TA	36.7	0.6025	0.707407	8	0.707107	0.1124	0.512424	4	0.512398	−3.80	1.15
LW04-2	TA	36.7	0.6231	0.707401	12	0.707091	0.1133	0.512438	6	0.512412	−3.53	1.13
LW04-10	TA	36.7	0.6383	0.707437	12	0.707120	0.1083	0.512433	6	0.512408	−3.60	1.14
LW05-1	T	35.9	0.5900	0.707468	10	0.707165	0.1165	0.512457	2	0.512430	−3.22	0.99
LW05-8	T	35.9	0.6261	0.707505	6	0.707183	0.1204	0.512467	2	0.512438	−3.05	0.97

$^{87}Rb/^{86}Sr$ and $^{147}Sm/^{144}Nd$ are calculated using whole-rock Rb, Sr, Sm and Nd values in Table 3. Chondritic Uniform Reservoir (CHUR) at the present day [$(^{87}Rb/^{86}Sr)_{CHUR}$ = 0.0847 (McCulloch and Black, 1984); $(^{87}Sr/^{86}Sr)_{CHUR}$ = 0.7045 (DePaolo, 2012); $(^{147}Sm/^{144}Nd)_{CHUR}$ = 0.1967 (Jacobsen and Wasserburg, 1980); $(^{143}Nd/^{144}Nd)_{CHUR}$ = 0.512638 (Goldstein et al., 1984)] was used for the calculations. Nd depleted mantle model ages (T_{DM}) were calculated using $(^{147}Sm/^{144}Nd)_{DM}$ = 0.2137 and $(^{143}Nd/^{144}Nd)_{DM}$ = 0.51315 (Peucat et al., 1989) at the present day. The details for two-stage (T_{DM2}) Nd model age calculations are given by Wu et al. (2002). Two-stage Nd model age (T_{DM2}) is calculated using the same formulation as Keto and Jacobsen (1987). Initial $^{87}Sr/^{86}Sr$ ratios and ε_{Nd}(t)

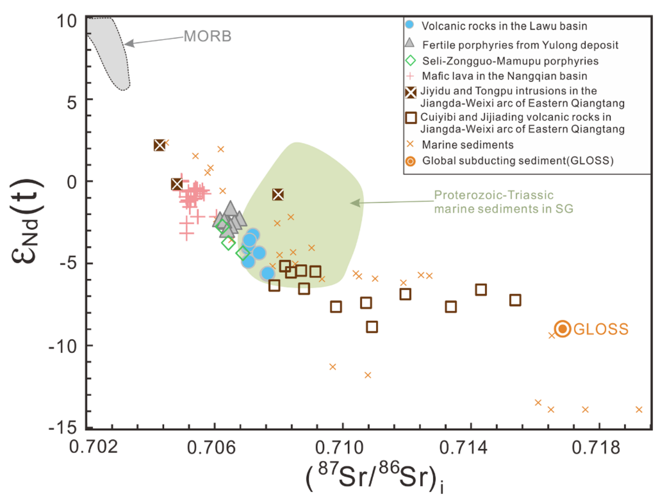

Fig. 8. ε_{Nd}(t) vs $(^{87}Sr/^{86}Sr)_i$; the mantle end-numbers (MORB; Zindler and Hart, 1986) are shown for reference. The isotope data for the Yulong fertile porphyries (Jiang et al., 2006), Seli-Zongguo-Mamupu porphyries (Zhang et al., 1998), the Nangqian mafic lavas (Deng et al., 2001; Spurlin et al., 2005; Xu et al., 2019b), Cuiyibi and Jijiading volcanic rocks in the Jiangda-Weixi arc belt (Wang et al., 2014a,b; Zi et al., 2012a), Jiyidu and Tongpu intrusions in the Jiangda-Weixi arc belt (Wu et al., 2013a,b; Zi et al., 2012b) the Proterozoic–-Triassic marine sediments in the Songpan-Ganze (SG) (Chen et al., 2006; She et al., 2006), and marine sediments and GLOSS (global subducting sediment) (Plank and Langmuir, 1998) were plotted for comparison. Initial $^{87}Sr/^{86}Sr$ ratios and ε_{Nd} (t) values of igneous rocks in the Jiangda-Weixi arc belt are calculated using ages of 36 Ma.

may suggest significant genetical relationship for them. The higher SiO_2 contents, incompatible trace element (e.g. Rb, Sr, Ba) and lower TFe_2O_3, TiO_2, MgO, CaO contents of the porphyries than the volcanic rocks (Figs. 6 and 7), indicate that, the porphyries are more evolved than the volcanic rocks. The slightly younger age (Appendix Fig. A1 and Table A3) and less evolved nature of volcanic rocks than the porphyries may be related to episodic magmatism, like proposed petrogenetic model for the volcanic and plutonic rocks in the Herberton Sn-W-Mo Mineral Field, Queensland, Australia (Cheng et al., 2018). In this model, volcanic rocks were erupted from large magma reservoirs at depth that underwent crystallization with periodic tapping of the chambers. The crystal-rich nature of the Lawu volcanic rocks reflects inefficient separation of crystal from liquid (Cheng et al., 2018; Parmigiani et al., 2016). Episodic termination of the volcanic connection (possibly due to regional compressional regime) may lead to fractionation of magmas within high-level magma chambers to generate large amount of more fractionated melts without loss of volatile components (Cheng et al., 2018). This process can explain the compositional differences and genetical relationship between the Seli-Zongguo-Mamupu porphyries and Lawu volcanic rocks over the time period from 39 to 35 Ma.

5.2. Petrogenesis of the volcanic rocks in the Lawu basin

The Lawu volcanic rocks with primarily intermediate compositions are temporally coeval with the felsic granite porphyry plutons from the giant Yulong deposit (Yulong granite porphyries) and the mafic lavas in the Nangqian basin (Nangqian mafic lavas) (Fig. 1b). A key question for the origin of the Lawu volcanic rocks is to account for its temporal, spatial and genetic relationships with the mafic and felsic end-members in the neighboring Nangqian mafic lavas and Yulong granites. Thus, we choose the Nangqian mafic lavas and Yulong granites for comparison to discuss the petrogenesis of the Lawu volcanic rocks.

5.2.1. Partial melting, binary mixing or crustal assimilation?

Direct partial melting of the mantle cannot generate melts with SiO_2 compositions over 57 wt% (Baker et al., 1995; Lloyd et al., 1985). However, the high SiO_2 contents of the volcanic rocks (54.25–64.73 wt %) in the Lawu basin probably didn't support a direct partial melting model of the mantle. The intermediate rocks are usually proposed to be the products of binary mixing between basaltic and felsic magmas (e.g. Lu et al., 2013; Streck et al., 2007), and assimilation and fractional crystallization (AFC) (e.g. Castillo et al., 1999; Miller et al., 1999; Turner et al., 1996) or fractional crystallization (FC) from parental mafic melts (e.g. Richards et al., 2013, 2018; Wang et al., 2006).

A possible petrogenetic model for the Lawu volcanic rocks is binary mixing between the mafic and felsic magmas as represented by the coeval mantle-derived Nangqian mafic lavas (Xu et al., 2016b) and crust-derived Yulong granite porphyries (Hou and Cook, 2009; Li et al., 2012), respectively. If possible, the magma mixing should produce straight arrays in the binary plots (Fig. 6d–f). However, the Lawu volcanic rocks have higher $(^{87}Sr/^{86}Sr)_i$ ratios and lower ε_{Nd}(t) values than the felsic end member, which is clearly inconsistent with the mixing model (Fig. 9a, b).

Alternative petrogenetic models for the Lawu volcanic rocks are the crustal assimilation or AFC of the mafic parental melts during their ascent from depth. However, significant crustal assimilation for the Lawu volcanic rocks can be ruled out by the following evidences: (1) lack of crustal xenoliths in the field observations; (2) absence of ancient

Table 5
Hf-O isotopic data for the magmatic zircons in the volcanic rocks from the Lawu basin.

Spots	$^{176}Yb/^{177}Hf$	$^{176}Lu/^{177}Hf$	$^{176}Hf/^{177}Hf$	1 σ	$\varepsilon_{Hf}(t)$	2 σ	T_{DM2} (Ga)	$\delta^{18}O$ (‰)	2 σ
LW01-1(trachyte; 35.53 ± 0.28 Ma)									
1	0.038637	0.001523	0.282826	0.000011	2.68	0.75	0.94	7.73	0.35
2	0.042808	0.001633	0.282799	0.000012	1.71	0.86	1.00	7.49	0.24
3	0.038968	0.001445	0.282799	0.000008	1.73	0.54	1.00	7.97	0.37
4	0.046360	0.001716	0.282767	0.000009	0.58	0.63	1.08	8.15	0.24
5	0.035501	0.001438	0.282856	0.000014	3.74	0.98	0.87	8.00	0.35
6	0.061863	0.002576	0.282867	0.000015	4.09	1.03	0.85	7.33	0.21
7	0.043178	0.001757	0.282772	0.000012	0.78	0.84	1.06	8.42	0.46
8	0.100388	0.003455	0.282825	0.000015	2.59	1.08	0.95	7.38	0.29
9	0.082081	0.002877	0.282787	0.000012	1.27	0.86	1.03	7.49	0.38
10	0.038766	0.001430	0.282813	0.000009	2.23	0.62	0.97	7.41	0.40
11	0.094062	0.003261	0.282803	0.000018	1.81	1.27	1.00	8.32	0.38
LW04-2(trachy-andesite; 35.37 ± 0.25 Ma)									
1	0.033650	0.001041	0.282810	0.000010	2.12	0.72	0.98	7.30	0.25
2	0.037889	0.001340	0.282795	0.000010	1.57	0.72	1.01	7.27	0.35
3	0.039029	0.001327	0.282800	0.000010	1.77	0.74	1.00	7.56	0.21
4	0.049007	0.001562	0.282785	0.000010	1.20	0.71	1.04	7.46	0.38
5	0.045026	0.001576	0.282738	0.000010	−0.44	0.69	1.14	—	—
6	0.041987	0.001322	0.282818	0.000010	2.40	0.70	0.96	6.73	0.25
7	0.032594	0.001177	0.282785	0.000012	1.23	0.84	1.03	7.46	0.28
8	0.039527	0.001331	0.282838	0.000012	3.09	0.82	0.92	6.99	0.22
9	0.038160	0.001328	0.282805	0.000012	1.93	0.88	0.99	—	—
10	0.044290	0.001440	0.282724	0.000011	−0.92	0.74	1.17	7.58	0.46
11	0.035739	0.001258	0.282799	0.000011	1.73	0.77	1.00	6.83	0.22
12	0.037256	0.001276	0.282781	0.000013	1.09	0.89	1.04	6.92	0.22
13	0.051412	0.001559	0.282799	0.000012	1.72	0.88	1.00	—	—
14	0.036401	0.001142	0.282836	0.000014	3.04	0.99	0.92	7.16	0.24
15	0.039197	0.001265	0.282776	0.000013	0.91	0.93	1.05	7.41	0.30
16	0.038566	0.001216	0.282802	0.000011	1.82	0.78	1.00	7.38	0.22
17	0.035319	0.001160	0.282752	0.000013	0.07	0.92	1.11	7.17	0.38
18	0.077994	0.002236	0.282753	0.000013	0.08	0.90	1.11	7.40	0.27
19	0.033650	0.001041	0.282810	0.000010	2.12	0.72	0.98	7.30	0.25
LW05-1(trachyte; 36.10 ± 0.28 Ma)									
1	0.053806	0.001664	0.282810	0.000012	2.08	0.87	0.98	6.97	0.23
2	0.040899	0.001435	0.282816	0.000011	2.33	0.81	0.96	6.67	0.31
3	0.030090	0.001039	0.282796	0.000011	1.63	0.80	1.01	6.82	0.41
4	0.041529	0.001464	0.282815	0.000012	2.28	0.85	0.97	—	—
5	0.041247	0.001457	0.282812	0.000012	2.17	0.87	0.97	6.79	0.48
6	0.034115	0.001235	0.282806	0.000013	1.96	0.90	0.99	6.94	0.25
7	0.024076	0.000894	0.282829	0.000009	2.77	0.66	0.94	6.88	0.35
8	0.043754	0.001413	0.282809	0.000013	2.08	0.90	0.98	6.75	0.25
9	0.040573	0.001393	0.282802	0.000011	1.81	0.75	1.00	7.43	0.36
10	0.040408	0.001366	0.282782	0.000011	1.11	0.79	1.04	7.00	0.32
11	0.028299	0.001072	0.282755	0.000011	0.18	0.76	1.10	7.20	0.35
12	0.038749	0.001248	0.282783	0.000012	1.13	0.82	1.04	7.13	0.27
13	0.070326	0.002125	0.282765	0.000011	0.51	0.81	1.08	7.38	0.23
14	0.033747	0.001151	0.282767	0.000010	0.58	0.72	1.08	7.43	0.26
15	0.037654	0.001302	0.282707	0.000010	−1.53	0.69	1.21	7.50	0.22

$\varepsilon_{Hf}(t) = 10000\ [(^{176}Hf/^{177}Hf)_S-(^{176}Lu/^{177}Hf)_S(e^{\lambda t}-1)]/[(^{176}Hf/^{177}Hf)_{CHUR,0}-(^{176}Lu/^{177}Hf)_{CHUR}(e^{\lambda t}-1)]-1$. Values for $(^{176}Hf/^{177}Hf)_{CHUR,0}$ (0.282785) and $(^{176}Lu/^{177}Hf)_{CHUR}$ (0.0336) are from Bouvier et al. (2008). $\varepsilon_{Hf}(t)$ calculated using a Lu decay constant of $1.865 \times 10^{-11}\ a^{-1}$ (Scherer et al., 2001). Two-stage Hf model age (T_{DM2}) calculated using the initial $^{176}Hf/^{177}Hf$ ratios of the zircons and the depleted mantle, the U-Pb age and the $^{176}Lu/^{177}Hf$ ratios of the average continental crust ($^{176}Lu/^{177}Hf = 0.015$; Griffin et al., 2002). Present-day $^{176}Lu/^{177}Hf$ ratio and $^{176}Hf/^{177}Hf$ ratio of the depleted mantle are 0.0384 and 0.28325, respectively (Griffin et al., 2000).

inherited zircons; (3) relatively uniform zircon $\varepsilon_{Hf}(t)$ values and $\delta^{18}O$ values with the increasing SiO_2 contents (Fig. 9c, d). Therefore, fractional crystallization of the mantle-derived mafic parental melts is the most possible model for the formation of the Lawu volcanic rocks.

5.2.2. Magma source and fractional crystallization

The Lawu volcanic rocks have obviously higher $(^{87}Sr/^{86}Sr)_i$ ratios and lower $\varepsilon_{Nd}(t)$ values, and much lower zircon $\varepsilon_{Hf}(t)$ values than the Nangqian mafic lavas (Figs. 8 and 9a,b and 12b). This indicates that mafic parental magmas that produced the Lawu volcanic rocks are obviously different from the Nangqian mafic lavas in Sr-Nd-Hf isotopic compositions, suggesting that the Lawu volcanic rocks have source most likely different from the Nangqian mafic lavas. Therefore, the elemental and isotopic compositions of the Lawu volcanic rocks may reflect a distinct magma source and fractional crystallization process.

The Lawu volcanic rocks show trace element and REE patterns with variable enrichments in incompatible large-ion lithophile elements (LILE) and Pb, and relative depletions in Nb, Ta and Ti and P, similar to the typical subduction-related arc rocks, and the Triassic Cuiyibi and Jijiading volcanic rocks in the Jiangda-Weixi arc belt, which originated from the Paleo-Tethyan subduction-enriched lithospheric mantle (Fig. 7c, d; Donnelly et al., 2004; Tatsumi, 1986; Wang et al., 2014a,b;

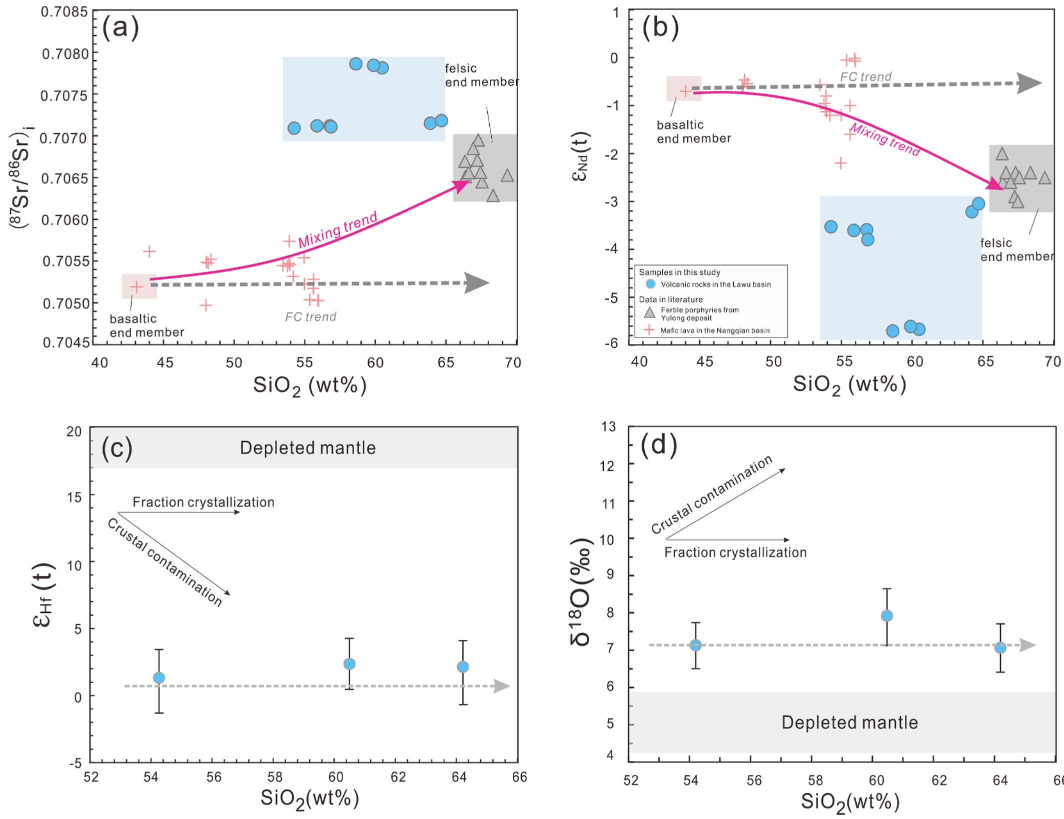

Fig. 9. Plots of SiO_2 vs Sr-Nd-Hf-O values of the Lawu volcanic rocks. (a) $(^{87}Sr/^{86}Sr)_i$ vs SiO_2; (b) $\varepsilon_{Nd}(t)$ vs SiO_2; (c) ε_{Hf} (t) vs SiO_2; (d) $\delta^{18}O$ (‰) vs SiO_2. The felsic end member is represented by Yulong intrusions and the mafic end member is represented by mafic lavas in the Nangqian basin. The $\delta^{18}O$ values for depleted mantle zircons are from Valley et al. (2005). Other data (e.g., Yulong and Nangqian) are the same as in Fig. 8.

Zi et al., 2012a). Furthermore, Sr–Nd isotopic values of the Lawu volcanic rocks are close to those (calculated back to 36 Ma) of the Cuiyibi and Jijiading volcanic rocks (Fig. 8; Wang et al., 2014a,b; Zi et al., 2012a). These suggest that, the Lawu volcanic rocks could share similar mantle sources with the Cuiyibi and Jijiading volcanic rocks. The slightly different Sr–Nd isotopic compositions between the Cuiyibi-Jijiading volcanic rocks and the Lawu volcanic rocks may suggest different degrees of involvement of marine sediments in the sources (Fig. 8). High zircon $\delta^{18}O$ values (6.67–8.42‰) of the Lawu volcanic rocks (Fig. 12a), also suggest that, supracrustal materials, probably the subducted marine sediments, were most likely involved in the mantle source (Cavosie et al., 2005; Hawkesworth and Kemp, 2006; Valley et al., 2005).

The listric-shaped REE patterns (steeper slope from LREE to MREE, then shallow to flat slope from MREE to HREE; Fig. 7b, d) for the Lawu volcanic rocks indicate their formation by a "wet" fractional crystallization of amphibole ± titanite from hydrous mafic parental magmas (e.g. Bachmann et al., 2005; Gromet and Silver, 1983; Green and Pearson, 1985; Klein et al., 1997; Prowatke and Klemme, 2006; Richards et al., 2006, 2013; Rollinson, 2014; Sisson, 1994); this is different from the Nangqian mafic lavas formed by a "dry" fractional crystallization of olivine, clinopyroxene and plagioclase from mafic parental magmas (Xu et al., 2016b).

Westward subduction of the Jinshajiang Paleo-Tethyan oceanic slab beneath the Eastern Qiangtang terrane from the early Permian to the late Triassic, which carried abundant H_2O-rich marine sediments into

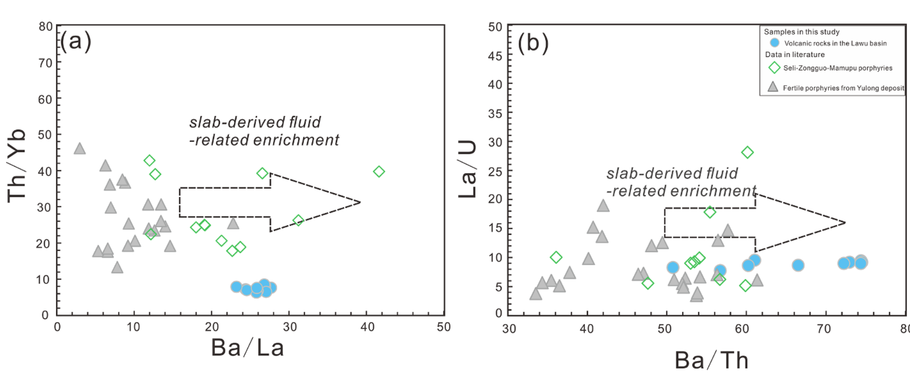

Fig. 10. (a) Th/Nb vs. Ba/La diagram and (b) La/U vs. Ba/Th diagram for the studied Lawu volcanic rocks. The arrow indicates the trend of slab-derived fluid-related enrichment. The data of Seli-Zongguo-Mamupu Cu prospects are from Chen et al. (2016) and data of Yulong deposit are from Hou et al. (2003) and Jiang et al. (2006).

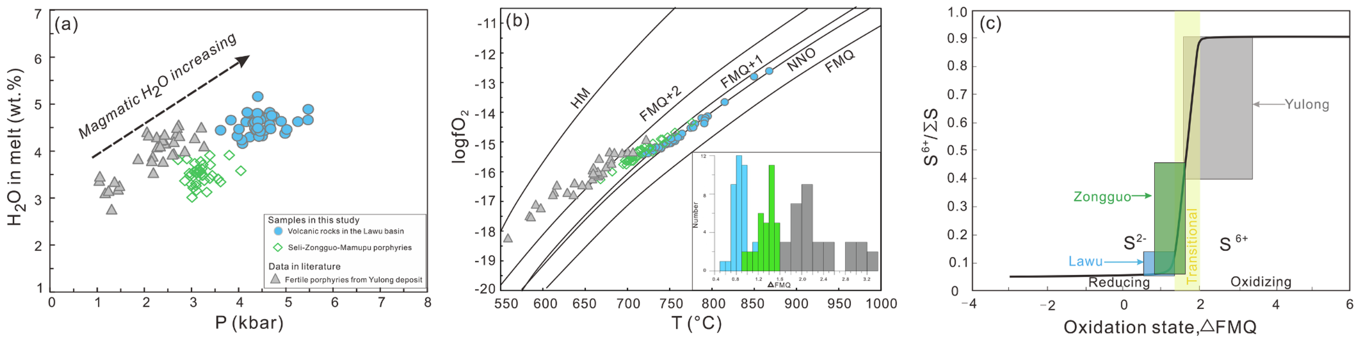

Fig. 11. Discrimination diagram and plots of crystallization pressure, temperature, magmatic water content and oxidation state estimated from amphibole compositions from the Lawu volcanic rocks and Zongguo porphyries. (a) Magmatic water contents (wt.%) vs. pressure (kbar); (b) Oxygen fugacity ($logfO_2$) vs. temperature (°C); (c) Variation of sulfur species with varying oxidation states (ΔFMQ) (modified after Wallace and Carmichael (1994)). The crystallization pressures are calculated by using the equation of Mutch et al. (2016). The crystallization temperatures are calculated using the equation of Ridolfi and Renzulli (2012). The magmatic water content and oxygen fugacity ($logfO_2$) are calculated by using the spread sheet of Ridolfi et al. (2010). The oxidation state (ΔFMQ) was calculated by using the equation of O'Neill (1987). The FMQ (fayalite-magnetite-quartz), FMQ + 1 and FMQ + 2 buffer curves are after O'Neill (1987); the NNO (nickel nickel oxide) buffer curve is after O'Neill and Pownceby (1993); the HM (hematite magnetite) buffer curve is after Chou (1978). Amphibole data of the Yulong intrusions is after Huang et al. (2019) (Appendix Table A1).

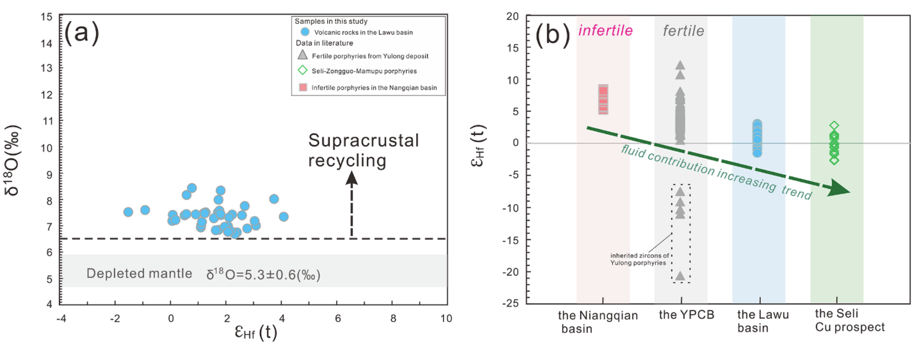

Fig. 12. (a) Combined zircon Hf-O isotope diagram for the Lawu volcanic rocks. The gray band represents the range of igneous zircons in high-temperature equilibrium with the Depleted Mantle ($\delta^{18}O = 5.3 \pm 0.6$ (‰); Valley et al., 2005). Zircon $\delta^{18}O$ values higher than 6.5‰ indicate important supracrustal material contribution (Cavosie et al., 2005; Valley et al., 2005; Hawkesworth and Kemp, 2006). (b) Plots of the zircon Hf isotopic compositions of the Lawu volcanic rocks. The data of the Yulong giant deposit (Jiang et al., 2006; Li et al., 2012), Seli prospect (Chen et al., 2016) and Nangqian basin (Xu et al., 2016b) were plotted for comparison. The green arrow indicates an increasing trend of fluid contribution. (For interpretation of the references to color in this figure legend, the reader is referred to the web version of this article.)

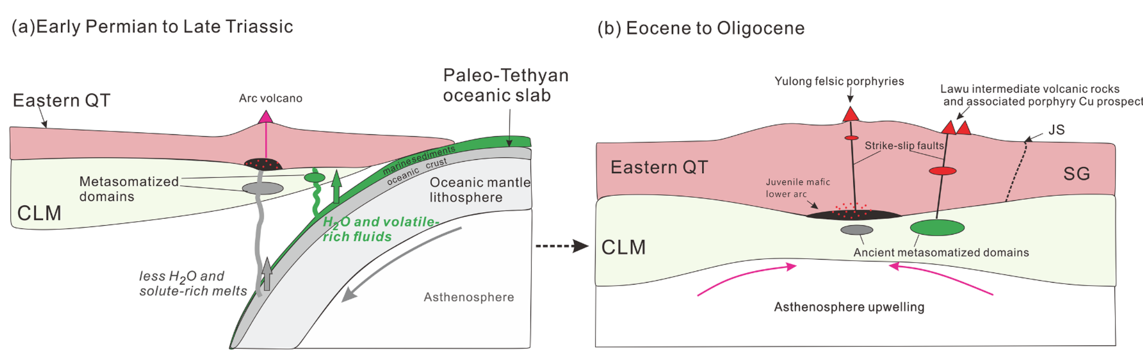

Fig. 13. A suggested model to produce fertile igneous rocks in the Eastern Qiangtang (QT) terrane. (a) During the early Permian to late Triassic, Paleo-Tethyan oceanic subduction from the eastern margin of the Eastern QT produced metasomatic domains within continental lithospheric mantle (CLM) and lower crust. Initial slab fluids released from subducted sediments at collisional edge were water- and volatiles-rich, whereas slab melts at subarc depth became less H_2O-rich and more solute-rich (modified from Riberio et al. (2015) and Richards (2009)). (b) During the Eocene-Oligocene time, the India-Asia collision-related strike-slip faults caused upwelling of the asthenosphere, which provided heat for remelting of Paleozoic metasomatic domains within CLM and lower arc, to produce the Lawu and associated metal prospects and the Yulong deposit, respectively. QT, Qiangtang; SG, Songpan-Ganze; JS, Jinshajiang suture.

the mantle, might play a significant role in producing the arc magmas of this age and enriched mantle source that later became the source of the Lawu volcanic rocks (Fig. 13a; Fan et al., 2010; Hou et al., 2003; Wang et al., 2014a,b; Xu et al., 2012, 2016a; Zhang and Xie, 1997; Zi et al., 2012a, 2013). During the Eocene-Oligocene time, the Indo-Asian collision might cause the crustal-scale strike-slip faulting and asthenospheric upwelling which triggered remelting of the ancient metasomatized domains at the Eastern Qiangtang edge to form the parental magmas of the Lawu volcanic rocks (Fig. 13b; Hou et al., 2003; Xu et al., 2016a).

5.3. Metallogenic implications

High magmatic H_2O contents and fO_2 conditions are the major controlling factors on the fertility of the evolved porphyry magmas (Ballard et al., 2002; Loucks, 2014; Mungall, 2002; Rohrlach et al., 2005; Richards, 2009; Richards and Celâl Şengör, 2017). In the co-magmatic system, the volcanic rocks can provide significant information on some physical-chemical conditions (e.g., oxidation states, water contents, sulfur fugacity, etc.,) of the parental magmas (Carmichael, 1991; de Hoog et al., 2004; Richards, 2003; Sillitoe, 2010). Therefore, we have used the magmatic H_2O-fO_2 conditions of the volcanic rocks to tentatively assess the fertility of the comagmatic porphyries in the Seli-Zonguo-Mamupu porphyry Cu prospects. In order to test this idea, we have also examined the magmatic H_2O-fO_2 conditions of the porphyries from one porphyry Cu prospect (e.g., Zongguo) for comparison.

Calculated H_2O contents of the magmas parental to the amphibole of the Lawu volcanic rocks are 4.2–5.2 wt% (ave. 4.6 ± 0.2 wt%), and furthermore, these amphibole grains have deep crystallization depths 13.8–20.9 km (ave. 17.1 ± 1.5 km), similar to those for amphiboles of early/deep crystallization in many porphyry Cu systems (Leng et al., 2018; Zhu et al., 2018). For the Zongguo porphyries, calculated amphibole crystallization depths and magmatic H_2O contents are 10.4–15.4 km (ave. 12.2 ± 1.0 km) and 3.0–3.9 wt% (ave. 3.5 ± 0.2 wt%), respectively. The lower magmatic H_2O contents for the Zongguo porphyries than the Lawu volcanic rocks may be attributed to the variable degassing during magmatic evolution, as high water contents could promote the exsolution of aqueous fluids at shallow depths (e.g. Cline, 2003; Richards, 2011b; Wang et al., 2014a,b). Nonethless, magmatic H_2O contents calculated from deepest-crystallized amphiboles indicate that, the Lawu volcanic rocks and Zongguo porphyries have initial magmatic H_2O contents as high as the fertile porphyries in the giant Yulong deposit (2.8–4.6 wt%, ave. 3.9 ± 0.5 wt %) in the same belt (Huang et al., 2019; Appendix Table A1), and typical porphyry Cu deposits (commonly > 4 wt%) worldwide (Fig. 11a; Burnham, 1979; Loucks, 2014; Naney, 1983; Richards, 2011a; Richards et al., 2012). Thus, the parental magmas for the Lawu volcanic rocks and their comagmatic porphyries (at least the Zongguo porphyries) in the Seli-Zongguo-Mamupu porphyry Cu prospects are enough in H_2O to produce concentrated hydrothermal fluids, once emplaced in appropriate depths for porphyry Cu systems (Richards, 2003; Sillitoe, 2010). This interpretation is coincident with the hydrothermal alteration developed within and around the porphyries in the Seli-Zongguo-Mamupu porphyry Cu prospects (Chen et al., 2016; Hou et al., 2003).

Except the magmatic H_2O contents, the calculated magmatic fO_2 (ΔFMQ) of the Lawu volcanic rocks and Zongguo porphyries are 0.6–1.3 (ave. 0.9 ± 0.1) and 0.9–1.7 (ave. 1.4 ± 0.2), respectively. The slightly higher magmatic fO_2 for the Zongguo porphyries than the Lawu volcanic rocks may be also attributed to the variably degassing during magmatic evolution, because fluid exsolution generally can lead to increase in magmatic fO_2 (e.g. Cline, 2003; Richards, 2011b; Wang et al., 2014a,b). Nevertheless, magmatic fO_2 for the Lawu volcanic rocks and Zongguo porphyries are still much lower than that for the fertile porphyries in the giant Yulong deposit (ΔFMQ = 1.6–3.3; ave. 2.3 ± 0.5) and typical porphyry Cu deposits (commonly ΔFMQ > 2) worldwide (Fig. 11b; Mungall, 2002; Richards et al., 2015). Such low magmatic fO_2 conditions will make most of the sulfur in the magmas existing as S^{2-} rather than S^{6+}, which will enhance early formation of Cu-rich sulfides, and thus will be unfavorable for metal Cu transportation and enrichment during magma evolution and emplacement (Fig. 11c; Mungall, 2002; Richards, 2015; Wallace and Carmichael, 1994). The sharp decrease in Cu with increasing SiO_2 contents of the Lawu volcanic rocks may indicate significant amounts of Cu-rich sulfide precipitation in magmatic stage (Fig. A2). This suggests that the comagmatic porphyries (at least the Zongguo porphyries) of the Lawu volcanic rocks in the Seli-Zongguo-Mamupu porphyry Cu prospects are unlikely to produce large-scale porphyry Cu mineralization like the giant Yulong deposit. This inference is generally consistent with the sub-economic mineralization of the porphyries in the Seli-Zongguo-Mamupu porphyry Cu prospects (Chen et al., 2016; Hou et al., 2003).

For the high H_2O contents of magmas parental to the Lawu volcanic rocks and the comagmatic porphyries in the Seli-Zongguo-Mamupu porphyry Cu prospect, fluids released from the Paleo-Tethyan oceanic slab during early subduction could play a significant role in elevating the H_2O contents of the metasomatized mantle domain and magmas generated in this domain (Fig. 13a). This inference is supported by the higher Ba/Th and Ba/La ratios, and higher $(^{87}Sr/^{86}Sr)_i$, and lower ε_{Nd} (t) and ε_{Hf} (t) values of the Lawu volcanic rocks and porphyries in the Seli-Zongguo-Mamupu porphyry Cu prospects than the Yulong fertile porphyries (Figs. 8, 10 and 12; Woodhead et al., 2001). However, for the low fO_2 conditions of magmas parental to the Lawu volcanic rocks and their comagmatic porphyries in the Seli-Zongguo-Mamupu porphyry Cu prospects, marine sediments released from the Paleo-Tethyan oceanic slab during early subduction could be responsible for lowering the fO_2 of the metasomatized mantle domain and magmas generated in this domain (Mungall, 2002; Richards, 2015). This inference is also supported by the higher $(^{87}Sr/^{86}Sr)_i$, and lower ε_{Nd} (t) and ε_{Hf} (t) values of the Lawu volcanic rocks and porphyries in the Seli-Zongguo-Mamupu porphyry Cu prospects than the Yulong fertile porphyries (Figs. 8 and 12; Dobosi et al., 2003; Plank and Langmuir, 1998; Roberts et al., 2013).

6. Conclusions

(1) The spatial-temporal relationships, and geochemical similarity suggest a closely comagmatic relation between the Lawu volcanic rocks and the porphyries in the Seli-Zongguo-Mamupu porphyry Cu prospects.
(2) The Lawu volcanic rocks were probably formed by fractional crystallization (FC) of mantle-derived mafic magmas that originated from the metasomatized mantle domains modified by significant amount of H_2O-rich marine sediments of the Paleo-Tethyan oceanic slab.
(3) The Lawu volcanic rocks and the Zongguo porphyries have initial magmatic H_2O contents as high as the fertile porphyries in the giant Yulong deposit and other typical porphyry Cu deposits worldwide, but have magmatic fO_2 much lower than them. These suggest that, the comagmatic porphyries (at least the Zongguo porphyries) of the Lawu volcanic rocks in the Seli-Zongguo-Mamupu porphyry Cu prospects likely won't produce large-scale porphyry Cu mineralization like the giant Yulong deposit in the same ore belt.

Acknowledgements

This study was jointly supported by the National Key R&D Program of China (2018YFC0309802), the National Basic Research Program, China (2015CB452603), the Strategic Priority Research Program (B) of the Chinese Academy of Sciences, China (XDB18000000), the Natural Science Foundation of China, China (41873052), the13th Five-Year Plan Program of the China Ocean Mineral Resources Research and Development Association Research, China (DY135-S2-2-08), the China Postdoctoral Science Foundation, China (2017M610403), the Taishan Scholar Project Funding, China (No. tspd20161007), and the 100 Innovative Talents of Guizhou province to Xian-Wu Bi. The kind help during fieldwork from staff of the Yunnan Copper Industry Co. Ltd. and the Tibet Yulong Copper Industry Co. Ltd is gratefully acknowledged. We thank Professor Xianhua Li (Institute of Geology and Geophysics, Chinese Academy of Sciences) for the SIMS zircon analysis. Constructive comments from two anonymous reviewers as well as insightful guidance from Editor-in-Chief Prof. Franco Pirajno and Managing Guest Editor Prof. Xiaoyong Yang are greatly appreciated.

Appendix

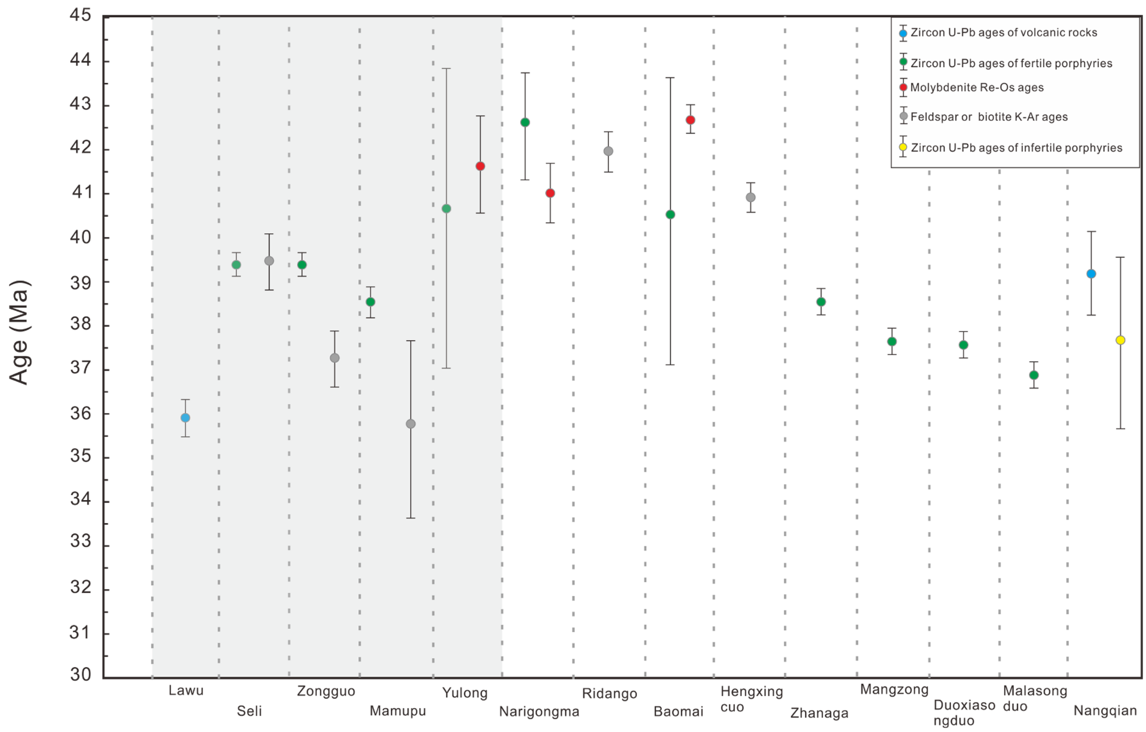

Fig. A1. Summary of ages of volcanic rocks and porphyries in the basins and Cu deposits of YPCB. Grey area marks the ages of the Lawu basin, Seli-Mamupu-Zongguo prospects and Yulong giant Cu deposits that are the focus of this study. Data sources are as in the Appendix Table A3.

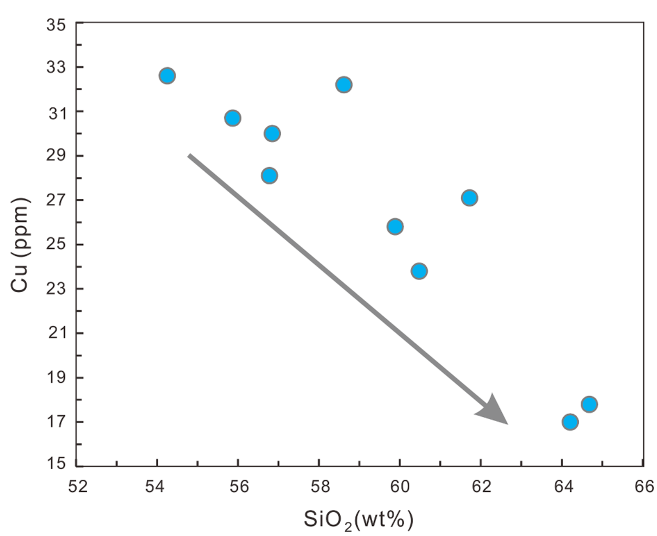

Fig. A2. Plots of ore-forming elements Cu (ppm) vs SiO_2 (wt%) contents.

Table A1
Amphibole compositions, atomic proportions, and physical-chemical conditions of the Lawu volcanic rocks, Zongguo porphyries and Yulong fertile porphyries.

Atomic proportions per 13 cations[1] Analyses[1–4]	SiO2	TiO_2	Al_2O_3	Cr_2O_3	FeO	MnO	MgO	CaO	Na2O	K_2O	F	Cl	H_2Ocalc
Volcanic rocks from Lawu basin													
LW05-1@1	43.32	1.67	9.82	0.03	16.71	0.33	10.29	11.57	1.89	1.49	0.17	0.07	1.89
LW05-1@2	43.15	1.70	10.05	0.03	16.94	0.35	9.98	11.75	1.83	1.63	0.40	0.05	1.78
LW05-1@3	43.02	1.68	9.87	0.02	16.96	0.33	10.17	11.71	1.77	1.46	0.20	0.06	1.88
LW05-1@4	42.41	1.73	10.47	0.01	17.35	0.30	9.73	11.47	1.85	1.61	0.48	0.07	1.74
LW05-1@5	43.36	1.69	9.85	0.00	17.02	0.31	10.06	11.58	1.77	1.51	0.33	0.05	1.82
LW05-1@6	42.91	1.69	10.15	0.03	17.36	0.36	9.98	11.87	1.79	1.58	0.52	0.05	1.72
LW05-1@7	42.73	2.66	11.55	0.03	14.25	0.22	11.41	11.49	2.10	1.61	0.44	0.07	1.79
LW05-1@8	42.02	2.84	11.74	0.03	14.43	0.23	11.08	11.54	2.12	1.54	0.23	0.07	1.88
LW05-1@9	42.61	1.86	10.27	0.00	16.86	0.29	9.96	11.81	1.92	1.71	0.31	0.10	1.81
LW05-1@10	42.82	1.74	10.19	0.00	17.12	0.35	9.93	11.82	1.87	1.55	0.24	0.07	1.85
LW05-1@11	42.89	1.73	9.91	0.10	16.89	0.32	10.13	11.88	1.86	1.63	0.40	0.07	1.77
LW05-1@12	42.74	1.84	10.71	0.01	17.54	0.28	9.84	11.44	1.84	1.68	0.27	0.08	1.83
LW05-1@13	43.01	1.88	10.18	0.35	17.06	0.31	10.07	11.74	1.86	1.62	0.37	0.02	1.81
LW05-1@14	42.58	1.70	10.46	0.17	17.31	0.31	9.85	11.68	1.83	1.64	0.33	0.02	1.82
LW05-1@15	42.92	1.86	10.26	0.06	17.20	0.34	9.97	11.92	1.91	1.54	0.22	0.06	1.86
LW05-1@16	42.70	1.63	10.22	0.01	16.87	0.33	10.08	11.82	1.73	1.64	0.74	0.07	1.61
LW05-8@1	42.45	1.80	10.00	0.03	17.44	0.32	9.97	11.17	1.83	1.54	0.49	0.18	1.70
LW05-8@2	42.19	1.80	10.29	0.00	17.65	0.33	9.69	11.25	1.83	1.67	0.46	0.17	1.71
LW05-8@3	41.47	1.87	10.68	0.01	17.31	0.36	9.59	11.44	1.79	1.70	0.53	0.17	1.68
LW05-8@4	42.70	1.76	10.10	0.01	16.94	0.38	9.96	11.31	1.79	1.41	0.47	0.18	1.72
LW05-8@5	43.31	1.52	9.26	0.02	16.45	0.33	10.45	11.42	1.79	1.36	0.51	0.14	1.71
LW05-8@6	42.51	1.73	9.97	0.03	17.02	0.32	9.85	11.32	1.89	1.55	0.56	0.18	1.67
LW05-8@7	42.68	1.79	10.13	0.01	17.30	0.40	9.97	11.37	1.85	1.48	0.50	0.18	1.70
LW05-8@8	42.14	1.90	10.45	0.02	17.79	0.32	9.53	11.28	1.81	1.69	0.37	0.16	1.76
LW05-8@9	41.37	2.08	10.78	0.00	16.98	0.39	9.52	11.28	1.80	1.83	0.48	0.15	1.71
LW05-8@10	40.92	2.10	11.43	0.02	17.53	0.31	9.22	11.39	1.78	1.90	0.49	0.16	1.69
LW05-8@11	42.40	1.86	10.10	0.03	17.00	0.32	9.89	11.38	1.86	1.67	0.44	0.19	1.72
LW05-8@12	43.98	1.46	8.98	0.02	16.41	0.33	10.79	11.24	1.88	1.31	0.33	0.17	1.80
LW05-8@13	41.89	1.94	10.45	0.00	17.25	0.31	9.72	11.27	1.74	1.61	0.43	0.15	1.74
LW05-8@14	42.54	1.72	9.58	0.01	16.96	0.32	10.19	11.32	1.79	1.57	0.48	0.16	1.71
LW05-8@15	42.78	1.67	9.58	0.00	17.12	0.37	10.12	11.19	1.91	1.52	0.56	0.18	1.67
LW05-8@16	42.15	1.72	10.00	0.02	17.28	0.31	9.92	11.33	1.81	1.57	0.49	0.17	1.70
LW05-8@17	42.67	1.76	10.13	0.03	17.07	0.31	10.11	11.33	1.81	1.55	0.47	0.17	1.72
LW05-8@18	42.35	1.79	10.16	0.02	17.19	0.33	10.00	11.26	1.86	1.61	0.46	0.19	1.72
LW05-8@19	42.48	1.85	10.08	0.00	17.13	0.32	9.80	11.24	1.94	1.59	0.44	0.18	1.72
LW05-8@20	43.25	1.66	9.54	0.00	16.90	0.30	10.54	11.43	1.90	1.44	0.43	0.17	1.74
LW05-8@21	41.26	2.01	10.85	0.03	17.57	0.34	9.49	11.29	1.79	1.78	0.45	0.17	1.71
LW05-8@22	43.14	1.60	9.55	0.02	16.57	0.35	10.59	11.33	1.75	1.45	0.59	0.17	1.67
LW05-8@23	41.68	1.84	10.40	0.01	17.31	0.35	9.86	11.24	1.63	1.70	0.71	0.18	1.59
porphyries from Zongguo prospect													
83-86@1	44.36	1.60	8.76	0.03	16.55	0.30	10.80	11.37	2.06	1.55	0.16	0.20	1.87
83-86@2	44.69	1.52	8.74	0.04	16.77	0.29	11.04	11.26	2.05	1.54	0.23	0.18	1.84
83-86@3	45.88	1.31	8.08	0.01	16.12	0.28	11.68	11.31	2.01	1.38	0.10	0.18	1.92
83-86@4	45.83	1.32	8.35	0.05	15.94	0.30	11.71	11.30	2.10	1.40	0.24	0.17	1.85
83-86@5	45.85	1.26	7.92	0.05	15.94	0.30	11.78	11.43	1.75	1.29	0.18	0.16	1.88
83-86@6	47.17	1.09	7.69	0.00	15.66	0.28	12.21	11.46	1.84	1.25	0.14	0.16	1.91
83-86@7	45.42	1.29	8.19	0.05	16.10	0.32	11.38	11.39	1.91	1.38	0.14	0.18	1.89
83-86@8	45.15	1.48	8.10	0.05	16.38	0.30	11.57	11.25	2.14	1.42	0.11	0.19	1.90
83-86@9	45.29	1.33	8.29	0.04	16.09	0.32	11.59	11.48	1.88	1.42	0.21	0.18	1.86
83-86@10	45.10	1.31	8.40	0.05	16.15	0.32	11.41	11.39	1.86	1.40	0.21	0.19	1.85
83-86@11	45.15	1.36	8.44	0.05	16.32	0.31	11.24	11.36	1.84	1.51	0.24	0.18	1.84

(*continued on next page*)

Table A1 (*continued*)

	Atomic proportions per 13 cations[1] Analyses[1–4]	SiO2	TiO_2	Al_2O_3	Cr_2O_3	FeO	MnO	MgO	CaO	Na2O	K_2O	F	Cl	H_2Ocalc
	83-86@12	43.81	1.77	8.93	0.00	17.11	0.30	10.49	11.35	1.97	1.62	0.16	0.21	1.86
	83-86@13	45.33	1.33	8.28	0.02	16.27	0.30	11.60	11.35	2.22	1.36	0.06	0.17	1.93
	83-86@14	45.37	1.30	8.09	0.02	16.46	0.31	11.57	11.37	2.06	1.39	0.11	0.16	1.91
	83-86@15	45.50	1.51	8.33	0.04	16.37	0.28	11.28	11.31	1.92	1.45	0.13	0.18	1.90
	83-86@16	45.44	1.30	8.45	0.01	16.26	0.30	11.48	11.38	2.06	1.42	0.29	0.17	1.82
	83-86@17	45.60	1.32	8.23	0.07	16.38	0.28	11.64	11.41	2.03	1.33	0.25	0.15	1.85
	83-86@18	45.33	1.43	8.38	0.04	16.74	0.30	11.06	11.24	2.17	1.41	0.14	0.21	1.88
	83-86@19	45.50	1.32	8.10	0.04	15.98	0.31	11.76	11.44	1.97	1.33	0.15	0.19	1.89
	83-86@20	44.87	1.44	8.24	0.02	16.59	0.29	11.46	11.26	2.04	1.43	0.14	0.19	1.89
	83-86@21	46.11	1.33	8.08	0.01	16.15	0.30	11.74	11.37	1.97	1.37	0.17	0.17	1.89
	83-86@22	43.39	1.83	9.71	0.01	16.86	0.28	10.52	11.28	2.28	1.62	0.14	0.17	1.88
	83-86@23	45.07	1.45	8.77	0.02	16.53	0.29	11.10	11.39	1.91	1.46	0.17	0.17	1.88
	83-86@24	44.67	1.60	8.62	0.02	16.71	0.30	11.07	11.33	2.22	1.54	0.15	0.19	1.87
	83-86@25	44.88	1.60	8.77	0.02	16.48	0.33	11.12	11.29	2.00	1.47	0.11	0.20	1.90
	83-86@26	45.35	1.41	8.19	0.05	16.33	0.27	11.78	11.47	2.00	1.40	0.12	0.17	1.90
	83-86@27	44.62	1.56	8.50	0.06	16.35	0.30	11.10	11.29	2.12	1.47	0.18	0.18	1.87
	83-86@28	45.15	1.46	8.50	0.05	16.69	0.30	11.19	11.45	2.12	1.44	0.15	0.17	1.88
	83-86@29	43.72	1.71	9.00	0.00	17.29	0.30	10.38	11.21	2.14	1.62	0.19	0.20	1.84
	83-86@30	45.61	1.33	7.83	0.01	15.80	0.30	11.87	11.32	1.94	1.32	0.17	0.15	1.89
	83-86@31	44.90	1.43	8.44	0.02	16.55	0.30	11.35	11.32	1.83	1.46	0.11	0.18	1.90
	83-86@32	45.24	1.49	8.50	0.04	16.30	0.31	11.19	11.28	1.94	1.46	0.17	0.17	1.88
	83-86@33	45.34	1.43	8.25	0.01	16.22	0.27	11.37	11.24	2.23	1.43	0.06	0.19	1.92
	83-86@34	45.11	1.38	8.51	0.02	16.54	0.29	11.33	11.49	2.02	1.46	0.16	0.17	1.88
	83-86@35	44.49	1.54	9.42	0.00	16.65	0.31	10.73	11.43	2.12	1.58	0.16	0.15	1.88
Early stage	Literature data of Yulong intrusions[*7]													
	ZK1007-454@1-1	46.39	0.93	7.00	0.03	14.86	0.37	12.74	11.46	1.77	0.82	0.40	0.05	1.69
	ZK1007-454@1-2	47.58	0.92	6.53	0.02	13.42	0.37	13.76	11.29	1.76	0.77	0.20	0.06	1.80
	ZK1007-454@1-3	47.37	1.11	6.57	0.01	13.02	0.28	14.12	11.32	1.83	0.78	0.48	0.07	1.67
	ZK1007-454@2-3	47.12	1.12	6.88	0.03	14.87	0.35	12.72	11.35	1.74	0.82	0.23	0.07	1.78
	ZK1007-454@2-4	46.52	1.22	6.97	0.00	14.93	0.38	12.77	11.55	1.79	0.91	0.31	0.10	1.73
	ZK1007-454@3	46.14	0.93	7.46	0.00	15.17	0.43	12.41	11.38	1.77	0.92	0.24	0.07	1.76
	ZK1007-454@4-1	47.74	0.77	6.70	0.10	13.73	0.43	13.20	11.19	1.91	0.75	0.40	0.07	1.70
	ZK1007-454@4-2	45.44	1.04	7.81	0.01	15.09	0.40	12.54	11.39	1.88	1.00	0.27	0.08	1.74
	ZK1007-454@5-3	46.35	1.00	7.42	0.06	13.78	0.31	13.41	11.40	1.79	0.91	0.22	0.06	1.78
	ZK1007-454@6-1	46.18	0.90	7.35	0.01	14.51	0.41	13.05	11.47	1.86	0.91	0.74	0.07	1.54
	ZK1007-454@6-2	48.66	0.73	5.87	0.00	13.16	0.40	14.27	11.44	1.72	0.64	0.57	0.05	1.65
	ZK1007-473@5-1	48.03	0.87	6.56	0.03	13.61	0.48	14.13	11.10	1.74	0.76	0.41	0.05	1.72
	ZK1007-473@5-2	45.90	1.02	7.56	0.06	15.13	0.39	12.34	11.40	1.77	0.85	0.23	0.07	1.76
	ZK1007-473@5-3	47.37	0.82	7.00	0.05	14.51	0.35	13.11	11.43	1.87	0.79	0.65	0.06	1.60
	ZK1007-473@6-2	47.76	0.82	6.26	0.17	13.74	0.55	13.65	11.21	1.39	0.66	0.32	0.07	1.74
	ZK1007-473@7-1	44.70	1.18	8.51	0.04	15.85	0.37	11.88	11.26	2.07	1.10	0.41	0.09	1.67
	ZK1007-473@7-2	46.25	0.92	7.42	0.03	14.92	0.37	12.75	11.56	1.90	0.85	0.02	0.06	1.87
	ZK1007-473@8-1	46.50	0.82	7.57	0.00	15.15	0.42	12.75	11.35	1.69	0.88	0.29	0.08	1.75
	ZK1007-473@8-2	44.97	1.25	8.15	0.06	14.99	0.47	12.26	11.36	1.81	1.02	0.46	0.10	1.64
	ZK1007-473@9-1	48.03	0.98	6.35	0.00	14.09	0.35	13.22	11.34	1.66	0.70	0.27	0.06	1.77
	ZK1007-473@9-2	46.30	1.10	7.68	0.02	15.59	0.36	12.53	11.36	1.82	0.89	0.29	0.06	1.75
	ZK1007-473@9-3	47.38	0.93	6.74	0.04	13.80	0.45	13.64	11.14	1.62	0.79	0.34	0.07	1.73
	ZK1007-473@10-1	47.24	0.93	6.87	0.00	14.02	0.42	13.34	11.38	1.74	0.82	0.44	0.06	1.69
	ZK1007-473@10-3	44.73	1.17	8.36	0.02	15.46	0.45	11.75	11.25	1.97	1.01	0.31	0.08	1.70
	ZK1007-473@11	46.76	0.87	7.05	0.02	15.35	0.38	12.90	11.40	1.52	0.82	0.49	0.07	1.66
Late stage	ZK1007-454@1-4	51.43	0.42	3.95	0.00	11.48	0.38	16.19	11.38	1.36	0.48	0.33	0.05	1.79
	ZK1007-454@2-1	50.08	0.57	4.79	0.03	12.02	0.37	15.48	11.53	1.50	0.61	0.52	0.05	1.69
	ZK1007-454@2-2	50.59	0.73	4.39	0.03	11.83	0.32	15.96	11.41	1.46	0.61	0.44	0.07	1.73

(continued on next page)

Table A1 (*continued*)

	Atomic proportions per 13 cations[1] Analyses[1–4]	SiO2	TiO_2	Al_2O_3	Cr_2O_3	FeO	MnO	MgO	CaO	Na2O	K_2O	F	Cl	H_2Ocalc
	ZK1007-454@5-1	52.05	0.32	3.47	0.35	11.33	0.34	16.15	11.69	1.18	0.38	0.37	0.02	1.79
	ZK1007-454@5-2	52.04	0.41	3.52	0.17	11.13	0.40	15.96	11.84	1.21	0.40	0.33	0.02	1.80
	ZK1007-454@7-1	49.92	0.67	4.87	0.00	12.10	0.37	15.36	11.54	1.43	0.63	0.20	0.06	1.83
	ZK1007-454@7-2	51.15	0.54	4.19	0.00	12.31	0.35	15.59	11.61	1.36	0.56	0.44	0.05	1.74
ZK1007-473@ 10-2	50.33	0.57	4.57	0.06	12.40	0.43	15.37	11.64	1.44	0.53	0.49	0.05	1.71	−0.22

	Atomic proportions per 13 cations[1] O = F,Cl	Total	Si	Al^{IV}	Ti^{4+}	**ΣT**	Ti^{4+}	Al^{VI}	Fe^{3+}	Mn^{2+}	Fe^{2+}	Mg^{2+}	**ΣC**	Mn^{2+}
	Volcanic rocks from Lawu basin													
	−0.09	97.26	6.59	1.42	0.00	**8**	0.19	0.34	0.00	0.01	2.12	2.33	**5**	0.04
	−0.18	97.69	6.55	1.45	0.00	**8**	0.20	0.35	0.01	0.04	2.14	2.26	**5**	0.01
	−0.10	97.13	6.55	1.45	0.00	**8**	0.19	0.32	0.05	0.01	2.11	2.31	**5**	0.03
	−0.22	97.25	6.48	1.52	0.00	**8**	0.20	0.37	0.06	0.00	2.15	2.22	**5**	0.04
	−0.15	97.38	6.59	1.41	0.00	**8**	0.19	0.35	0.04	0.02	2.12	2.28	**5**	0.02
	−0.23	98.05	6.51	1.49	0.00	**8**	0.19	0.32	0.04	0.02	2.16	2.26	**5**	0.02
	−0.20	98.35	6.36	1.64	0.00	**8**	0.30	0.39	0.04	0.01	1.74	2.53	**5**	0.02
	−0.11	97.76	6.30	1.70	0.00	**8**	0.32	0.38	0.03	0.01	1.78	2.48	**5**	0.02
	−0.15	97.54	6.49	1.51	0.00	**8**	0.21	0.34	0.00	0.04	2.15	2.26	**5**	
	−0.11	97.57	6.51	1.49	0.00	**8**	0.20	0.34	0.02	0.03	2.16	2.25	**5**	0.01
	−0.18	97.62	6.53	1.47	0.00	**8**	0.20	0.31	0.01	0.04	2.14	2.30	**5**	0.01
	−0.13	98.15	6.46	1.54	0.00	**8**	0.21	0.37	0.09	0.00	2.12	2.22	**5**	0.04
	−0.16	98.31	6.49	1.51	0.00	**8**	0.21	0.31	0.04	0.02	2.12	2.27	**5**	0.02
	−0.14	97.75	6.47	1.53	0.00	**8**	0.20	0.34	0.05	0.01	2.15	2.23	**5**	0.03
	−0.11	98.15	6.49	1.51	0.00	**8**	0.21	0.32	0.02	0.04	2.16	2.25	**5**	0.01
	−0.33	97.50	6.51	1.49	0.00	**8**	0.19	0.35	0.04	0.02	2.12	2.29	**5**	0.02
	−0.25	96.96	6.50	1.50	0.00	**8**	0.21	0.31	0.12	0.00	2.08	2.28	**5**	0.04
	−0.23	97.10	6.47	1.53	0.00	**8**	0.21	0.33	0.10	0.00	2.15	2.22	**5**	0.04
	−0.26	96.64	6.40	1.60	0.00	**8**	0.22	0.34	0.08	0.00	2.15	2.21	**5**	0.05
	−0.24	96.76	6.54	1.47	0.00	**8**	0.20	0.36	0.09	0.00	2.08	2.27	**5**	0.05
	−0.24	96.31	6.64	1.36	0.00	**8**	0.18	0.32	0.06	0.01	2.05	2.39	**5**	0.04
	−0.27	96.63	6.54	1.46	0.00	**8**	0.20	0.34	0.06	0.01	2.13	2.26	**5**	0.03
	−0.25	97.41	6.51	1.49	0.00	**8**	0.21	0.33	0.10	0.00	2.10	2.27	**5**	0.05
	−0.19	97.26	6.45	1.55	0.00	**8**	0.22	0.34	0.10	0.00	2.17	2.18	**5**	0.04
	−0.24	96.43	6.39	1.61	0.00	**8**	0.24	0.36	0.06	0.02	2.13	2.19	**5**	0.04
	−0.24	97.02	6.30	1.70	0.00	**8**	0.24	0.38	0.07	0.00	2.18	2.12	**5**	0.04
	−0.23	96.91	6.50	1.50	0.00	**8**	0.22	0.33	0.06	0.01	2.13	2.26	**5**	0.03
	−0.18	96.73	6.69	1.31	0.00	**8**	0.17	0.30	0.09	0.00	1.99	2.45	**5**	0.04
	−0.21	96.54	6.45	1.55	0.00	**8**	0.23	0.34	0.10	0.00	2.11	2.23	**5**	0.04
	−0.24	96.39	6.55	1.45	0.00	**8**	0.20	0.29	0.09	0.00	2.09	2.34	**5**	0.04
	−0.27	96.73	6.57	1.43	0.00	**8**	0.19	0.30	0.09	0.00	2.10	2.32	**5**	0.05
	−0.24	96.52	6.49	1.51	0.00	**8**	0.20	0.31	0.10	0.00	2.11	2.28	**5**	0.04
	−0.23	97.17	6.51	1.49	0.00	**8**	0.20	0.33	0.10	0.00	2.07	2.30	**5**	0.04
	−0.23	96.97	6.49	1.51	0.00	**8**	0.21	0.32	0.10	0.00	2.09	2.28	**5**	0.04
	−0.23	96.81	6.52	1.48	0.00	**8**	0.21	0.34	0.06	0.01	2.14	2.24	**5**	0.04
	−0.22	97.33	6.58	1.42	0.00	**8**	0.19	0.29	0.09	0.00	2.04	2.39	**5**	0.04
	−0.23	96.79	6.36	1.64	0.00	**8**	0.23	0.33	0.10	0.00	2.15	2.18	**5**	0.04
	−0.29	96.81	6.59	1.41	0.00	**8**	0.18	0.31	0.11	0.00	1.99	2.41	**5**	0.05
	−0.34	96.54	6.43	1.57	0.00	**8**	0.21	0.32	0.14	0.00	2.07	2.27	**5**	0.05
	porphyries from Zongguo prospect													
	−0.11	97.63	6.71	1.29	0.00	**8**	0.18	0.27	0.03	0.02	2.06	2.44	**5**	0.02
	−0.14	98.19	6.71	1.29	0.00	**8**	0.17	0.26	0.08	0.00	2.02	2.47	**5**	0.04

(*continued on next page*)

Table A1 (*continued*)

	Atomic proportions per 13 cations[1]													
	O = F,Cl	Total	Si	Al^{IV}	Ti^{4+}	**ΣT**	Ti^{4+}	Al^{VI}	Fe^{3+}	Mn^{2+}	Fe^{2+}	Mg^{2+}	**ΣC**	Mn^{2+}
	−0.08	98.25	6.84	1.16	0.00	**8**	0.15	0.26	0.07	0.00	1.93	2.59	**5**	0.04
	−0.14	98.56	6.81	1.19	0.00	**8**	0.15	0.27	0.07	0.00	1.91	2.59	**5**	0.04
	−0.11	97.79	6.85	1.15	0.00	**8**	0.14	0.25	0.09	0.00	1.89	2.62	**5**	0.04
	−0.09	98.86	6.94	1.06	0.00	**8**	0.12	0.28	0.08	0.00	1.85	2.68	**5**	0.04
	−0.10	97.64	6.82	1.18	0.00	**8**	0.15	0.27	0.06	0.01	1.96	2.55	**5**	0.03
	−0.09	98.04	6.77	1.23	0.00	**8**	0.17	0.20	0.09	0.00	1.96	2.59	**5**	0.04
	−0.13	97.98	6.78	1.22	0.00	**8**	0.15	0.25	0.08	0.00	1.93	2.59	**5**	0.04
	−0.13	97.65	6.78	1.22	0.00	**8**	0.15	0.27	0.08	0.00	1.94	2.56	**5**	0.04
	−0.14	97.86	6.78	1.22	0.00	**8**	0.15	0.28	0.07	0.00	1.98	2.52	**5**	0.04
	−0.11	97.59	6.65	1.35	0.00	**8**	0.20	0.25	0.06	0.01	2.12	2.37	**5**	0.03
	−0.06	98.24	6.77	1.23	0.00	**8**	0.15	0.23	0.07	0.00	1.96	2.59	**5**	0.04
	−0.08	98.13	6.79	1.21	0.00	**8**	0.15	0.22	0.09	0.00	1.96	2.58	**5**	0.04
	−0.09	98.21	6.80	1.20	0.00	**8**	0.17	0.27	0.06	0.00	1.98	2.51	**5**	0.04
	−0.16	98.40	6.78	1.22	0.00	**8**	0.15	0.27	0.07	0.00	1.96	2.55	**5**	0.04
	−0.14	98.56	6.79	1.21	0.00	**8**	0.15	0.23	0.09	0.00	1.94	2.59	**5**	0.04
	−0.11	98.34	6.79	1.22	0.00	**8**	0.16	0.26	0.06	0.01	2.04	2.47	**5**	0.03
	−0.11	97.98	6.81	1.20	0.00	**8**	0.15	0.23	0.08	0.00	1.91	2.62	**5**	0.04
	−0.10	97.86	6.75	1.26	0.00	**8**	0.16	0.21	0.11	0.00	1.96	2.57	**5**	0.04
	−0.11	98.65	6.84	1.16	0.00	**8**	0.15	0.26	0.08	0.00	1.92	2.60	**5**	0.04
	−0.10	97.99	6.56	1.44	0.00	**8**	0.21	0.29	0.05	0.01	2.08	2.37	**5**	0.03
	−0.11	98.21	6.75	1.25	0.00	**8**	0.16	0.29	0.07	0.00	2.00	2.48	**5**	0.04
	−0.11	98.29	6.71	1.29	0.00	**8**	0.18	0.23	0.05	0.01	2.05	2.48	**5**	0.03
	−0.09	98.15	6.72	1.28	0.00	**8**	0.18	0.27	0.07	0.00	1.99	2.48	**5**	0.04
	−0.09	98.45	6.76	1.24	0.00	**8**	0.16	0.20	0.10	0.00	1.92	2.62	**5**	0.03
	−0.12	97.60	6.73	1.27	0.00	**8**	0.18	0.25	0.05	0.01	2.01	2.50	**5**	0.03
	−0.10	98.56	6.75	1.25	0.00	**8**	0.16	0.25	0.06	0.01	2.03	2.49	**5**	0.03
	−0.13	97.63	6.64	1.36	0.00	**8**	0.20	0.25	0.06	0.01	2.14	2.35	**5**	0.03
	−0.11	97.54	6.84	1.16	0.00	**8**	0.15	0.22	0.08	0.00	1.89	2.65	**5**	0.04
	−0.08	97.80	6.75	1.26	0.00	**8**	0.16	0.24	0.11	0.00	1.95	2.54	**5**	0.04
	−0.11	97.97	6.78	1.22	0.00	**8**	0.17	0.28	0.06	0.00	1.98	2.50	**5**	0.04
	−0.07	97.98	6.80	1.20	0.00	**8**	0.16	0.25	0.04	0.01	1.99	2.54	**5**	0.03
	−0.11	98.38	6.75	1.25	0.00	**8**	0.16	0.25	0.07	0.00	2.00	2.53	**5**	0.04
	−0.10	98.49	6.66	1.34	0.00	**8**	0.17	0.33	0.04	0.02	2.05	2.40	**5**	0.02
Early stage	Literature data of Yulong intrusions[*7]													
	−0.18	98.66	6.98	1.02	0.00	**8**	0.11	0.22	0.00	0.00	1.81	2.86	**5**	0.05
	−0.10	98.72	7.07	0.93	0.00	**8**	0.10	0.21	0.13	0.00	1.51	3.05	**5**	0.05
	−0.22	98.76	7.03	0.97	0.00	**8**	0.12	0.18	0.13	0.00	1.45	3.12	**5**	0.04
	−0.11	99.26	7.01	0.99	0.00	**8**	0.13	0.22	0.11	0.00	1.72	2.82	**5**	0.04
	−0.15	99.30	6.94	1.06	0.00	**8**	0.14	0.17	0.11	0.00	1.75	2.84	**5**	0.05
	−0.11	98.91	6.92	1.08	0.00	**8**	0.10	0.24	0.13	0.00	1.75	2.78	**5**	0.05
	−0.18	98.76	7.10	0.90	0.00	**8**	0.09	0.28	0.09	0.00	1.62	2.93	**5**	0.05
	−0.13	98.95	6.83	1.17	0.00	**8**	0.12	0.21	0.15	0.00	1.71	2.81	**5**	0.05
	−0.11	98.76	6.92	1.08	0.00	**8**	0.11	0.22	0.14	0.00	1.54	2.99	**5**	0.04
	−0.33	99.04	6.91	1.09	0.00	**8**	0.10	0.20	0.14	0.00	1.65	2.91	**5**	0.05
	−0.25	99.24	7.17	0.83	0.00	**8**	0.08	0.19	0.12	0.00	1.48	3.13	**5**	0.05
	−0.18	99.84	7.06	0.94	0.00	**8**	0.10	0.19	0.20	0.00	1.42	3.10	**5**	0.06
	−0.11	98.72	6.90	1.10	0.00	**8**	0.12	0.24	0.13	0.00	1.75	2.77	**5**	0.05
	−0.29	99.64	7.02	0.98	0.00	**8**	0.09	0.24	0.12	0.00	1.66	2.90	**5**	0.04
	−0.15	98.69	7.10	0.91	0.00	**8**	0.09	0.19	0.28	0.00	1.42	3.02	**5**	0.07
	−0.19	99.34	6.73	1.27	0.00	**8**	0.13	0.24	0.15	0.00	1.81	2.67	**5**	0.05
	−0.02	99.22	6.91	1.09	0.00	**8**	0.10	0.22	0.12	0.00	1.72	2.84	**5**	0.05
	−0.14	99.59	6.92	1.08	0.00	**8**	0.09	0.25	0.18	0.00	1.66	2.83	**5**	0.05
	−0.21	98.69	6.78	1.22	0.00	**8**	0.14	0.23	0.14	0.00	1.73	2.76	**5**	0.06

(*continued on next page*)

Table A1 (*continued*)

	Atomic proportions per 13 cations[1] O = F,Cl	Total	Si	Al^{IV}	Ti^{4+}	**ΣT**	Ti^{4+}	Al^{VI}	Fe^{3+}	Mn^{2+}	Fe^{2+}	Mg^{2+}	**ΣC**	Mn^{2+}
	−0.13	98.94	7.12	0.88	0.00	**8**	0.11	0.23	0.10	0.00	1.64	2.92	**5**	0.04
	−0.14	100.08	6.87	1.13	0.00	**8**	0.12	0.22	0.17	0.00	1.72	2.77	**5**	0.05
	−0.16	98.98	7.03	0.97	0.00	**8**	0.10	0.21	0.18	0.00	1.48	3.02	**5**	0.06
	−0.20	99.09	7.02	0.98	0.00	**8**	0.10	0.22	0.13	0.00	1.59	2.96	**5**	0.05
	−0.15	98.45	6.78	1.23	0.00	**8**	0.13	0.27	0.12	0.00	1.82	2.65	**5**	0.06
	−0.22	99.59	6.96	1.04	0.00	**8**	0.10	0.20	0.20	0.00	1.65	2.86	**5**	0.05
Late stage	−0.15	99.52	7.43	0.57	0.00	**8**	0.05	0.10	0.24	0.00	1.12	3.49	**5**	0.05
	−0.23	99.38	7.30	0.70	0.00	**8**	0.06	0.12	0.20	0.00	1.25	3.36	**5**	0.05
	−0.20	99.80	7.33	0.68	0.00	**8**	0.08	0.08	0.24	0.00	1.16	3.44	**5**	0.04
	−0.16	99.60	7.53	0.47	0.00	**8**	0.04	0.12	0.17	0.00	1.20	3.48	**5**	0.04
	−0.14	99.27	7.54	0.46	0.00	**8**	0.04	0.14	0.09	0.02	1.26	3.45	**5**	0.03
	−0.10	99.24	7.28	0.72	0.00	**8**	0.07	0.12	0.20	0.00	1.26	3.34	**5**	0.05
	−0.20	100.05	7.39	0.61	0.00	**8**	0.06	0.11	0.19	0.00	1.28	3.36	**5**	0.04
ZK1007-473@ 10-2	99.74	7.32	0.68	0.00	**8**	0.06	0.10	0.21	0.00	1.30	3.33	**5**	0.05	0.01

	Atomic proportions per 13 cations[1] Fe^{2+}	Ca^{2+}	Na^{+}	**ΣB**	Na	K	**ΣA**	P (kbar)[2]	T (°C)[6]	H_2Omelt (wt.%)[3]	depth (km)[4]	$logfO_2$	**$logfO_2$ (FMQ)**[5]	**ΔFMQ**[5]
	Volcanic rocks from Lawu basin													
		1.89	0.08	**2**	0.48	0.29	**0.77**	4.2	743	4.6	15.9	−15.1	−16.0	1.0
		1.91	0.08	**2**	0.46	0.32	**0.77**	4.3	779	4.6	16.4	−14.4	−15.2	0.8
		1.91	0.06	**2**	0.46	0.28	**0.75**	4.2	741	4.8	16.0	−15.1	−16.1	0.9
		1.88	0.09	**2**	0.46	0.32	**0.78**	4.7	751	4.8	17.8	−15.0	−15.8	0.8
		1.89	0.09	**2**	0.43	0.29	**0.72**	4.2	740	4.8	16.0	−15.2	−16.1	0.9
		1.93	0.05	**2**	0.48	0.31	**0.79**	4.4	757	4.7	16.7	−14.9	−15.7	0.8
		1.83	0.15	**2**	0.46	0.31	**0.77**	5.3	850	4.6	20.0	−12.8	−13.7	0.9
		1.86	0.13	**2**	0.49	0.29	**0.78**	5.5	868	4.9	20.9	−12.6	−13.4	0.8
		1.93	0.07	**2**	0.49	0.33	**0.83**	4.5	795	4.3	17.2	−14.1	−14.9	0.7
		1.93	0.06	**2**	0.49	0.30	**0.79**	4.4	775	4.8	16.9	−14.5	−15.3	0.8
		1.94	0.06	**2**	0.49	0.32	**0.81**	4.2	788	4.3	16.1	−14.2	−15.0	0.8
	0.01	1.85	0.10	**2**	0.44	0.32	**0.77**	4.8	758	4.7	18.1	−14.9	−15.7	0.8
		1.90	0.08	**2**	0.47	0.31	**0.78**	4.4	815	4.4	16.6	−13.7	−14.4	0.8
		1.90	0.07	**2**	0.47	0.32	**0.79**	4.6	780	4.7	17.6	−14.4	−15.2	0.8
		1.93	0.06	**2**	0.50	0.30	**0.80**	4.4	792	4.7	16.9	−14.2	−14.9	0.7
		1.93	0.05	**2**	0.46	0.32	**0.78**	4.5	758	4.7	17.0	−14.8	−15.7	0.9
	0.03	1.83	0.10	**2**	0.45	0.30	**0.75**	4.3	750	4.5	16.6	−14.9	−15.9	1.0
	0.02	1.85	0.09	**2**	0.45	0.33	**0.78**	4.6	750	4.4	17.4	−15.1	−15.9	0.8
		1.89	0.06	**2**	0.47	0.34	**0.81**	4.9	763	4.6	18.7	−14.8	−15.6	0.8
	0.00	1.85	0.10	**2**	0.44	0.27	**0.71**	4.4	740	5.2	16.8	−15.2	−16.1	0.9
		1.88	0.09	**2**	0.45	0.27	**0.71**	3.8	725	4.7	14.6	−15.4	−16.5	1.1
		1.87	0.10	**2**	0.46	0.30	**0.76**	4.3	756	4.6	16.6	−14.9	−15.7	0.8
	0.00	1.86	0.09	**2**	0.46	0.29	**0.75**	4.4	746	4.8	16.8	−15.1	−16.0	0.9
	0.01	1.85	0.10	**2**	0.44	0.33	**0.77**	4.7	756	4.6	17.8	−15.0	−15.7	0.8
		1.87	0.10	**2**	0.44	0.36	**0.80**	5.0	792	4.4	19.0	−14.3	−14.9	0.7
	0.00	1.88	0.08	**2**	0.46	0.37	**0.83**	5.5	791	4.7	20.9	−14.4	−14.9	0.6
		1.87	0.10	**2**	0.45	0.33	**0.78**	4.4	765	4.3	16.9	−14.7	−15.5	0.8
	0.01	1.83	0.12	**2**	0.44	0.26	**0.69**	3.6	718	4.4	13.8	−15.4	−16.7	1.3
	0.02	1.86	0.09	**2**	0.43	0.32	**0.75**	4.7	755	4.8	17.9	−14.9	−15.8	0.8
	0.01	1.87	0.08	**2**	0.45	0.31	**0.76**	4.1	731	4.2	15.6	−15.3	−16.3	1.0
	0.01	1.84	0.11	**2**	0.46	0.30	**0.76**	4.1	737	4.2	15.5	−15.2	−16.2	1.0
	0.02	1.87	0.07	**2**	0.47	0.31	**0.78**	4.4	746	4.5	16.7	−15.0	−16.0	0.9

(*continued on next page*)

Table A1 (*continued*)

	Atomic proportions per 13 cations[1]													
	Fe^{2+}	Ca^{2+}	Na^{+}	**ΣB**	Na	K	**ΣA**	P (kbar)[2]	T (°C)[6]	H_2Omelt (wt.%)[3]	depth (km)[4]	$logfO_2$	**$logfO_2$ (FMQ)**[5]	**ΔFMQ**[5]
	0.02	1.85	0.09	**2**	0.44	0.30	**0.75**	4.4	749	4.6	16.8	−14.9	−15.9	1.0
	0.02	1.85	0.10	**2**	0.46	0.31	**0.77**	4.5	755	4.4	17.0	−14.8	−15.8	0.9
		1.85	0.12	**2**	0.46	0.31	**0.77**	4.4	760	4.5	16.8	−14.8	−15.7	0.8
	0.01	1.86	0.09	**2**	0.48	0.28	**0.75**	4.0	734	4.3	15.1	−15.2	−16.3	1.1
	0.02	1.87	0.08	**2**	0.46	0.35	**0.81**	5.0	778	4.5	19.1	−14.5	−15.2	0.7
	0.02	1.85	0.09	**2**	0.43	0.28	**0.72**	4.0	729	4.5	15.3	−15.2	−16.4	1.2
	0.03	1.86	0.07	**2**	0.42	0.33	**0.76**	4.7	752	4.5	17.8	−14.9	−15.8	1.0
	porphyries from Zongguo prospect													
		1.84	0.14	**2**	0.47	0.30	**0.77**	3.4	748	3.5	13.1	−14.8	−15.9	1.1
	0.01	1.81	0.14	**2**	0.45	0.29	**0.75**	3.4	725	3.4	12.9	−15.2	−16.5	1.3
	0.01	1.81	0.15	**2**	0.43	0.26	**0.69**	3.0	699	3.5	11.3	−15.7	−17.2	1.5
	0.00	1.80	0.16	**2**	0.44	0.27	**0.71**	3.1	717	3.5	11.9	−15.2	−16.7	1.5
	0.01	1.83	0.12	**2**	0.39	0.25	**0.63**	2.9	682	3.8	11.1	−16.0	−17.6	1.6
	0.01	1.81	0.15	**2**	0.38	0.24	**0.61**	2.7	668	3.8	10.4	−16.3	−18.0	1.7
		1.83	0.14	**2**	0.42	0.26	**0.69**	3.1	707	3.7	11.7	−15.5	−17.0	1.4
	0.01	1.81	0.14	**2**	0.48	0.27	**0.75**	3.0	722	3.0	11.5	−15.1	−16.6	1.4
	0.00	1.84	0.11	**2**	0.43	0.27	**0.70**	3.1	701	3.5	11.9	−15.6	−17.1	1.5
	0.01	1.84	0.12	**2**	0.42	0.27	**0.69**	3.2	701	3.8	12.2	−15.6	−17.1	1.5
	0.00	1.83	0.13	**2**	0.40	0.29	**0.69**	3.2	699	3.6	12.3	−15.8	−17.2	1.4
		1.85	0.12	**2**	0.46	0.31	**0.77**	3.6	730	3.4	13.6	−15.3	−16.4	1.0
	0.00	1.82	0.14	**2**	0.50	0.26	**0.76**	3.1	720	3.3	11.8	−15.2	−16.6	1.4
	0.01	1.82	0.13	**2**	0.47	0.27	**0.73**	3.0	705	3.3	11.4	−15.5	−17.0	1.5
	0.00	1.81	0.15	**2**	0.40	0.28	**0.68**	3.1	705	3.6	11.9	−15.7	−17.0	1.3
	0.00	1.82	0.14	**2**	0.46	0.27	**0.73**	3.2	708	3.6	12.2	−15.5	−16.9	1.4
	0.02	1.82	0.13	**2**	0.46	0.25	**0.71**	3.1	711	3.6	11.6	−15.4	−16.8	1.5
		1.80	0.17	**2**	0.46	0.27	**0.73**	3.2	726	3.5	12.1	−15.2	−16.5	1.2
	0.01	1.83	0.12	**2**	0.45	0.26	**0.70**	3.0	704	3.5	11.4	−15.5	−17.0	1.5
	0.02	1.81	0.13	**2**	0.47	0.28	**0.74**	3.1	715	3.2	11.8	−15.3	−16.7	1.4
	0.01	1.81	0.15	**2**	0.42	0.26	**0.68**	3.0	695	3.5	11.3	−15.8	−17.3	1.5
		1.83	0.15	**2**	0.52	0.31	**0.84**	4.0	776	3.6	15.4	−14.3	−15.3	0.9
	0.00	1.83	0.14	**2**	0.42	0.28	**0.70**	3.4	707	3.9	12.9	−15.6	−16.9	1.3
		1.82	0.15	**2**	0.50	0.29	**0.79**	3.3	742	3.1	12.7	−14.9	−16.1	1.2
	0.00	1.81	0.15	**2**	0.43	0.28	**0.72**	3.4	720	3.7	13.0	−15.4	−16.6	1.3
	0.02	1.83	0.11	**2**	0.47	0.27	**0.73**	3.0	713	3.2	11.6	−15.3	−16.8	1.5
		1.83	0.15	**2**	0.47	0.28	**0.76**	3.3	740	3.4	12.5	−14.9	−16.1	1.2
		1.83	0.14	**2**	0.48	0.27	**0.75**	3.2	727	3.5	12.3	−15.2	−16.4	1.3
		1.83	0.14	**2**	0.49	0.31	**0.80**	3.6	743	3.3	13.8	−15.1	−16.0	1.0
	0.01	1.82	0.13	**2**	0.43	0.25	**0.68**	2.9	697	3.4	10.9	−15.6	−17.2	1.6
	0.02	1.82	0.12	**2**	0.42	0.28	**0.70**	3.2	703	3.5	12.3	−15.6	−17.0	1.4
		1.81	0.15	**2**	0.41	0.28	**0.69**	3.2	713	3.7	12.4	−15.5	−16.8	1.3
		1.81	0.17	**2**	0.48	0.27	**0.75**	3.1	730	3.3	11.8	−15.0	−16.4	1.3
	0.00	1.84	0.12	**2**	0.47	0.28	**0.75**	3.2	711	3.5	12.3	−15.5	−16.9	1.4
		1.84	0.15	**2**	0.47	0.30	**0.77**	3.8	756	3.9	14.5	−14.7	−15.7	1.1
Early stage	Literature data of Yulong intrusions[*7]													
	0.06	1.85	0.05	**2**	0.47	0.16	**0.63**	2.4	659	4.2	9.3	−16.2	−18.3	2.0
	0.03	1.80	0.13	**2**	0.38	0.15	**0.52**	2.2	659	3.9	8.3	−15.9	−18.3	2.3
	0.04	1.80	0.13	**2**	0.40	0.15	**0.55**	2.2	679	3.5	8.4	−15.3	−17.7	2.4
	0.02	1.81	0.13	**2**	0.38	0.16	**0.53**	2.3	654	4.2	8.9	−16.4	−18.4	2.0
	0.01	1.85	0.09	**2**	0.43	0.17	**0.60**	2.4	666	3.8	9.2	−16.1	−18.1	1.9
	0.02	1.83	0.10	**2**	0.42	0.18	**0.59**	2.7	667	4.4	10.2	−16.1	−18.0	1.9
	0.00	1.78	0.17	**2**	0.39	0.14	**0.53**	2.3	661	4.3	8.6	−16.0	−18.2	2.1
	0.04	1.83	0.08	**2**	0.47	0.19	**0.66**	2.9	694	4.0	10.9	−15.4	−17.3	1.9

(continued on next page)

Table A1 (*continued*)

	Atomic proportions per 13 cations[1] Fe^{2+}	Ca^{2+}	Na^{+}	**ΣB**	Na	K	**ΣA**	P (kbar)[2]	T (°C)[6]	H_2Omelt (wt.%)[3]	depth (km)[4]	$\log fO_2$	**$\log fO_2$ (FMQ)**[5]	**ΔFMQ**[5]
	0.04	1.82	0.10	**2**	0.42	0.17	**0.59**	2.6	685	3.9	10.0	−15.3	−17.5	2.2
	0.03	1.84	0.08	**2**	0.46	0.17	**0.63**	2.6	680	3.9	9.9	−15.6	−17.7	2.1
	0.02	1.81	0.12	**2**	0.37	0.12	**0.49**	1.9	637	3.8	7.1	−16.4	−18.9	2.5
	0.06	1.75	0.14	**2**	0.36	0.14	**0.50**	2.2	667	3.8	8.2	−15.5	−18.0	2.5
	0.02	1.84	0.09	**2**	0.43	0.16	**0.59**	2.7	671	4.6	10.4	−16.0	−17.9	1.9
	0.02	1.81	0.12	**2**	0.42	0.15	**0.57**	2.4	661	4.2	9.1	−16.1	−18.2	2.1
	0.01	1.78	0.14	**2**	0.27	0.12	**0.39**	2.1	629	4.4	7.8	−16.7	−19.1	2.5
	0.04	1.82	0.10	**2**	0.51	0.21	**0.72**	3.3	722	4.1	12.5	−14.9	−16.6	1.7
	0.02	1.85	0.08	**2**	0.47	0.16	**0.63**	2.6	675	4.2	10.0	−15.8	−17.8	2.0
	0.05	1.81	0.09	**2**	0.40	0.17	**0.57**	2.7	665	4.5	10.3	−16.0	−18.1	2.1
	0.02	1.84	0.08	**2**	0.45	0.20	**0.64**	3.1	700	4.3	11.7	−15.3	−17.1	1.8
	0.01	1.80	0.14	**2**	0.33	0.13	**0.47**	2.1	636	4.3	8.0	−16.8	−18.9	2.2
	0.05	1.81	0.10	**2**	0.43	0.17	**0.60**	2.7	681	4.3	10.5	−15.7	−17.6	1.9
	0.05	1.77	0.13	**2**	0.34	0.15	**0.49**	2.3	660	4.1	8.7	−15.9	−18.2	2.4
	0.02	1.81	0.12	**2**	0.39	0.15	**0.54**	2.3	660	4.1	8.9	−16.0	−18.2	2.2
	0.01	1.83	0.10	**2**	0.48	0.20	**0.67**	3.2	707	4.5	12.2	−15.3	−17.0	1.6
	0.07	1.82	0.07	**2**	0.37	0.16	**0.52**	2.4	647	4.4	9.3	−16.4	−18.6	2.2
Late stage	0.02	1.76	0.17	**2**	0.21	0.09	**0.30**	1.2	592	3.1	4.5	−17.1	−20.4	3.3
	0.01	1.80	0.14	**2**	0.28	0.11	**0.40**	1.4	613	3.2	5.5	−16.7	−19.6	3.0
	0.03	1.77	0.16	**2**	0.25	0.11	**0.36**	1.3	617	2.8	5.0	−16.4	−19.5	3.1
	0.01	1.81	0.14	**2**	0.19	0.07	**0.26**	1.0	559	3.4	4.0	−18.2	−21.5	3.3
	0.00	1.84	0.14	**2**	0.20	0.07	**0.28**	1.1	584	3.5	4.0	−17.5	−20.6	3.1
	0.01	1.80	0.14	**2**	0.27	0.12	**0.38**	1.5	612	3.3	5.6	−16.8	−19.7	2.9
	0.01	1.80	0.15	**2**	0.23	0.10	**0.34**	1.2	586	3.2	4.7	−17.5	−20.5	3.0
ZK1007-473@ 10-2	1.81	0.13	**2**	0.28	0.10	**0.38**	1.4	598	3.3	5.2	−17.2	−20.2	2.9	

Note: General formula: $A_{0-1}B_2C_5T_8O_{22}(OH, F, Cl)_2$.

[1] Atomic proportions based on 13 cations were calculated by using the spreadsheet given by Locock (2014).

[2] Amphibole crystallization pressures are calculated using the equation of Mutch et al. (2016).

[3] Amphibole crystallization water contents in melt, and *f*O2 are calculated from equations of Ridolfi et al. (2010).

[4] Amphibole crystallization depth was caculated assuming conditions of lithostatic pressure, $\rho = 2.7 \times 10^3\, kg/m^{3.}$

[5] ΔFMQ is calculated using the equation of HSC O'Neill (1987).

[6] Amphibole crystallization temperatures are calculated using the equation of Ridolfi and Renzulli (2012).

*7 Amphibole data of the Yulong intrusions is after Huang et al. (2019).

Table A2
Summary of the geology of Cu prospects and deposits of the yulong porphyry Cu belt.

Deposits	Scale, metal tonnage and grade	Controlled structure	Wall rocks	Fertile rock type	Alteration	Ore structure	Sulfide assemblage	Metallic type	References
Seli-Zongguo-Mamupu porphyry Cu prospects									
Seli	Cu prospect	N-S Ailao Shan- Red River fault and Seli anticline	Upper Triassic sandstone and shale	Monzogranite porphyry	Propylitic and potassic	Disseminated	Ccp + Py ± Po	Cu ± Mo	Chen et al. (2016); Zhang et al. (1998); this study
Zongguo	Cu prospect	N-S Ailao Shan- Red River fault	Upper Triassic sandstone, shale and tuff	Quartz monzonite porphyry	Hornfelsed and propylitic	Disseminated	Ccp	Cu	Chen et al. (2016); this study
Mamupu	Cu prospect	N-S Ailao Shan- Red River fault and Jicuo anticline	Upper Triassic sandstone and shale	Syenite porphyry	Hornfelsed and propylitic	Disseminated	Ccp + Py + Gn	Cu ± Au ± Ag	Chen et al. (2016); Zhang et al. (2012); this study
Giant Cu deposit									
Yulong	Giant (6.22 Mt Cu) Cu: 0.99%; Mo: 0.028%; Au: 0.35 ppm	NW-SE strike-slip faults and Ganlongla anticline	Upper Triassic crystalline limestone	Monzogranite porphyry; Alkali-feldspar granite porphyry; Quartz monzonite porphyry; Syenogranite porphyry	Potassic, propylitic, phyllic, argillic and skarn	Disseminated, stockwork and massive	Ccp + Mol + Py + -Bn + Cct + Ttr + C-pr ± Gn ± Sp	Cu + Mo ± Au ± -Ag ± Re ± Pt ± -Pd ± Co ± Pb ± -Zn	Hou et al. (2003); Jiang et al. (2006); Wu et al. (2013a,b)
Large Cu deposits									
Malasongduo	Large (1.00 Mt Cu) Cu: 0.44%; Mo: 0.14%; Au: 0.06 ppm	NW-SE strike-slip faults	Upper mudstone and sandstone, lower Triassic rhyolite and tuff	Monzogranite porphyry; Syenogranite porphyry	Potassic, phyllic and argillic	Veinlet-disseminated	Ccp + Mol	Cu + Mo ± Au ± -Ag ± Re ± Pt ± -Pd	Hou et al. (2003); Liang et al. (2009)
Duoxiasongduo	Large (0.50 Mt Cu) Cu: 0.38%; Mo: 0.04%; Au: 0.05 ppm	NW-SE strike-slip faults and Mangzong anticline	Upper Triassic sandstone, mudstone and shale	Monzogranite porphyry; Alkali-feldspar granite porphyry	Potassic, phyllic and propylitic	Veinlet-disseminated, stockwork	Ccp + Py ± Mol ± Bn ± Mag	Cu + Mo ± Au ± -Ag	Hou et al. (2003); Wu et al. (2013a,b)
Medium Cu deposits									
Narigongma	Medium (0.25 Mt Cu) Cu: 0.33%; Mo: 0.079%	NW-SE strike-slip faults and Zaduo anticline	Lower Permian intermediate-mafic volcanic rocks	Biotite granite porphyry	Potassic, propylitic, phyllic and argillic	Vein-veinlet	Ccp + Mol + Cct + -Az + Py ± Gn ± S-p	Cu + Mo	Yang et al. (2008, 2014); Wang et al. (2008a,b)
Baomai	Medium (0.21 Mt Cu) Cu: 0.22%; Mo: 0.06%	NW-SE strike-slip faults and Xiariduo anticline	Early Paleozoic gneiss and middle Triassic limestone and shale	Biotite granite porphyry; Biotite monzogranite porphyry	Potassic, propylitic, phyllic, argillic and skarn	Disseminated and vein, veinlet	Ccp + Mol + Py + -Eng	Cu + Mo ± Fe ± -Ag ± Pb ± Zn	Lin et al. (2018)
Zhanaga	Medium (0.30 Mt Cu) Cu: 0.36%; Mo: 0.03%; Au: 0.03 ppm	NW-SE strike-slip faults	Lower Permian volcanic rocks and upper Triassic sandstone and mudstone	Monzogranite porphyry; Syenogranite porphyry	Potassic, propylitic, phyllic and argillic	Disseminated	Ccp + Mol + Py + -Mag + Cct ± Gn ± Sp	Cu + Mo + Au ± F-e ± Pb ± Zn	He et al. (2014); Hou et al. (2003)
Mangzong	Medium (0.25 Mt Cu) Cu: 0.34%; Mo: 0.03%; Au: 0.02 ppm	NW-SE strike-slip faults and Mangzong anticline	Upper Triassic sandy mudstone	Monzogranite porphyry	Potassic, propylitic, phyllic	Veinlet and disseminated	Ccp + Mol + Py ± Gn ± Sp	Cu + Mo + Au	Hou et al. (2003); Wu et al. (2011)

Abbreviations: Az = azurite; Bn = bornite; Cct = chalcocite; Ccp = chalcopyrite; Cpr = cuprite; Eng = enargite; Gn = galena; Po = pyrrhotite; Py = pyrite; Mag = magnetite; Mol = molybdenite; Sp = sphalerite; Ttr = tetrahedrite.

Table A3
Summary of ages of volcanic rocks and porphyries in the basins and Cu deposits of the Yulong porphyry Cu belt.

Locality	Rock type	Analyzed phase	Method	Age (Ma)	References
Lawu basin	Volcanic rocks	Zircon	U-Pb	35.37 ± 0.25–36.10 ± 0.28	This study
Seli	Porphyries	Zircon	U-Pb	39.4 ± 0.2	Chen et al. (2016)
		Biotite	K-Ar	39.5 ± 0.6	Zhang and Xie (1997)
Mamupu	Porphyries	Zircon	U-Pb	38.5 ± 0.3	Chen et al. (2016)
		Biotite	K-Ar	34.2 ± 0.6–37.1 ± 0.6	Zhang and Xie (1997)
Zongguo	Porphyries	Zircon	U-Pb	39.4 ± 0.2	Chen et al. (2016)
		Biotite	K-Ar	37.2 ± 0.6	Zhang and Xie (1997)
Yulong	Fertile porphyries	Zircon	U-Pb	41.0 ± 1.0–43.6 ± 0.8	Guo et al. (2006)
		Molybdenite	Re-Os	41.6 ± 1.4	Tang et al. (2009)
		Zircon	U-Pb	41.4 ± 0.6–43.9 ± 0.6	Wang et al. (2009)
		Zircon	U-Pb	41.3 ± 0.2	Liang et al. (2008)
		Zircon	U-Pb	40.7–41.2	Li et al. (2012)
		Zircon	U-Pb	37–40	Jiang et al. (2006)
Narigongma	Fertile porphyries	Zircon	U-Pb	43.3 ± 0.5	Yang et al. (2008)
		Zircon	U-Pb	41.44 ± 0.23	Song et al. (2011)
		Zircon	U-Pb	42.9 ± 0.3–43.4 ± 0.4	Hao et al. (2012)
		Molybdenite	Re-Os	40.8 ± 0.4	Hao et al. (2012)
		Molybdenite	Re-Os	40.8 ± 0.4–40.86 ± 0.85	Wang et al. (2008b)
Ridanguo	Fertile porphyries	Feldspar and K feldspar	K-Ar	41.5–42.3	Hou et al. (2003)
Baomai	Fertile porphyries	Zircon	U-Pb	41.9 ± 0.4–43.6 ± 0.4; 37.0 ± 0.7–38.7 ± 0.5	Lin et al. (2018)
		Molybdenite	Re-Os	42.6 ± 0.3	Lin et al. (2018)
Hengxingcuo	Fertile porphyries	K feldspar	K-Ar	40.7–41.0	Tang and Luo (1995)
Zhanaga	Fertile porphyries	Zircon	U-Pb	38.5 ± 0.2	Liang et al. (2006)
Mangzong	Fertile porphyries	Zircon	U-Pb	37.6 ± 0.2	Liang et al. (2006)
Duoxiasongduo	Fertile porphyries	Zircon	U-Pb	37.4 ± 0.3–37.6 ± 0.2	Liang et al. (2006)
Malasongduo	Fertile porphyries	Zircon	U-Pb	36.8 ± 0.3–36.9 ± 0.3	Liang et al. (2006)
Nangqian basin	Volcanic rocks	Zircon	U-Pb	38.2 ± 0.3–40.1 ± 0.3	Xu et al. (2019a,b)
	Infertile porhyries	Zircon	U-Pb	35.6 ± 0.3–39.5 ± 0.3	Xu et al. (2016b)

References

Andersen, T., 2002. Correction of common lead in U-Pb analyses that do not report ^{204}Pb. Chem. Geol. 192, 59–79.
Bachmann, O., Dungan, M., Bussy, F., 2005. Insights into shallow magmatic processes in large silicic magma bodies: the trace element record in the Fish Canyon magma body, Colorado. Contrib. Miner. Petrol. 149, 338–349.
Baker, M., Hirschmann, M., Ghiorso, M., Stolper, E., 1995. Compositions of near-solidus peridotite melts from experiments and thermodynamic calculations. Nature 375, 308–311.
Ballard, J.R., Palin, M.J., Campbell, I.H., 2002. Relative oxidation states of magmas inferred from Ce (IV)/Ce (III) in zircon: application to porphyry copper deposits of northern Chile. Contrib. Miner. Petrol. 144, 347–364.
Bouvier, A., Vervoort, J.D., Patchett, P.J., 2008. The Lu–Hf and Sm–Nd isotopic composition of CHUR: constraints from unequilibrated chondrites and implications for the bulk composition of terrestrial planets. Earth Planet. Sci. Lett. 273, 48–57.
Burnham, C.W., 1979. Magmas and hydrothermal fluids. Geochem. Hydrother. Ore Depos. 71–136.
Carmichael, I.S.E., 1991. The redox states of basic and silicic magmas: a reflection of their source regions? Contrib. Miner. Petrol. 106, 129–141.
Castillo, P.R., Janney, P.E., Solidum, R.U., 1999. Petrology and geochemistry of Camiguin Island, southern Philippines: insights to the source of adakites and other lavas in a complex arc setting. Contrib. Miner. Petrol. 134, 33–51.
Cavosie, A., Valley, J., Wilde, S., 2005. Magmatic δ18O in 4400–3900 Ma detrital zircons: a record of the alteration and recycling of crust in the Early Archean. Earth Planet. Sci. Lett. 235, 663–681.
Chang, J., Li, J.W., Selby, D., Liu, J.C., Deng, X.D., 2017. Geological and chronological constraints on the long-lived Eocene Yulong porphyry Cu-Mo deposit, eastern Tibet, China: implications for lifespan of magmatic-hydrothermal processes forming giant and supergiant porphyry Cu deposits. Econ. Geol. 112, 1719–1746.
Chen, X.L., Huang, W.T., Zou, Y.Q., Liang, H.Y., Zhang, J., Zhang, Y.Q., 2016. Zircon U-Pb geochronology and geochemistry of ore-bearing porphyries in the southern Yulong porphyry copper belt, and factors resulting in the differences in scale of mineralization between the southern and northern Yulong porphyry copper belt. Acta Petrol. Sin. 32, 2522–2534 (in Chinese with English abstract).
Cheng, Y., Spandler, C., Chang, Z., Clarke, G., 2018. Volcanic–plutonic connections and metal fertility of highly evolved magma systems: a case study from the Herberton Sn–W–Mo Mineral Field, Queensland, Australia. Earth Planet. Sci. Lett. 486, 84–93.
Chen, Y.-L., Tang, J.-R., Liu, F., Zhang, H.-F., Nie, L.-S., Jiang, L.-T., 2006. Elemental and Sm-Nd isotopic geochemistry of clastic sedimentary rocks in the Garzê-Songpan block and Longmen Mountains. Geol. China 33, 109–118 (in Chinese with English abstract).
Chou, I.-M., 1978. Calibration of oxygen buffers at elevated P and T using the hydrogen fugacity sensor. Am. Mineral. 63, 690–703.
Cline, J.S., 2003. How to concentrate copper. Science 302, 2075–2076.
DeCelles, P.G., Robinson, D.M., Zandt, G., 2002. Implications of shortening in the Himalayan fold-thrust belt for uplift of the Tibetan Plateau. Tectonics 21, 12-1-12-25.
Deng, J., Wang, Q., Li, G., Li, C., Wang, C., 2014a. Tethys tectonic evolution and its bearing on the distribution of important mineral deposits in the Sanjiang region, SW China. Gondwana Res. 26, 419–437.
Deng, J., Wang, Q., Li, G., Santosh, M., 2014b. Cenozoic tectono-magmatic and metallogenic processes in the Sanjiang region, southwestern China. Earth Sci. Rev. 138, 268–299.
Deng, W., Sun, H., Zhang, Y., 2001. Petrogenesis of cenozoic potassic volcanic rocks in nangqen basin. Chin. J. Geol. 36, 304–318 (in Chinese with English abstract).
DePaolo, D.J., 2012. Neodymium Isotope Geochemistry: An Introduction. Springer Science & Business Media, pp. 230.
de Hoog, J.C.M., Hattori, K.H., Hoblitt, R.P., 2004. Oxidized sulfur-rich mafic magma at Mount Pinatubo, Philippines. Contrib. Miner. Petrol. 146, 750–761.
Ding, L., Maksatbek, S., Cai, F.L., Wang, H.Q., Song, P.P., Ji, W.Q., Xu, Q., Zhang, L.Y., Muhammad, Q., Upendra, B., 2017. Processes of initial collision and suturing between India and Asia. Sci. China Earth Sci. 60, 635–651.
Ding, L., Qasim, M., Jadoon, I.A.K., Khan, M.A., Xu, Q., Cai, F.L., Wang, H.Q., Baral, U., Yue, Y.H., 2016. The India-Asia collision in north Pakistan: INSIGHT from the U-Pb detrital zircon provenance of Cenozoic foreland basin. Earth Planet. Sci. Lett. 455, 49–61.
Donnelly, K.E., Goldstein, S.L., Langmuir, C.H., Spiegelman, M., 2004. Origin of enriched ocean ridge basalts and implications for mantle dynamics. Earth Planet. Sci. Lett. 226, 347–366.
Dobosi, G., Kempton, P.D., Downes, H., Embey-Isztin, A., Thirlwall, M., Greenwood, P., 2003. Lower crustal granulite xenoliths from the Pannonian Basin, Hungary, Part 2: Sr–Nd–Pb–Hf and O isotope evidence for formation of continental lower crust by tectonic emplacement of oceanic crust. Contrib. Miner. Petrol. 144, 671–683.
Fan, W.-M., Guo, F., Wang, Y.-J., Lin, G., 2003. Late mesozoic calc-alkaline volcanism of post-orogenic extension in the northern Da Hinggan Mountains, northeastern China. J. Volcanol. Geoth. Res. 121, 115–135.
Fan, W., Wang, Y., Zhang, A., Zhang, F., Zhang, Y., 2010. Permian arc–back-arc basin development along the Ailaoshan tectonic zone: geochemical, isotopic and geochronological evidence from the Mojiang volcanic rocks, Southwest China. Lithos 119, 553–568.
Gerdes, A., Zeh, A., 2006. Combined U-Pb and Hf isotope LA-(MC-) ICP-MS analyses of detrital zircons: comparison with SHRIMP and new constraints for the provenance and age of an Armorican metasediment in Central Germany. Earth Planet. Sci. Lett. 249, 47–61.
Gill, J., 2012. Orogenic Andesites and Plate Tectonics. Springer Science & Business Media,

pp. 358.
Goldstein, S., O'nions, R., Hamilton, P., 1984. A Sm-Nd isotopic study of atmospheric dusts and particulates from major river systems. Earth Planet. Sci. Lett. 70, 221–236.
Green, T., Pearson, N., 1985. Experimental determination of REE partition coefficients between amphibole and basaltic to andesitic liquids at high pressure. Geochim. Cosmochim. Acta 49, 1465–1468.
Griffin, W., Pearson, N., Belousova, E., Saeed, A., 2006. Comment: Hf-isotope heterogeneity in zircon 91500. Chem. Geol. 233, 358–363.
Griffin, W., Pearson, N., Belousova, E., Jackson, S., Van Achterbergh, E., O'Reilly, S.Y., Shee, S., 2000. The Hf isotope composition of cratonic mantle: LAM-MC-ICPMS analysis of zircon megacrysts in kimberlites. Geochim. Cosmochim. Acta 64, 133–147.
Griffin, W., Wang, X., Jackson, S., Pearson, N., O'Reilly, S.Y., Xu, X., Zhou, X., 2002. Zircon chemistry and magma mixing, SE China: in-situ analysis of Hf isotopes, Tonglu and Pingtan igneous complexes. Lithos 61, 237–269.
Gromet, L.P., Silver, L.T., 1983. Rare earth element distributions among minerals in a granodiorite and their petrogenetic implications. Geochim. Cosmochim. Acta 47, 925–939.
Guo, L., Liu, Y., Xu, W., Zhang, X., Qin, K., Li, T., Shi, Y., 2006. Constraints to the mineralization age of the Yulong porphyry copper deposit from SHRIMP U-Pb zircon data in Tibet. Acta Petrol. Sin. 22, 1009–1016 (in Chinese with English abstract).
Hao, J., Chen, J., Dong, Q., Tian, Y., Li, Y., Chen, D., 2012. Zircon LA-ICP-MS U-Pb dating for Narigongma porphyry molybdenite copper deposit in southern Qinghai Province and its geological implication. Geoscience 26, 45–53 (in Chinese with English abstract).
Hawkesworth, C., Kemp, A., 2006. Using hafnium and oxygen isotopes in zircons to unravel the record of crustal evolution. Chem. Geol. 226, 144–162.
He, S.P., Li, R.S., Wang, C., Zhang, H.F., Ji, W.H., Yu, P.S., Gu, P.Y., Shi, C., He, S.P., Li, R.S., 2011. Discovery of ~4.0 Ga detrital zircons in the Changdu Block, North Qiangtang, Tibetan Plateau. Sci. Bull. 56, 647–658.
He, G., Wang, G., Huang, W., Zou, Y., Wu, J., Liang, H., Zhang, Y., Allen, C., 2014. Zircon LA-ICP-MS U-Pb age of the zalaga porphyry associated with Cu-Mo mineralization in the yulong ore belt and its geological implication. Geochimica 43, 399–407 (in Chinese with English abstract).
Horton, B.K., Yin, A., Spurlin, M.S., Zhou, J., Wang, J., 2002. Paleocene-Eocene syncontractional sedimentation in narrow, lacustrine-dominated basins of east-central Tibet. Geol. Soc. Am. Bull. 114, 771–786.
Hou, Z., Hongwen, M., Zaw, K., Yuquan, Z., Mingjie, W., Zeng, W., Guitang, P., Renli, T., 2003. The Himalayan Yulong porphyry copper belt: product of large-scale strike-slip faulting in eastern Tibet. Econ. Geol. 98, 125–145.
Hou, Z., Cook, N.J., 2009. Metallogenesis of the Tibetan collisional orogen: a review and introduction to the special issue. Ore Geol. Rev. 36, 2–24.
Huang M-L, Bi X-W, Hu R-Z, Gao J-F, Xu L-L, Zhu J-J., 2019. Geochemistry, in-situ Sr-Nd-Hf-O isotopes, and mineralogical constraints on origin and magmatic-hydrothermal evolution of the Yulong porphyry Cu-Mo deposit, Eastern Tibet. Gondwana Research, Submitted.
Hu, X.M., Wang, J., An, W., Garzanti, E., Li, J., 2017. Constraining the timing of the India-Asia continental collision by the sedimentary record. Sci. China Earth Sci. 60, 603–625.
Irvine, T., Baragar, W., 1971. A guide to the chemical classification of the common volcanic rocks. Can. J. Earth Sci. 8, 523–548.
Jacobsen, S.B., Wasserburg, G., 1980. Sm-Nd isotopic evolution of chondrites. Earth Planet. Sci. Lett. 50, 139–155.
Jiang, Y.-H., Jiang, S.-Y., Ling, H.-F., Dai, B.-Z., 2006. Low-degree melting of a metasomatized lithospheric mantle for the origin of Cenozoic Yulong monzogranite-porphyry, east Tibet: geochemical and Sr–Nd–Pb–Hf isotopic constraints. Earth Planet. Sci. Lett. 241, 617–633.
Kemp, A.I.S., Hawkesworth, C.J., 2003. Granitic perspectives on the generation and secular evolution of the continental crust In: ed. Rudnick, R. L., The Crust. Treatise on Geochemistry 3, pp. 349–410.
Keto, L.S., Jacobsen, S.B., 1987. Nd and Sr isotopic variations of early paleozoic oceans. Earth Planet. Sci. Lett. 84, 27–41.
Klein, M., Stosch, H.-G., Seck, H., 1997. Partitioning of high field-strength and rare-earth elements between amphibole and quartz-dioritic to tonalitic melts: an experimental study. Chem. Geol. 138, 257–271.
Kohn, M.J., Parkinson, C.D., 2002. Petrologic case for EOCENE slab breakoff during the Indo-Asian collision. Geology 30, 591–594.
Le Maitre, R.W., Bateman, P., Dudek, A., Keller, J., Lameyre, J., Le Bas, M., Sabine, P., Schmid, R., Sorensen, H., Streckeisen, A., 1989. In: A Classification of Igneous Rocks and Glossary of Terms: Recommendations of. Blackwell Oxford, pp. 193.
Li, J., Qin, K., Li, G., Cao, M., Xiao, B., Chen, L., Zhao, J., Evans, N.J., McInnes, B.I., 2012. Petrogenesis and thermal history of the Yulong porphyry copper deposit, Eastern Tibet: insights from U-Pb and U-Th/He dating, and zircon Hf isotope and trace element analysis. Mineral. Petrol. 105, 201–221.
Li, Q.-L., Li, X.-H., Liu, Y., Tang, G.-Q., Yang, J.-H., Zhu, W.-G., 2010a. Precise U-Pb and Pb–Pb dating of phanerozoic baddeleyite by SIMS with oxygen flooding technique. J. Anal. At. Spectrom. 25, 1107–1113.
Li, X.-H., Li, W.-X., Li, Q.-L., Wang, X.-C., Liu, Y., Yang, Y.-H., 2010b. Petrogenesis and tectonic significance of the~ 850 Ma Gangbian alkaline complex in South China: evidence from in situ zircon U-Pb dating, Hf–O isotopes and whole-rock geochemistry. Lithos 114, 1–15.
Li, X., Tang, G., Gong, B., Yang, Y., Hou, K., Hu, Z., Li, Q., Liu, Y., Li, W., 2013. Qinghu zircon: a working reference for microbeam analysis of U-Pb age and Hf and O isotopes. Chin. Sci. Bull. 58, 4647–4654.
Li, X.H., Liu, Y., Li, Q.L., Guo, C.H., Chamberlain, K.R., 2009. Precise determination of Phanerozoic zircon Pb/Pb age by multicollector SIMS without external standardization. Geochem. Geophys. Geosyst. 10, 4.
Liang, H.-Y., Campbell, I.H., Allen, C., Sun, W.-D., Liu, C.-Q., Yu, H.-X., Xie, Y.-W., Zhang, Y.-Q., 2006. Zircon Ce^{4+}/Ce^{3+} ratios and ages for Yulong ore-bearing porphyries in eastern Tibet. Miner. Depos. 41, 152–159.
Liang, H.Y., Campbell, I.H., Allen, C.M., Sun, W.D., Yu, H.X., Xie, Y.W., Zhang, Y.Q., 2007. The age of the potassic alkaline igneous rocks along the Ailao Shan-Red River shear zone: implications for the onset age of left-lateral shearing. J. Geol. 115, 231–242.
Liang, H., Mo, J., Sun, W., Yu, H., Zhang, Y., Charllote, M., 2008. Study on the duration of the ore-forming system of the Yulong giant porphyry copper deposit in eastern Tibet, China. Acta Petrol. Sin. 24, 2352–2358 (in Chinese with English abstract).
Liang, H.-Y., Mo, J.-H., Sun, W.-D., Zhang, Y.-Q., Zeng, T., Hu, G.-Q., M, A.C., 2009. Study on geochemical composition and isotope ages of the Malasongduo porphyry associated with Cu-Mo mineralization. Acta Petrol. Sin. 25, 385–392.
Leng, C.-B., Gao, J.-F., Chen, W.T., Zhang, X.-C., Tian, Z.-D., Guo, J.-H., 2018. Platinum-group elements, zircon Hf-O isotopes, and mineralogical constraints on magmatic evolution of the Pulang porphyry Cu-Au system, SW China. Gondwana Res. 62, 163–177.
Lin, B., Wang, L., Tang, J., Song, Y., Cao, H., Baker, M.J., Zhang, L., Zhou, X., 2018. Geology, geochronology, geochemical characteristics and origin of Baomai porphyry Cu (Mo) deposit, Yulong Belt. Tibet. Ore Geol. Rev. 92, 186–204.
Lloyd, F., Arima, M., Edgar, A., 1985. Partial melting of a phlogopite-clinopyroxenite nodule from south-west Uganda: an experimental study bearing on the origin of highly potassic continental rift volcanics. Contrib. Miner. Petrol. 91, 321–329.
Loucks, R., 2014. Distinctive composition of copper-ore-forming arc magmas. Aust. J. Earth Sci. 61, 5–16.
Locock, A.J., 2014. An Excel spreadsheet to classify chemical analyses of amphiboles following the IMA 2012 recommendations. Comput. Geosci. 62, 1–11.
Lu, Y.-J., Kerrich, R., Mccuaig, T.C., Li, Z.-X., Hart, C.J., Cawood, P.A., Hou, Z.-Q., Bagas, L., Cliff, J., Belousova, E.A., 2013. Geochemical, Sr–Nd–Pb, and zircon Hf–O isotopic compositions of eocene-oligocene shoshonitic and potassic adakite-like felsic intrusions in western Yunnan, SW China: petrogenesis and tectonic implications. J. Petrol. 54, 1309–1348.
Lu, Y.-J., Loucks, R.R., Fiorentini, M., McCuaig, T.C., Evans, N.J., Yang, Z.-M., Hou, Z.-Q., Kirkland, C.L., Parra-Avila, L.A., Kobussen, A., 2016. Zircon compositions as a pathfinder for porphyry Cu ± Mo ± Au deposits. Soc. Econ. Geol. Spec. Publ. 19, 329–347.
Ludwig, K., 2012. A Geochronological Toolkit for Microsoft Excel. Berkeley Geochronology Center Special Publications, pp. 1–75.
McCulloch, M., Black, L., 1984. Sm Nd isotopic systematics of enderby land granulites and evidence for the redistribution of Sm and Nd during metamorphism. Earth Planet. Sci. Lett. 71, 46–58.
Metcalfe, I., 2013. Gondwana dispersion and Asian accretion: tectonic and palaeogeographic evolution of eastern Tethys. J. Asian Earth Sci. 66, 1–33.
Miller, C., Schuster, R., Klötzli, U., Frank, W., Purtscheller, F., 1999. Post-collisional potassic and ultrapotassic magmatism in SW Tibet: geochemical and Sr–Nd–Pb–O isotopic constraints for mantle source characteristics and petrogenesis. J. Petrol. 40, 1399–1424.
Mo, X., Lu, F., Shen, S., Zhu, Q., Hou, Z., 1993. The Tethyan Volcanism and Mineralization in the Sanjiang Region. Geological Publishing House, Beijing, pp. 250 (in Chinese with English abstract.
Mungall, J.E., 2002. Roasting the mantle: slab melting and the genesis of major Au and Au-rich Cu deposits. Geology 30, 915–918.
Mutch, E., Blundy, J., Tattitch, B., Cooper, F., Brooker, R., 2016. An experimental study of amphibole stability in low-pressure granitic magmas and a revised Al-in-hornblende geobarometer. Contrib. Miner. Petrol. 171, 85.
Naney, M., 1983. Phase equilibria of rock-forming ferromagnesian silicates in granitic systems. Am. J. Sci. 283, 993–1033.
Nasdala, L., Hofmeister, W., Norberg, N., Martinson, J.M., Corfu, F., Dörr, W., Kamo, S.L., Kennedy, A.K., Kronz, A., Reiners, P.W., 2008. Zircon M257-a homogeneous natural reference material for the ion microprobe U-Pb analysis of zircon. Geostand. Geoanal. Res. 32, 247–265.
O'Neill, H.S., 1987. Quartz-fayalite-iron and quartz-fayalite-magnetite equilibria and the free energy of formation of fayalite (Fe2SiO4) and magnetite (Fe3O4). Am. Mineral. 72, 67–75.
O'Neill, H.S.C., Pownceby, M.I., 1993. Thermodynamic data from redox reactions at high temperatures. I. An experimental and theoretical assessment of the electrochemical method using stabilized zirconia electrolytes, with revised values for the Fe-"FeO", Co-CoO, Ni-NiO and Cu-Cu_2O oxygen buffers, and new data for the W-WO_2 buffer. Contrib. Miner. Petrol. 114, 296–314.
Pan, G., Wang, L., Zhang, W., Wang, B., 2010. In: Geotectonic Map and Specification of the Qinghai-Tibet Plateau and Its Adjacent areas (1:1500000). Geological Publishing, Beijing, pp. 75.
Parmigiani, A., Faroughi, S., Huber, C., Bachmann, O., Su, Y., 2016. Bubble accumulation and its role in the evolution of magma reservoirs in the upper crust. Nature 532, 492.
Peccerillo, A., Taylor, S.R., 1976. Geochemistry of Eocene calc-alkaline volcanic rocks from the Kastamonu area, northern Turkey. Contrib. Miner. Petrol. 58, 63–81.
Peucat, J., Vidal, P., Bernard-Griffiths, J., Condie, K., 1989. Sr, Nd, and Pb isotopic systematics in the archean low-to high-grade transition zone of Southern India: syn-accretion vs. post-accretion granulites. J. Geol. 537–549.
Plank, T., Langmuir, C.H., 1998. The chemical composition of subducting sediment and its consequences for the crust and mantle. Chem. Geol. 145, 325–394.
Prowatke, S., Klemme, S., 2006. Rare earth element partitioning between titanite and silicate melts: Henry's law revisited. Geochim. Cosmochim. Acta 70, 4997–5012.
Pullen, A., Kapp, P., Gehrels, G.E., Vervoort, J.D., Ding, L., 2008. Triassic continental subduction in central Tibet and Mediterranean-style closure of the Paleo-Tethys

Ocean. Geology 36, 351–354.
Qi, L., Jing, H., Gregoire, D.C., 2000. Determination of trace elements in granites by inductively coupled plasma mass spectrometry. Talanta 51, 507–513.
Ribeiro, J.M., Stern, R.J., Kelley, K.A., Shaw, A.M., Martinez, F., Ohara, Y., 2015. Composition of the slab-derived fluids released beneath the Mariana forearc: evidence for shallow dehydration of the subducting plate. Earth Planet. Sci. Lett. 418, 136–148.
Richard, P., Shimizu, N., Allegre, C., 1976. ^{143}Nd/^{146}Nd, a natural tracer: an application to oceanic basalts. Earth Planet. Sci. Lett. 31, 269–278.
Richards, J., 2003. Tectono-magmatic precursors for porphyry Cu-(Mo-Au) deposit formation. Econ. Geol. 98, 1515–1533.
Richards, J.P., 2009. Postsubduction porphyry Cu-Au and epithermal Au deposits: products of remelting of subduction-modified lithosphere. Geology 37, 247–250.
Richards, J., Jourdan, F., Creaser, R., Maldonado, G., DuFrane, S., 2013. Geology, geochemistry, geochronology, and economic potential of Neogene volcanic rocks in the Laguna Pederal and Salar de Aguas Calientes segments of the Archibarca lineament, northwest Argentina. J. Volcanol. Geoth. Res. 258, 47–73.
Richards, J.P., 2015. The oxidation state, and sulfur and Cu contents of arc magmas: implications for metallogeny. Lithos 233, 27–45.
Richards, J.P., 2011a. High Sr/Y arc magmas and porphyry Cu ± Mo ± Au deposits: just add water. Econ. Geol. 106, 1075–1081.
Richards, J.P., 2011b. Magmatic to hydrothermal metal fluxes in convergent and collided margins. Ore Geol. Rev. 40, 1–26.
Richards, J.P., Celâl Şengör, A.M., 2017. Did Paleo-Tethyan anoxia kill arc magma fertility for porphyry copper formation? Geology 45, 591–594.
Richards, J.P., Razavi, A.M., Spell, T.L., Locock, A., Sholeh, A., Aghazadeh, M., 2018. Magmatic evolution and porphyry–epithermal mineralization in the Taftan volcanic complex, southeastern Iran. Ore Geol. Rev. 95, 258–279.
Richards, J.P., Spell, T., Rameh, E., Razique, A., Fletcher, T., 2012. High Sr/Y magmas reflect arc maturity, high magmatic water content, and porphyry Cu ± Mo ± Au potential: examples from the Tethyan arcs of Central and Eastern Iran and Western Pakistan. Econ. Geol. 107, 295–332.
Richards, J.P., Ullrich, T., Kerrich, R., 2006. The late Miocene-Quaternary Antofalla volcanic complex, southern Puna, NW Argentina: protracted history, diverse petrology, and economic potential. J. Volcanol. Geoth. Res. 152, 197–239.
Ridolfi, F., Renzulli, A., Puerini, M., 2010. Stability and chemical equilibrium of amphibole in calc-alkaline magmas: an overview, new thermobarometric formulations and application to subduction-related volcanoes. Contrib. Miner. Petrol. 160, 45–66.
Ridolfi, F., Renzulli, A., 2012. Calcic amphiboles in calc-alkaline and alkaline magmas: thermobarometric and chemometric empirical equations valid up to 1,130° C and 2.2 GPa. Contrib. Miner. Petrol. 163, 877–895.
Roberts, D.A., Birchenough, S.N., Lewis, C., Sanders, M.B., Bolam, T., Sheahan, D., 2013. Ocean acidification increases the toxicity of contaminated sediments. Glob. Change Biol. 19, 340–351.
Rollinson, H.R., 2014. Using Geochemical Data: Evaluation, Presentation, Interpretation. Routledge, pp. 352.
Roger, F., Tapponnier, P., Arnaud, N., SchaÈrer, U., Brunel, M., Zhiqin, X., Jingsui, Y., 2000. An Eocene magmatic belt across central Tibet: mantle subduction triggered by the Indian collision? Terra Nova 12, 102–108.
Rohrlach, B.D., Loucks, R.R., Porter, T., 2005. Multi-million-year cyclic ramp-up of volatiles in a lower crustal magma reservoir trapped below the Tampakan copper-gold deposit by Mio-Pliocene crustal compression in the southern Philippines. Super porphyry copper and gold deposits: A global perspective 2, pp. 369–407.
Scherer, E., Münker, C., Mezger, K., 2001. Calibration of the lutetium-hafnium clock. Science 293, 683–687.
Shen, P., Hattori, K., Pan, H., Jackson, S., Seitmuratova, E., 2015. Oxidation condition and metal fertility of granitic magmas: zircon trace-element data from porphyry Cu deposits in the Central Asian Orogenic Belt. Econ. Geol. 110, 1861–1878.
She, Z., Ma, C., Mason, R., Li, J., Wang, G., Lei, Y., 2006. Provenance of the triassic songpan-Ganzi flysch, west China. Chem. Geol. 231, 159–175.
Sillitoe, R.H., 2010. Porphyry copper systems. Econ. Geol. 105, 3–41.
Sisson, T., 1994. Hornblende-melt trace-element partitioning measured by ion microprobe. Chem. Geol. 117, 331–344.
Sláma, J., Košler, J., Condon, D.J., Crowley, J.L., Gerdes, A., Hanchar, J.M., Horstwood, M.S., Morris, G.A., Nasdala, L., Norberg, N., 2008. Plešovice zircon—a new natural reference material for U-Pb and Hf isotopic microanalysis. Chem. Geol. 249, 1–35.
Song, Z., Jia, Q.-Z., Chen, X.-Y., Chen, B., Zhang, Y.-L., Zhang, X.-F., Quan, S.-C., 2011. The petrogenic age of narigongma granitic diorite-porphyry in the northern part of the sanjiang region and its geological implications. Acta Geosci. Sin. 32, 154–162 (in Chinese with English abstract).
Spurlin, M.S., Yin, A., Horton, B.K., Zhou, J., Wang, J., 2005. Structural evolution of the Yushu-Nangqian region and its relationship to syncollisional igneous activity, east-central Tibet. Geol. Soc. Am. Bull. 117, 1293–1317.
Stacey, J.t., Kramers, J., 1975. Approximation of terrestrial lead isotope evolution by a two-stage model. Earth Planet. Sci. Lett. 26, 207–221.
Streck, M.J., Leeman, W.P., Chesley, J., 2007. High-magnesian andesite from Mount Shasta: a product of magma mixing and contamination, not a primitive mantle melt. Geology 35, 351–354.
Sun, S.-S., McDonough, W.F., 1989. Chemical and Isotopic Systematics of Oceanic Basalts: Implications for Mantle Composition and Processes, vol. 42, 313–345 Special Publications.
Tang, G.-Q., Li, X.-H., Li, Q.-L., Liu, Y., Ling, X.-X., Yin, Q.-Z., 2015. Deciphering the physical mechanism of the topography effect for oxygen isotope measurements using a Cameca IMS-1280 SIMS. J. Anal. At. Spectrom. 30, 950–956.
Tang, J., Wang, C., Qu, W., Du, A., Ying, L., Gao, Y., 2009. Re–Os isotopic dating of molybdenite from the Yulong porphyry copper–molybdenum deposit in Tibet and its metallogenic significance. Rock Miner. Anal. 28, 215–218 (in Chinese with English abstract).
Tang, R., Luo, H., 1995. The Geology of Yulong Porphyry Copper (molybdenum) ore Belt. Geological Publishing House, Beijing, Xizang (Tibet), pp. 320.
Tao, Y., Bi, X., Li, C., Hu, R., Li, Y., Liao, M., 2014. Geochronology, petrogenesis and tectonic significance of the Jitang granitic pluton in eastern Tibet, SW China. Lithos 184–187, 314–323.
Tapponnier, P., Zhiqin, X., Roger, F., Meyer, B., Arnaud, N., Wittlinger, G., Jingsui, Y., 2001. Oblique stepwise rise and growth of the Tibet Plateau. Science 294, 1671–1677.
Tatsumi, Y., 1986. Formation of the volcanic front in subduction zones. Geophys. Res. Lett. 13, 717–720.
Tera, F., Wasserburg, G., 1972. U-Th-Pb systematics in three Apollo 14 basalts and the problem of initial Pb in lunar rocks. Earth Planet. Sci. Lett. 14, 281–304.
Turner, S., Arnaud, N., LIU, J., Rogers, N., Hawkesworth, C., Harris, N., Kelley, S., Van Calsteren, P., Deng, W., 1996. Post-collision, shoshonitic volcanism on the Tibetan Plateau: implications for convective thinning of the lithosphere and the source of ocean island basalts. J. Petrol. 37, 45–71.
Usuki, T., Lan, C.Y., Wang, K.L., Chiu, H.Y., 2013. Linking the Indochina block and gondwana during the early Paleozoic: evidence from U-Pb ages and Hf isotopes of detrital zircons. Tectonophysics 586, 145–159.
Valley, J., Lackey, J., Cavosie, A., Clechenko, C., Spicuzza, M., Basei, M., Bindeman, I., Ferreira, V., Sial, A., King, E., 2005. 4.4 billion years of crustal maturation: oxygen isotope ratios of magmatic zircon. Contrib. Miner. Petrol. 150, 561–580.
Wang, B., Wang, L., Chen, J., Yin, F., Wang, D., Zhang, W., Chen, L., Liu, H., 2014a. Triassic three-stage collision in the Paleo-Tethys: constraints from magmatism in the Jiangda–Deqen–Weixi continental margin arc, SW China. Gondwana Res. 26, 475–491.
Wang, C., Tang, J., Chen, J., Hao, J., Gao, Y., Liu, Y., Fan, T., Zhang, Q., Ying, L., Chen, Z., 2009. Chronological research of Yulong copper–molybdenum porphyry deposit. Acta Geol. Sin. 83, 1445–1455 (in Chinese with English abstract).
Wang, Q., Deng, J., Li, C., Li, G., Yu, L., Qiao, L., 2013. The boundary between the Simao and Yangtze blocks and their locations in Gondwana and Rodinia: constraints from detrital and inherited zircons. Gondwana Res. 26, 438–448.
Wang, Q., Wyman, D.A., Xu, J.-F., Zhao, Z.-H., Jian, P., Xiong, X.-L., Bao, Z.-W., Li, C.-F., Bai, Z.-H., 2006. Petrogenesis of Cretaceous adakitic and shoshonitic igneous rocks in the Luzong area, Anhui Province (eastern China): implications for geodynamics and Cu–Au mineralization. Lithos 89, 424–446.
Wang, Q., Tang, G., Jia, X., Zi, F., Jiang, Z., Xu, J., Zhao, Z., 2008a. The metalliferous mineralization associated with adakitic rocks. Geol. J. China Univers. 14, 350–364 (in Chinese with English abstract).
Wang, Z.L., Yang, Z.M., Yang, Z.S., Tian, S.H., Liu, Y.C., Ma, Y.Q., Wang, G.R., Qu, W.J., 2008b. Narigongma porphery molybdenite copper deposit, northern extension of Yulong copper belt: evidence from the age of Re-Os isotope. Acta Petrol. Sin. 24, 503–510 (in Chinese with English abstract).
Wang, R., Richards, J.P., Hou, Z., Yang, Z., DuFrane, S.A., 2014b. Increased magmatic water content—The key to oligo-miocene porphyry Cu-Mo ± Au formation in the eastern gangdese belt. Tibet. Econ. Geol. 109, 1315–1339.
Wang, R., Weinberg, R.F., Collins, W.J., Richards, J.P., Zhu, D.C., 2018. Origin of post-collisional magmas and formation of porphyry Cu deposits in southern Tibet. Earth Sci. Rev. 181, 122–143.
Wang, Y., Qian, X., Cawood, P.A., Liu, H., Feng, Q., Zhao, G., Zhang, Y., He, H., Zhang, P., 2017. Closure of the east paleotethyan ocean and amalgamation of the eastern cimmerian and southeast asia continental fragments. Earth Sci. Rev. 186, 195–230.
Wallace, P.J., Carmichael, I.S., 1994. S speciation in submarine basaltic glasses as determined by measurements of S Kα X-ray wavelength shifts. Am. Mineral. 79, 161–167.
Woodhead, J., Hergt, J., Davidson, J., Eggins, S., 2001. Hafnium isotope evidence for 'conservative' element mobility during subduction zone processes. Earth Planet. Sci. Lett. 192, 331–346.
Wu, F.-Y., Yang, Y.-H., Xie, L.-W., Yang, J.-H., Xu, P., 2006. Hf isotopic compositions of the standard zircons and baddeleyites used in U-Pb geochronology. Chem. Geol. 234, 105–126.
Wu, F.-Y., Sun, D.-Y., Li, H., Jahn, B.-M., Wilde, S., 2002. A-type granites in northeastern China: age and geochemical constraints on their petrogenesis. Chem. Geol. 187, 143–173.
Wu, F.Y., Ji, W.Q., Wang, J.G., Liu, C.Z., Chung, S.L., 2014. Zircon U-Pb and Hf isotopic constraints on the onset time of India-Asia collision. Am. J. Sci. 314, 548–579.
Wu, W., Xia, B., Zhang, Y., Dong, B., Xia, Z., 2013a. Geochemical characteristics and metallogenic mechanism of the porphyry Cu-Mo deposits in the Yulong ore belt, Eastern Tibet: a case study of the Yulong and Duoxiasongduo porphyries. Geotect. Metall. 37, 440–454 (in Chinese with English abstract).
Wu, J., Liang, H., Mo, J., Zhang, Y., Hu, G., 2011. Petrochemistry and zircon LA–ICP–MS U-Pb age of the Mangzong porphyry associated with Cu–Mo mineralization in the Yulong ore belt. Geotect. Metall. 35, 300–306 (in Chinese with English abstract).
Wu, T., Xiao, L., Ma, C.Q., Huang, Q., 2013b. The geochronological, geochemical and Sr-Nd isotopic characteristics of the Tongpu intrusive complex and its implications. Acta Petrol. Sin. 29, 3567–3580 (in Chinese with English abstract).
Xu, L.-L., Bi, X.-W., Hu, R.-Z., Tang, Y.-Y., Wang, X.-S., Huang, M.-L., Wang, Y.-J., Ma, R., Liu, G., 2019a. Contrasting whole-rock and mineral compositions of ore-bearing (Tongchang) and ore-barren (Shilicun) granitic plutons in SW China: Implications for petrogenesis and ore genesis. Lithos 336–337, 54–66.
Xu, L., Bi, X., Hu, R., Qi, Y., Tang, Y., Wang, X., Zhu, J., 2016a. Redox states and genesis of magmas associated with intra-continental porphyry Cu-Au mineralization within the Jinshajiang-Red River alkaline igneous belt, SW China. Ore Geol. Rev. 73, 330–345.
Xu, L., Bi, X., Hu, R., Zhang, X., Su, W., Qu, W., Hu, Z., Tang, Y., 2012. Relationships

between porphyry Cu–Mo mineralization in the Jinshajiang-Red River metallogenic belt and tectonic activity: constraints from zircon U-Pb and molybdenite Re–Os geochronology. Ore Geol. Rev. 48, 460–473.
Xu, Y., Bi, X.W., Hu, R.Z., Chen, Y.W., Liu, H.Q., Xu, L.L., 2016b. Geochronology and geochemistry of Eocene potassic felsic intrusions in the Nangqian basin, eastern Tibet: tectonic and metallogenic implications. Lithos 246–247, 212–227.
Xu, Y., Zhu, J., Hu, R., Bi, X., Yu, H., Xu, L., Liu, B., Huang, M., Sheng, X., 2019b. Heterogeneous lithospheric mantle beneath the Southeastern Tibetan Plateau: evidence from Cenozoic high-Mg potassic volcanic rocks in the Jinshajiang-Ailaoshan Cenozoic magmatic belt. J. Asian Earth Sci. https://doi.org/10.1016/j.jseaes.2019.04.018.
Yang, Z., Hou, Z., Xu, J., Bian, X., Wang, G., Yang, Z., Tian, S., Liu, Y., Wang, Z., 2014. Geology and origin of the post-collisional Narigongma porphyry Cu–Mo deposit, southern Qinghai. Tibet Gondwana Res. 26, 536–556.
Yang, Z.M., Hou, Z.Q., Yang, Z.S., Wang, S.X., Wang, G.R., Tian, S.H., Wen, D.Y., Wang, Z.L., Liu, Y.C., 2008. Genesis of porphyries and tectonic controls on the Narigongma porphyry Mo (-Cu) deposit, southern Qinghai. Acta Petrol. Sin. 24, 489–502 (in Chinese with English abstract).
Yin, A., Harrison, T.M., 2000. Geologic evolution of the himalayan-tibetan orogen. Annu. Rev. Earth Planet. Sci. 28, 211–280.
Zhang, H.-F., Sun, M., Zhou, X.-H., Fan, W.-M., Zhai, M.-G., Yin, J.-F., 2002. Mesozoic lithosphere destruction beneath the North China Craton: evidence from major-, trace-element and Sr–Nd–Pb isotope studies of Fangcheng basalts. Contrib. Miner. Petrol. 144, 241–254.
Zhang, H., He, H., Wang, J., Xie, G., 2005. $^{40}Ar/^{39}Ar$ chronology and geochemistry of high-K volcanic rocks in the Mangkang basin. Tibet. Sci. China Ser. D Earth Sci. 48, 1–12.
Zhang, Y., Xie, Y., 1997. Geochronology of Ailaoshan-Jinshajiang alkalirich intrusive rocks and their Sr and Nd isotopic characteristics. Sci. China Ser. D Earth Sci. 40, 524–529.
Zhang, Y., Xie, Y., Huaying, L., Qiu, H., Li, X., 1998. Petrogenesis series and the ore-bearing porphyries of the Yulong copper ore belt in eastern Tibet. Geochimica 27, 236–243 (in Chinese with English abstract).
Zhang, S.M., Xiao, Y.F., Gong, T.T., He, J.L., Wang, Q., Zhang, L., Sun, J.D., 2012. Optimal selection assessment on geochemical anomalies at Gegongnong, Hengxingcuo, Mamupu in the Yulong metallogenic zone. Tibet. Bull. Mineral. Petrol. Geochem. 31, 354–360 (in Chinese with English abstract).
Zheng, Y., Wu, F., 2018. The timing of continental collision between Indian and Asia. Sci. Bull. 63, 1649–1654.
Zhu, D.C., Zhao, Z.D., Niu, Y., Dilek, Y., Hou, Z.Q., Mo, X.X., 2013. The origin and pre-Cenozoic evolution of the Tibetan Plateau. Gondwana Res. 23, 1429–1454.
Zhu, D.C., Wang, Q., Zhao, Z.D., 2017. Constraining quantitatively the timing and process of continent-continent collision using magmatic record: method and examples. Sci. China Earth Sci. 60, 1040–1056.
Zi, J.-W., Cawood, P.A., Fan, W.-M., Wang, Y.-J., Tohver, E., McCuaig, T.C., Peng, T.-P., 2012a. Triassic collision in the paleo-tethys Ocean constrained by volcanic activity in SW China. Lithos 144, 145–160.
Zi, J.W., Cawood, P.A., Fan, W.M., Wang, Y.J., Tohver, E., 2012b. Contrasting rift and subduction-related plagiogranites in the Jinshajiang ophiolitic mélange, southwest China, and implications for the Paleo-Tethys. Tectonics 31.
Zi, J.W., Cawood, P.A., Fan, W.M., Tohver, E., Wang, Y.J., Mccuaig, T.C., Peng, T.P., 2013. Late permian-triassic magmatic evolution in the jinshajiang orogenic belt, SW China and implications for orogenic processes following closure of the Paleo-Tethys. Am. J. Sci. 313, 81–112.
Zindler, A., Hart, S., 1986. Chemical geodynamics. Annu. Rev. Earth Planet. Sci. 14, 493–571.
Zhu, J.-J., Richards, J.P., Rees, C., Creaser, R., DuFrane, S.A., Locock, A., Petrus, J.A., Lang, J., 2018. Elevated magmatic sulfur and chlorine contents in ore-forming magmas at the Red Chris porphyry Cu-Au deposit, Northern British Columbia, Canada. Econ. Geol. 113, 1047–1075.